ABSTRACT

A hybrid emulsion-spectrometer experiment (E531) was performed in the wide-band neutrino beam line at the Fermi National Accelerator Laboratory in Batavia, Illinois, U.S.A. The primary purpose of this experiment was to measure the lifetimes of weakly decaying, charmed particles. 1248 neutrino and antineutrino interactions were located of which 23 were reconstructed as charged, charmed candidates. From these 23 events the lifetime of the D^+ meson was determined to be $11.5^{+6.5}_{-3.0} \times 10^{-13}$ s, of the F^+ meson to be $1.9^{+1.3}_{-0.7} \times 10^{-13}$ s, and of the Λ_c^+ baryon to be $2.3^{+1.0}_{-0.7} \times 10^{-13}$ s.

The mass of the F^+ meson is measured to be 2057 ± 39 MeV/c^2.

Candidates for the decays $\Sigma_c \to \Lambda_c^+\pi$, $\Sigma_c^* \to \Lambda_c^+\pi$, $D^{+*} \to D^+\pi^o$, and $F^* \to F\gamma$ are also observed.

LIFETIME MEASUREMENTS OF THE D^+, F^+, AND Λ_c^+

Dale Barbara Pitman

A Thesis submitted in conformity with the requirements
for the Degree of Doctor of Philosophy in the
University of Toronto

© Dale Barbara Pitman
1982

ACKNOWLEDGEMENTS

I am grateful to the members of the collaboration who have made the experiment the success it has been. Anthony Kiang and Stephen Bracker, without whom the Toronto group and the experiment as a whole could not have managed, and John Martin and Steve Errede, who have inspired me with their enthusiasm, are to be thanked.

To have known Jim Prentice as my professor and friend has been my good fortune. I am grateful for the many kindnesses he has shown me, his inspiration, and his guidance.

David Bailey, my accomplice in whatever mischief was brought to the experiment during the months of data taking, who has more recently dispensed wisdom on a kaleidoscope of topics, deserves special thanks.

To my parents, I am thankful for their support. Lastly, there is Thomas, without whom I could not have written this thesis.

List of Collaborators

N. Ushida.
Department of Physics, Aichi University of Education, Igaya-cho, Kariya, Aichi 448, Japan.

T. Kondo.
Fermi National Accelerator Laboratory, Batavia, Illinois 60510, U.S.A.

F. Fujioka, H. Fukushima, Y. Takahashi, S. Tatsumi, and C. Yokoyama.
Physics Department, Kobe University, Rokkadai, Nada, Kobe 657, Japan.

Y. Homma and Y. Tsuzuki.
Faculty of Arts, Kobe University, Tsurukabuto, Nada, Kobe 657, Japan.

S. Bahk, C. Kim, J. Park, and J. Song.
Department of Physics, Korea University, Seoul 132, Korea.

D. Bailey, S. Conetti, J. Fischer, and J. Trischuk.
Department of Physics, McGill University, Montreal, Quebec H3A 2T8, Canada.

H. Fuchi, K. Hoshino, M. Miyanishi, K. Niu, K. Niwa, H. Shibuya, and Y. Yanagisawa.
Department of Physics, Nagoya University, Furo-Cho, Chikusa-Ku, Nagoya 464, Japan.

S. Errede, M. Gutzwiller, S. Kuramata, N. Reay, K. Reibel, T. Romanowski, R. Sidwell, and N. Stanton.
Physics Department, The Ohio State University, Columbus, Ohio 43210, U.S.A.

K. Moriyama and H. Shibata.
Physics Department, Okayama University, Okayama, Japan.

T. Hara, O. Kusumoto, Y. Noguchi, and M. Teranaka.
Physics Department, Osaka City University, Sugimoto-Cho, Sumiyoshi-Ku, Osaka 558, Japan.

H. Okabe and J. Yokota.
Science Education Institute of Osaka Prefecture, Karita-Cho 4, Sumiyoshi-Ku, Osaka 558, Japan.

J. Harnois, C. Hebert, J. Hebert, S. Lokanathan, and B. McLeod.
Department of Physics, University of Ottawa, Ottawa, Ontario, Canada.

S. Tasaka.
Institute for Cosmic Ray Research, University of Tokyo, Tokyo, Japan.

P. Davis, J. Martin, D. Pitman, J. Prentice, P. Sinervo, and T. Yoon.
Physics Department, University of Toronto, Toronto, Ontario M5S 1A7, Canada.

H. Kimura and Y. Maeda.
Faculty of Education, Yokohama National University, Hodogaya-Ku, Yokohama, Japan.

TABLE OF CONTENTS

		Page
1.	AN HISTORICAL PERSPECTIVE	1
2.	THEORY	11
	2.1 Production of Charm Quarks by Neutrinos	16
	2.2 Decays of Charmed Particles (Low-lying States)	20
	2.3 Decays of Charmed Particles (High Mass States)	27
3.	EQUIPMENT	28
	3.1 Neutrino Beam Line	31
	3.2 Emulsion	34
	3.3 Anti-coincidence Counter	41
	3.4 Time of Flight	42
	3.5 Drift Chambers	46
	3.5.1 Upstream Chambers	46
	3.5.2 Downstream Chambers	50
	3.5.3 Drift Chamber Electronic Data Collection System	52
	3.5.4 Calibration of Drift Chambers	53
	3.6 Magnet and Momentum Measurements	54
	3.7 Lead Glass	56
	3.8 Hadron Calorimeter	60
	3.9 Muon Identification Counters	62
	3.10 Data Acquisition	65

4. RESULTS 69

4.1 Reconstructed and Calculated Neutrino Event Samples 70
4.2 Emulsion Processing 73

5. DATA ANALYSIS 76

5.1 Neutrino Event Reconstruction Programs 76
5.2 Search for Neutrino Events in the Emulsion 80
5.3 Search for Charged Decays 85
5.3.1 Horizontal Emulsion Modules 85
5.3.2 Vertical Emulsion Modules 85
5.4 Search for Neutral Decays 88
5.4.1 Horizontal Emulsion Modules 88
5.4.2 Vertical Emulsion Modules 90
5.4.3 Overall Scanning Efficiencies 91
5.5 Backgrounds to Charm Decays 95
5.6 Analysis of Events with Short Decays 98

6. LIFETIME AND MASS CALCULATIONS 111

6.1 The $F^{\pm}$ 112
6.2 The Λ_c^+ 119
6.3 The $D^{\pm}$ 126
6.4 The Exotics 134
6.5 The Other Multi-prong Events 135

7. A SUMMARY 137

APPENDIX A. CHARM EVENTS 140

LIST OF FIGURES

FIGURE 1.	The Low-lying SU(4) hadrons.	4
FIGURE 2.	K^o-$\bar{K}^o$ mixing.	7
FIGURE 3.	Emission of the W boson.	17
FIGURE 4.	Neutral Current Processes.	18
FIGURE 5.	Decay of the W boson.	21
FIGURE 6.	Muon Decay and Charm Decay.	23
FIGURE 7.	Spectator Charm Decay.	24
FIGURE 8.	Alternative Charm Decay Mechanisms.	25
FIGURE 9.	Side View of the E531 apparatus.	30
FIGURE 10.	The Fermilab Neutrino Beam Line.	33
FIGURE 11.	The Neutrino Energy Spectrum.	35
FIGURE 12.	Placement of the Emulsion in the Beam Line.	37
FIGURE 13.	The Emulsion.	38
FIGURE 14.	The Time of Flight I Counter.	43
FIGURE 15.	The Time of Flight II Counter.	44
FIGURE 16.	Placement of the Upstream Chambers in the Beam Line.	47
FIGURE 17.	Cross-section of a Drift Chamber Cell.	49
FIGURE 18.	The Lead Glass Array.	58
FIGURE 19.	The Hadron Calorimeter.	61
FIGURE 20.	The Muon Detector.	64
FIGURE 21.	The Relative Timing of the Triggers.	66
FIGURE 22.	The Distribution of the Number of Reconstructed Tracks per Event.	79
FIGURE 23.	Z Coordinates of Found Events in the Emulsion Target.	82
FIGURE 24.	Differences between Predicted and Found Vertex Coordinates.	84
FIGURE 25.	Track Following Efficiency for Tracks of Various Angles.	86
FIGURE 26.	Charged Scanning Efficiency.	93
FIGURE 27.	Neutral Scanning Efficiency.	94
FIGURE 28.	Mass Spectrum Observed by Time of Flight.	102
FIGURE 29.	Relative Ionization Loss in Emulsion.	103
FIGURE 30.	Photomicrographs of Charged and Neutral Charm Candidates.	113
FIGURE 31.	Gaussian Ideograms of the Masses of Fitted $F^{\pm}$ Decays.	115
FIGURE 32.	Gaussian Ideograms of the Masses of Cabibbo-favoured $F^{\pm}$ Decay Modes.	116

FIGURE 33. Gaussian Ideograms of the Invariant $\Lambda_c^{\pm}\pi$ Mass Combinations. 122
FIGURE 34. Gaussian Ideograms of the Invariant $\Lambda_c^{+}\pi^{+}$ Mass Combinations. 123
FIGURE 35. Gaussian Ideograms of the Invariant $\Lambda_c^{+}\pi^{-}$ Mass Combinations. 124
FIGURE 36. Gaussian Ideograms of a Restricted Set of $\Lambda_c^{+}\pi$ Invariant Masses. 125
FIGURE 37. The 2-Dimensional Maximum Likelihood Function. 130
FIGURE 38. A Contour Plot of the Likelihood Function. 131
FIGURE 39. Gaussian Ideograms of the $D^{*} \rightarrow D\pi$ Mass Combinations. 133

LIST OF TABLES

TABLE 1.	Chemical composition of Fuji ET-7B emulsion.	36
TABLE 2.	Summary of Emulsion Scanning	92
TABLE 3.	Fitted $F^{\pm}$ Decays	114
TABLE 4.	Summary of F^{*} Production	117
TABLE 5.	Λ_c^+ Decays	120
TABLE 6.	Λ_c^+ Invariant Masses (MeV/c^2)	121
TABLE 7.	Summary of $D^{\pm}$ decays.	127
TABLE 8.	Summary of Exotic Decay Modes	134
TABLE 9.	Summary of Charm Candidates	136
TABLE 10.	Decay tracks for event 476-4449.	141
TABLE 11.	Summary of unconstrained decay hypothesis for event 476-4449.	142
TABLE 12.	Summary of constrained decay hypothesis for event 476-4449.	142
TABLE 13.	Decay tracks for event 493-1235.	144
TABLE 14.	Summary of decay hypotheses for event 493-1235.	145
TABLE 15.	Decay tracks for event 498-4985.	147
TABLE 16.	Decay hypotheses for event 498-4985.	148
TABLE 17.	Decay tracks for event 499-4713.	150
TABLE 18.	Summary of decay hypotheses for event 499-4713.	151
TABLE 19.	Decay tracks for event 512-5761.	153
TABLE 20.	Decay hypotheses for event 512-5761.	154
TABLE 21.	Decay tracks for event 522-2107.	156
TABLE 22.	Decay hypotheses for event 522-2107.	157
TABLE 23.	Decay tracks for event 527-3682.	159
TABLE 24.	Decay hypotheses for event 527-3682	160
TABLE 25.	Decay tracks for event 529-0271.	162
TABLE 26.	Summary of unconstrained decay hypotheses for event 529-0271.	163
TABLE 27.	Summary of constrained decay hypotheses for event 529-0271.	164
TABLE 28.	Decay tracks for event 533-7152.	165
TABLE 29.	Summary of decay hypotheses for event 533-7152.	166
TABLE 30.	Decay tracks for event 546-1339.	167
TABLE 31.	Summary of decay hypotheses for event 546-1339.	168
TABLE 32.	Decay tracks for event 547-3192.	170
TABLE 33.	Summary of constrained decay hypotheses for event 547-3192.	171
TABLE 34.	Summary of unconstrained decay hypotheses for event 547-3192.	172

TABLE 35. Decay tracks for event 549-4068. 175
TABLE 36. Summary of decay hypotheses for event 549-4068. 175
TABLE 37. Decay tracks for event 567-2596. 177
TABLE 38. Summary of decay hypotheses for event 567-2596. 178
TABLE 39. Decay tracks for event 580-4508. 180
TABLE 40. Summary of decay hypotheses for event 580-4508. 180
TABLE 41. Decay tracks for event 597-1851. 182
TABLE 42. Summary of decay hypotheses for event 597-1851. 183
TABLE 43. Decay tracks for event 598-1759. 186
TABLE 44. Summary of constrained decay hypotheses for event 598-1759. 186
TABLE 45. Summary of unconstrained decay hypotheses for event 598-1759. 187
TABLE 46. Decay tracks for event 602-2032. 189
TABLE 47. Summary of unconstrained decay hypothesis for event 602-2032. 189
TABLE 48. Summary of constrained decay hypothesis for event 602-2032. 190
TABLE 49. Decay tracks for event 610-4088. 191
TABLE 50. Summary of decay hypothesis for event 610-4088. 192
TABLE 51. Decay tracks for event 638-9417. 194
TABLE 52. Summary of decay hypotheses for event 638-9417. 194
TABLE 53. Decay tracks for event 650-6003. 196
TABLE 54. Decay hypotheses for event 650-6003. 197
TABLE 55. Decay Tracks for event 656-2631 198
TABLE 56. Summary of decay hypotheses for event 656-2631. 199
TABLE 57. Decay tracks for event 663-7758. 200
TABLE 58. Summary of decay hypotheses for event 663-7758. 201
TABLE 59. Decay tracks for event 671-7015. 204
TABLE 60. Summary of decay hypotheses for event 671-7015. 204

1. AN HISTORICAL PERSPECTIVE

The experimental discovery in 1974 of the J/ψ, which contains a charmed quark-antiquark pair, was in retrospect, the first new evidence supporting the conclusions of many years of theoretical work concerning the unification of the weak and electromagnetic forces. Prior to 1961, it was believed that the weak interactions were mediated by two charged, massive vector bosons, the W^+ and the W^- and that the electromagnetic interaction was mediated by a single vector boson, the photon. Although a unification of these two forces had been speculated upon earlier, it was Glashow who first proposed the addition of a neutral vector boson to the previously accepted triplet of intermediate vector fields -- the $W^{\pm}$ and the photon -- by which the theories could be unified [Glashow, 1961]. It was speculated that a linear combination of the two neutral fields corresponded to two physical particles: the photon, which accounted for electromagnetic interactions, and a neutral intermediary which coupled to a neutral lepton current.

Weinberg and Salam independently extended this model to include a spin-zero Higgs doublet [Weinberg, 1967 and Salam, 1968]. The model now involved the four vector fields, (the triplet, $\vec{W}_\mu$, and a singlet, B), the Higgs doublet, four

leptons, (the electron, the muon, the electron neutrino and the muon neutrino) and three quarks (now known as the u, d, and s quarks), which were the constituents of all the observable hadrons known at that time. The introduction of this doublet allowed the symmetry of the triplet and singlet to be spontaneously broken, leaving two massive charged bosons ($W^{\pm}$), a massive neutral boson (Z^{o}), and a massless boson (the photon). This spontaneous symmetry breaking, by which the particles are given masses is known as the Higgs Mechanism [Higgs, 1964]. Although it was not known at the time whether the model was renormalizable, it was later proven to be by t'Hooft and others [t'Hooft, 1971].

The appearance of the Z^{o} implied the existence of weak strangeness-changing currents, which was not supported by experimental evidence. In particular, in the Weinberg-Salam model first order terms existed which would give a K_1-K_2 mass splitting and contribute to unobserved decay modes such as $K^{+} \rightarrow \pi^{+}\ell\bar{\ell}$, where $\ell\bar{\ell}$ is a lepton-antilepton pair. Experimental evidence, however, implied that the K_1-K_2 mass splitting should arise from second order weak corrections.

To solve this difficulty, Glashow, Iliopoulos, and Maiani proposed the addition of a fourth quark, c, which carried the quantum number charm [Glashow, 1970]. (The concept of charm had

been previously proposed in 1964 by Bjorken and Glashow [Bjorken, 1964]. The authors presented the idea as a new quantum number, violated by the weak interaction, in order to develop a lepton-hadron symmetry.) The four-quark hadron sector could then be constructed analogously to the lepton sector, which at that time included the electron, the muon, and two neutrinos. The weak current was then expressed as a combination of the lepton and hadron currents.

In contrast to alternative schemes being presented at that time [Bars, 1972 and 1973 and deWit, 1974], the GIM model appeared to be the simplest modification to the Weinberg-Salam model and the most aesthetically pleasing. The observed selection rules remained preserved, in contrast with the three-quark model where a neutral current could not be introduced without contradicting experimental observations. No induced strangeness-changing couplings appeared in the neutral current. Several consequences resulted from this speculation:

- The weak bosons must be massive, of order 100 GeV/c^2, in order to have the electromagnetic and weak coupling constants of comparable magnitude;
- the weak neutral current would involve right-handed as well as left-handed terms; and
- The mass of the Z^o would not be equal to the mass of the $W^{\pm}$.

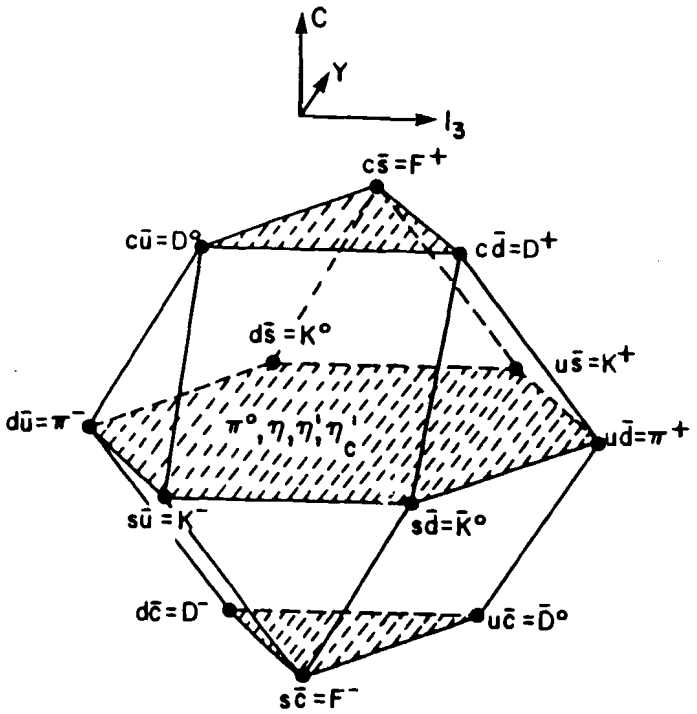

$J^P = 0^-$ MESONS

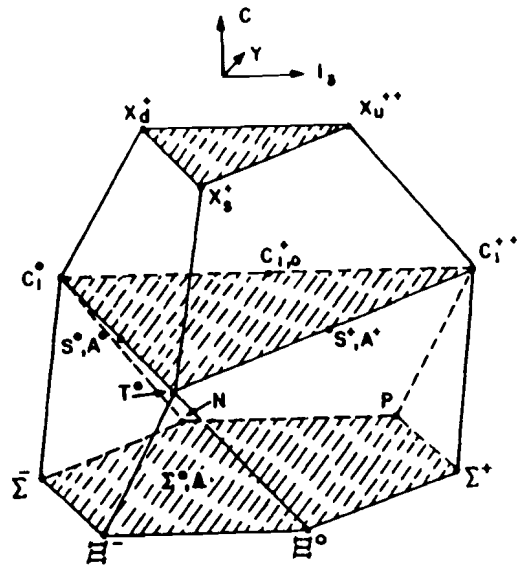

$J^P = \frac{1}{2}^+$ BARYONS

Figure 1. The low-lying SU(4) hadrons, showing the predicted charm states. The C_1^+ is now known as the Λ_c^+ and the C_0 as the Σ_c.

An extensive array of charmed hadron states was predicted. The states are shown in Figure 1. In the meson sector (that is, particles containing one quark and one antiquark) there exist two SU(3) triplets with one charm quark or antiquark. Among the baryons (particles containing three quarks) one expected a triplet and a sextet of singly charmed states and a doubly charmed triplet in the $J^P = \frac{1}{2}^+$ supermultiplet.

In their 1975 review paper, Gaillard, Lee, and Rosner elaborated upon the argument for the existence of charm (still to explain the absence of strangeness-changing neutral currents). The fundamental similarities between the quarks and leptons, which had been proposed by GIM, were presented explicitly: the fermions could be grouped in isodoublets for left-handed particles:

$$\begin{pmatrix} e \\ \nu_e \end{pmatrix}_L , \begin{pmatrix} \mu \\ \nu_\mu \end{pmatrix}_L , \text{ and } \begin{pmatrix} u \\ d_c \end{pmatrix}_L , \begin{pmatrix} c \\ s_c \end{pmatrix}_L , \tag{1}$$

where $d_c = d \cos \theta_c + s \sin \theta_c$, $s_c = s \cos \theta_c - d \sin \theta_c$, and θ_c is the Cabibbo angle. The right-handed fermions appeared as isosinglets:

$$(e)_R , (\mu)_R , (u)_R , (d)_R , (c)_R , (s)_R \tag{2}$$

Through the weak interaction a fermion may transform only within

its doublet. The charged vector bosons allow for transformations of the type $c \to s_c$. The Z^o boson accounts for the transitions $u \to u$, $c \to c$, $d_c \to d_c$, and $s_c \to s_c$. Thus the s quark always appears in the neutral current in the combination

$$\bar{d}_c d_c + \bar{s}_c s_c = \bar{d}d + \bar{s}s, \tag{3}$$

which does not involve a strangeness-changing part.

The mass of the charm quark could be predicted based on the amplitudes for second-order effects. (If the mass of the charm quark were equal to that of the up quark, there would be no large, strangeness-changing, neutral current effects). The magnitude of the second order effects is:

$$G_F \alpha (m_c^2 - m_u^2)/m_W^2 \cong G_F \alpha m_c^2/m_W^2 \ . \tag{4}$$

As it happens, the process which one would think might give the best prediction for the charm quark mass, $K_L^o \to \mu^+\mu^-$, occurs independently of m_c, because the relevant diagrams cancel. However, the K_L^o-K_S^o mass difference (which is related to K_o-$\bar{K}_o$ mixing, the higher order process shown in Figure 2), was used by the authors to successfully predict the mass of the charm quark.

It was at this time that two independent groups observed what would come to be interpreted as the ground state vector

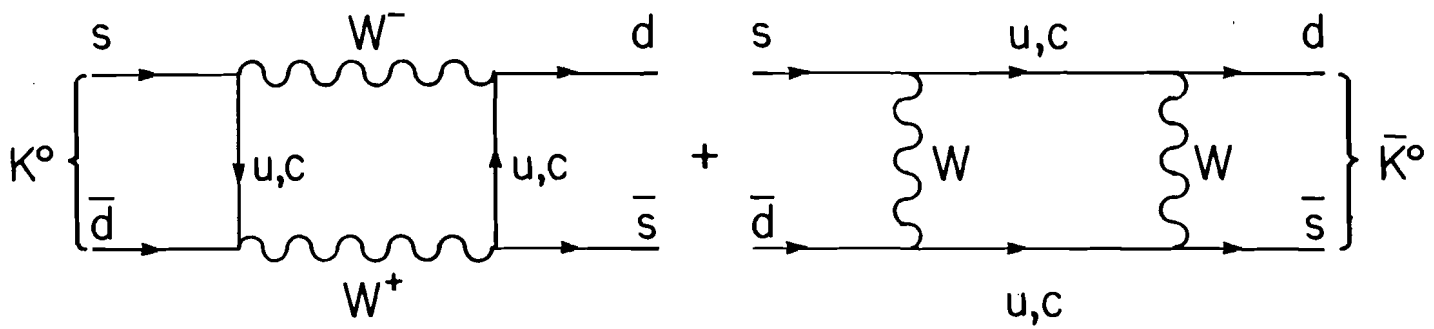

Figure 2. K^o-$\bar{K}^o$ mixing, a second-order, strangeness-changing weak process.

meson which contained "hidden" charm, $c\bar{c}$ [Aubert, 1974 and Augustin, 1974]. It is now known as the J/Ψ particle. Studying the reaction

$$p + Be \rightarrow e^+e^- + \text{anything} \tag{5}$$

Aubert, et al. at Brookhaven National Laboratory observed an enhancement in the invariant mass of the e^+e^- pair at 3.1 GeV/c^2. Using electron-positron colliding beams at SLAC, Augustin et al. observed a resonant peak at the same mass. In addition, the SLAC group observed a resonance at 3.7 GeV/c^2 (now interpreted as the radially excited state).

With this data, Gaillard, Lee, and Rosner were able to refine their predictions of the masses and lifetimes of charmed particles. They predicted the masses of the ground state charmed hadrons (for example: $c\bar{u}$, $c\bar{d}$, $c\bar{s}$, and cud) to be 2 - 2.5 GeV/c^2 and the lifetimes to be about 10^{-13} seconds [Gaillard, 1975].

Conclusive evidence for the existence of charmed mesons was presented in 1976 by an LBL-SLAC group working at SPEAR. Both the charged and neutral D particles ($c\bar{d}$ and $c\bar{u}$) were observed as final states in the reaction $e^+e^- \rightarrow$ hadrons. The mass of the D^o was found to be 1865±15 GeV/c^2 [Goldhaber, 1976], while that of the D^+ was 1876±15 GeV/c^2 [Peruzzi, 1976].

Evidence of the production and decay of charmed particles was amassed prior to and after this time using nuclear emulsion. As early as 1951 and 1956, events were found which could not be explained at the time, but which were later found to be consistent with the production of charm [Kaplon, 1952 and Nishikawa, 1959]. A 1971 cosmic ray emulsion experiment [Niu, 1971] observed an event which is now interpreted to be the associated production and decay of a pair of charmed particles. The observed decay times were 2.2×10^{-14} and 3.6×10^{-14} seconds. The masses were approximately 2 GeV/c^2.

Further visible evidence for the production and decay of charmed particles came from experiments which exposed nuclear emulsion in ν beam lines at both Fermilab and CERN [Burhop, 1976; Read, 1979]. In the CERN experiment a bubble chamber downstream of the target was used as a spectrometer. One event was kinematically reconstructed as a Λ_c^+ (cud) -> $p\pi^+K^-$ [Angelini, 1979]. The parent mass was calculated to be 2295±15 GeV/c^2 and the proper decay time was 7.3×10^{-13} seconds.

What was lacking in some of the early emulsion experiments, however, was a satisfactory method of identifying and measuring the momentum of the decay particles. Without such measurements, the mass of the parent particle could not be accurately determined, nor could the lifetime of the parent particle be

measured since the proper decay time is a function of the momentum:

$$L = \beta\gamma ct = \frac{p}{m}ct \ , \tag{6}$$

where L is the decay length, t is the decay time, p is the momentum, and m is the mass of the decaying particle. Given this situation, it seemed logical to combine the techniques of nuclear emulsion, in which decay lengths of several microns can be easily observed, with those of counter experiments, in which the mass and momentum of decay particles can be adequately measured. This thesis reports the results of such an experiment performed at the Fermi National Accelerator Laboratory from November 1978 to February 1979.

2. THEORY

Current theory holds that all matter is composed of quarks and leptons. Experimental evidence exists for five flavours of quarks: up (u), down (d), strange (s), charm (c), and beauty (b). In addition, a sixth quark, truth (t), is postulated. Each quark, which is of spin $\frac{1}{2}$, carries an electric and colour charge. Quarks themselves may not be observable as isolated particles but they are the constituents of the hadrons, for example the proton and the neutron, which are detectable. Hadrons may be grouped according to their quark content: Mesons are particles composed of a quark and an antiquark (not necessarily of identical flavour); baryons contain three quarks (again of any flavour). Symmetrically, there are six leptons: the electron, the muon, the tauon, and their respective neutrinos. Leptons are both elementary and observable in unbound states.

The standard theory of the weak interaction groups the quarks into left-handed doublets:

$$\begin{pmatrix} u \\ d' \end{pmatrix}_L , \begin{pmatrix} c \\ s' \end{pmatrix}_L , \begin{pmatrix} t \\ b' \end{pmatrix}_L ,$$

where the d', s', and b', the eigenstates of the weak interaction, are orthogonal linear combinations of the d, s, and b quarks. These are often expressed generically as

$$\begin{pmatrix} u \\ d' \end{pmatrix}$$

where the u is a quark of charge $\frac{2}{3}e$ and the d' is a quark of charge $-\frac{1}{3}e$. The right-handed quarks are singlets:

$$(u)_R \ , \ (d)_R \ , \ (c)_R \ , \ (s)_R \ , \ (t)_R \ , \text{ and } (b)_R \ .$$

In this theory, the weak interactions are mediated by two charged vector bosons $W^{\pm}$ and a neutral boson, Z^o, which account for charged and neutral current interactions. The weak interaction Lagrangian is expressed as:

$$\mathcal{L} = e \left[\frac{1}{\sin \theta_W \cos \theta_W} Z^o J^o + \frac{1}{\sqrt{2} \sin \theta_W}(W^+ J^+ + W^- J^-)\right] \qquad (7)$$

where J^o and $J^{\pm}$ are the weak interaction currents, and θ_W is the weak mixing angle which relates the physical fields A, the photon, and Z^o, the weak neutral boson, with the gauge fields W^o, the neutral member of the W triplet, and B, the U(1) singlet. These relations are

$$A = W^o \sin \theta_W + B \cos \theta_W, \qquad (8)$$

and

$$Z^{o} = W^{o}\cos\Theta_W - B\sin\Theta_W. \tag{9}$$

For the hadron sector

$$J_H^{+} = \bar{q}_u C_{KM}\,\gamma_\alpha \frac{(1-\gamma_5)}{2}\, q_d, \tag{10}$$

J_H^{-} is the adjoint of J_H^{+}, and

$$J_H^{o} = \bar{q}_d[-\frac{1}{2}\gamma_\alpha \frac{(1-\gamma_5)}{2} + \frac{1}{3}\sin^2\Theta_W\gamma_\alpha]q_d + \bar{q}_u[\frac{1}{2}\gamma_\alpha \frac{(1-\gamma_5)}{2} - \frac{2}{3}\sin^2\Theta_W\gamma_\alpha]q_u. \tag{11}$$

The q_u and q_d are the field operators where

$$q_u = \begin{bmatrix} u \\ c \\ t \end{bmatrix} \quad \text{and} \quad q_d = \begin{bmatrix} d \\ s \\ b \end{bmatrix}$$

respectively, The left-handed fields are projected by the operator $\frac{1}{2}(1-\gamma_5)$ and the right-handed fields by the operator $\frac{1}{2}(1+\gamma_5)$. The 3 x 3 Kobayashi-Maskawa mixing matrix, C_{KM}, which was developed as an extension for the four-quark scheme, is given by:

$$\begin{bmatrix} c_1 & s_1c_3 & s_1s_3 \\ -s_1c_2 & c_1c_2c_3+s_2s_3e^{i\delta} & c_1c_2c_3-s_2c_3e^{i\delta} \\ -s_1s_2 & c_1s_2c_3-c_2s_3e^{i\delta} & c_1s_2s_3+c_2c_3e^{i\delta} \end{bmatrix}$$

where $c_i = \cos\theta_i$ and $s_i = \sin\theta_i$. The charged current accounts for transitions of charge $\frac{2}{3}e$ quarks to $-\frac{1}{3}e$ quarks through the emission of a W^+. For example a charm quark can change into a strange quark by emitting a W^+ (Figure 3). Similarly, the W^- couples the antiquarks of charge $-\frac{2}{3}e$ to the antiquarks of charge $\frac{1}{3}e$. Particles are coupled to themselves through the Z^o. A quark may spontaneously emit a Z^o, or a Z^o may create a quark-antiquark pair from the vacuum (Figure 4).

The Kobayashi-Maskawa 6-quark model became experimentally relevant following the discovery of the b quark in the upsilon ($b\bar{b}$) particle [Herb, 1977]. However, since our discussion will involve primarily the first two quark generations, we shall neglect the effects of the generalized Kobayashi-Maskawa matrix which are minimal for charm decays. In the four-quark limit, $d' = d_c = d\cos\theta_c + s\sin\theta_c$ and $s' = s_c = s\cos\theta_c - d\sin\theta_c$, where θ_c is the Cabibbo angle and we recover the GIM scheme discussed in Chapter 1.

The left-handed leptons are also grouped into doublets:

$$\begin{pmatrix} e \\ \nu_e \end{pmatrix}_L, \quad \begin{pmatrix} \mu \\ \nu_\mu \end{pmatrix}_L, \quad \begin{pmatrix} \tau \\ \nu_\tau \end{pmatrix}_L$$

The right-handed leptons appear as weak-isospin singlets:

$$(e)_R, \ (\mu)_R, \text{ and } (\tau)_R.$$

The weak leptonic current

$$J_L^+ = \bar{\nu}_\ell \gamma_\alpha \frac{(1 - \gamma_5)}{2} \ell, \tag{12}$$

J^- is the adjoint of J^+, and

$$J_L^o = \bar{\nu}_\ell \left[\frac{1}{2}\gamma_\alpha \frac{(1 - \gamma_5)}{2}\right]\nu_\ell + \\ + \bar{\ell}\left[-\frac{1}{2}\gamma_\alpha \frac{(1 - \gamma_5)}{2} + \sin^2\theta_W \gamma_\alpha\right]\ell, \tag{13}$$

where ℓ is a lepton and ν_ℓ is its neutrino. The charged leptons couple to their neutrinos through the emission of a $W^\pm$ (Figure 3). A lepton may also spontaneously emit a Z^o or a Z^o may create a lepton-antilepton pair from the vacuum (Figure 4).

Since the discovery of parity violations in weak interactions, many theoretical models and much experimental evidence have indicated that the neutrinos are massless. It was therefore believed that, for the neutrinos, the weak interaction

eigenstates were the same as the mass eigenstates. Recently, considerable interest, both theoretical and experimental, has focused on the topic of massive neutrinos and neutrino mixing [Lubimov, 1980; Reines, 1980; Ushida, 1981].

2.1 Production of Charm Quarks by Neutrinos

Charm quarks may be produced by neutrinos in the presence of a nucleon by several processes. The most likely process will be that in which the neutrino changes into a lepton through the emission of a W^+, which then interacts with a d valence quark of the nucleus or with an s quark from the quark-antiquark sea to produce a charm quark. Another less likely process will be the neutral current reaction in which a Z^o, emitted by the neutrino, pulls a $c\bar{c}$ pair from the sea surrounding the nucleon. This process gives rise to associated production.

The charm quark, once created, combines with other quarks to produce detectable hadrons. Thus the states most easily produced using a neutrino beam will be those containing a single charm quark in combination with other quarks. These are called charmed particles in contrast to particles possessing hidden charm (a $c\bar{c}$ pair). The least massive of these states containing a charm quark are the mesons with $J^P = 0^-$. These are the (D^+, D^o)

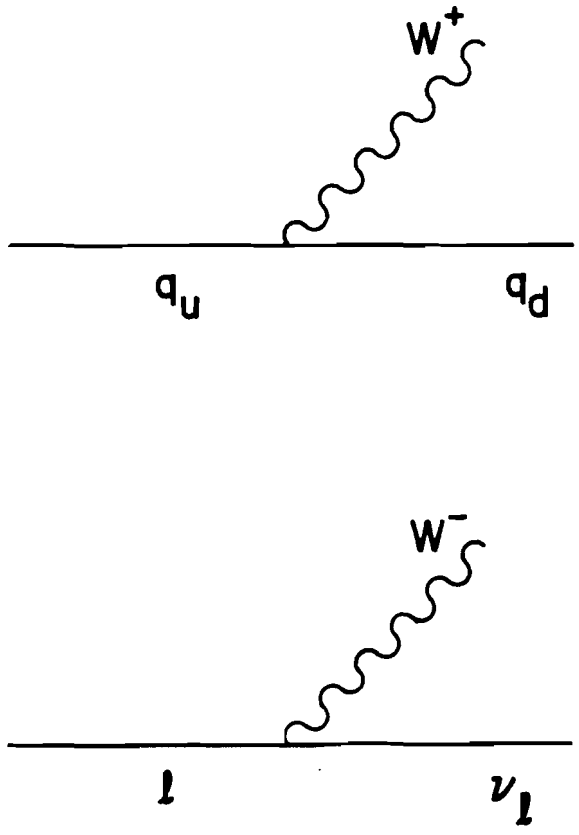

Figure 3. Emission of a W boson by a quark and by a lepton.

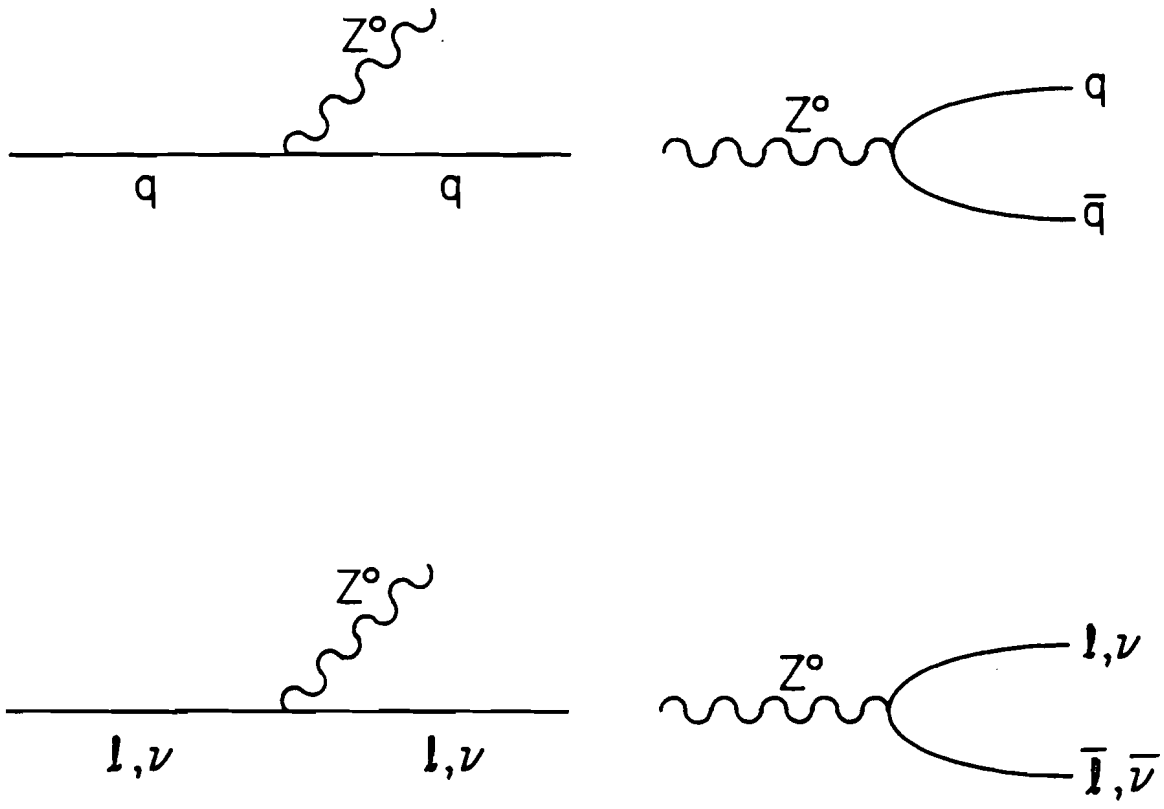

Figure 4. Neutral Current Processes.

isodoublet of quark content ($c\bar{d}$, $c\bar{u}$). Slightly more massive is the F^+ singlet ($c\bar{s}$). The most easily produced baryon state will be the Λ_c^+ (cud), which has $J^P = \frac{1}{2}^+$.

The antiparticles of the above states, that is those containing a charm antiquark will be produced by an antineutrino emitting a W^-, which then interacts with the nucleon. Since there are no valence antiquarks in the nucleon, anticharm production will occur only through a $\bar{d}$ or $\bar{s}$, which are part of the sea of quark-antiquark pairs.

There exist other more massive charmed states. In particular, the D and F mesons have related states having $J^P = 1^-$. These, the $D^{\pm *}$, $F^{\pm *}$, and D^{o*} and $\bar{D}^{o*}$, are spin excitations of the 0^- states.

There are also more massive weakly decaying baryons: A^+ (cus) and A^o (cds). Production of baryon states containing strange and charm quarks will presumably be less probable because the nucleon does not contain a strange valence quark and the m_s-m_d mass difference inhibits the production of $s\bar{s}$ pairs, relative to $d\bar{d}$ and $u\bar{u}$ pairs, during fragmentation. Many high mass charmed baryon states are predicted and are expected to decay to the Λ_c^+ through the strong interaction. The least massive of these are the triplets Σ_c ($J^P = \frac{1}{2}^+$) and Σ_c^* ($J^P = \frac{3}{2}^+$).

The Σ_c triplet consists of the Σ_c^{++} (cuu), the Σ_c^{+} (cud), and the Σ_c^{o} (cdd). The Σ_c^{++*} (cuu), the Σ_c^{+*} (cud), and the Σ_c^{o*} (cdd) make up the Σ_c^{*} triplet.

2.2 Decays of Charmed Particles (Low-lying States)

Charm is conserved by both the strong and the electromagnetic interactions. Thus the low-lying hadrons, the $D^{\pm}$, D^{o}, $\bar{D}^{o}$, $F^{\pm}$, and Λ_c^{+}, must decay through the weak interaction, in a manner similar to that in which they were created. The charm quark may emit a W^{+} boson and change to a d or s quark with amplitudes proportional to sin θ_c and cos θ_c respectively. The W^{+} will then "decay" to any one of the doublets to which it couples and for which enough energy is present, that is, a lepton and its antineutrino or a quark and an antiquark (for example $u\bar{d}$) as shown in Figure 5. Relative to the lepton-neutrino couplings, the quark-antiquark couplings are modified by the strengths cos θ_c and sin θ_c.

This model, in which the charm quark decays independently of the other quarks of the parent particle, is called the spectator quark model. Using this model, one would expect the lifetimes of all the charmed particles to be approximately the same. This lifetime can be calculated using the same formula as that for

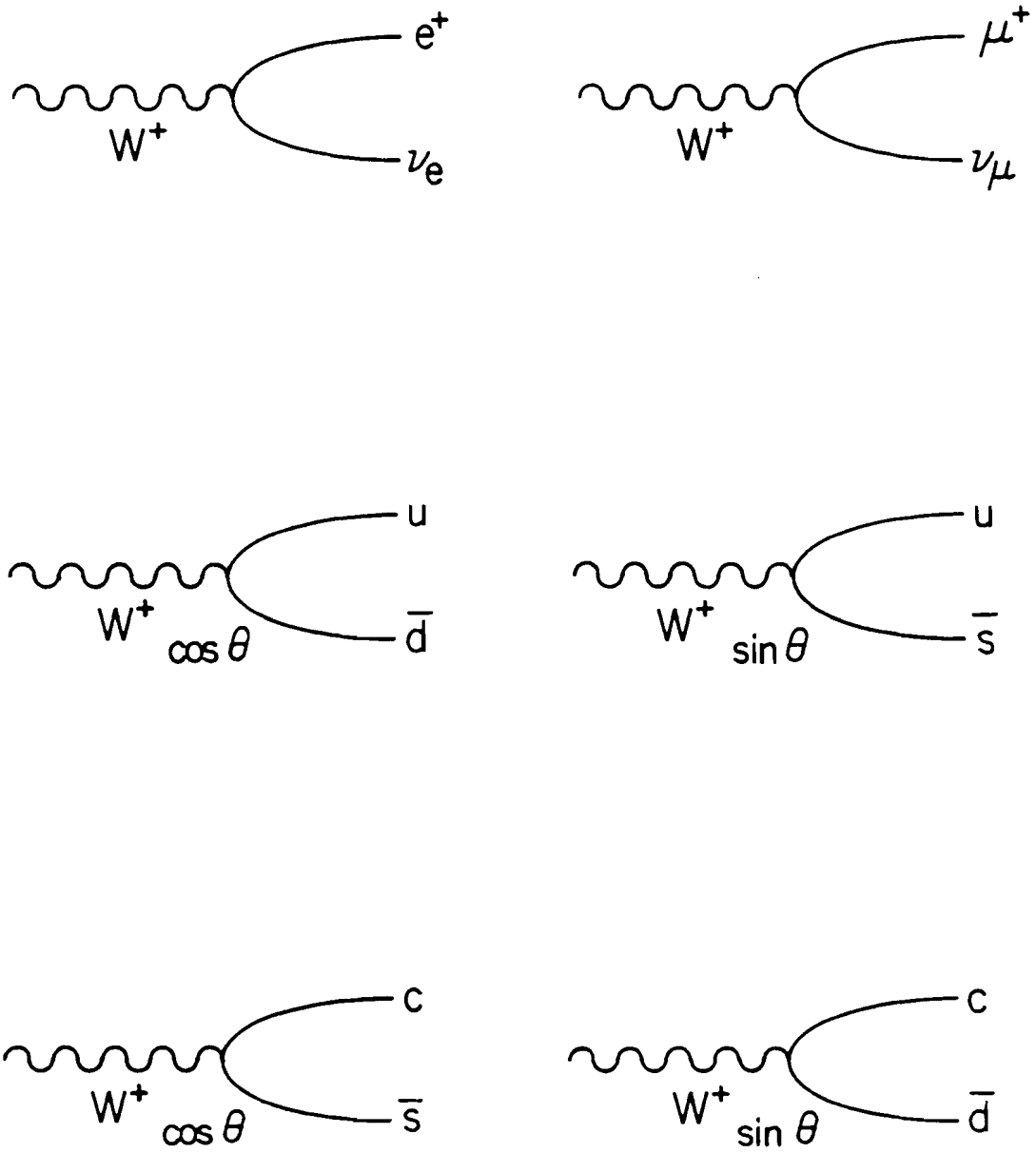

Figure 5. Decay of the W^+ to leptons and to quarks, with the relative coupling strengths.

muon decay, since the processes are quite similar, as shown in Figure 6. The rate for a charm quark decaying to a lepton and its neutrino is:

$$\Gamma_{total}(c \rightarrow X\ell\nu_\ell) \cong 192\pi^3 G_F^2 m_c^5, \tag{14}$$

where m_c is the mass of the charm quark and G_F is the coupling constant. A naive calculation for the total charm decay rate would be one which included all the decay diagrams shown in Figure 7, and the fact that the quark-antiquark pairs come in three colours. However, there are strong corrections to the non-leptonic decay modes, involving the radiation of gluons by the quarks, which increase the hadronic decay rates by approximately a factor of two [Leveille, 1981]. An inferred mass of 1.5 GeV/c^2 for the c quark, based on the K_L-K_S mass difference [Gaillard, 1975], gives for the lifetime of a weakly decaying charmed particle

$$\tau = \frac{1}{\Gamma_{total}} = \frac{1}{1.9 \times 10^{12}} \cong 5 \times 10^{-13} \text{ seconds.} \tag{15}$$

Initially, spectator decay was thought to be the only important process in charm decay. However, current experimental data lends support to more complicated mechanisms shown by the Feynman diagrams in Figure 8. In the annihilation process the

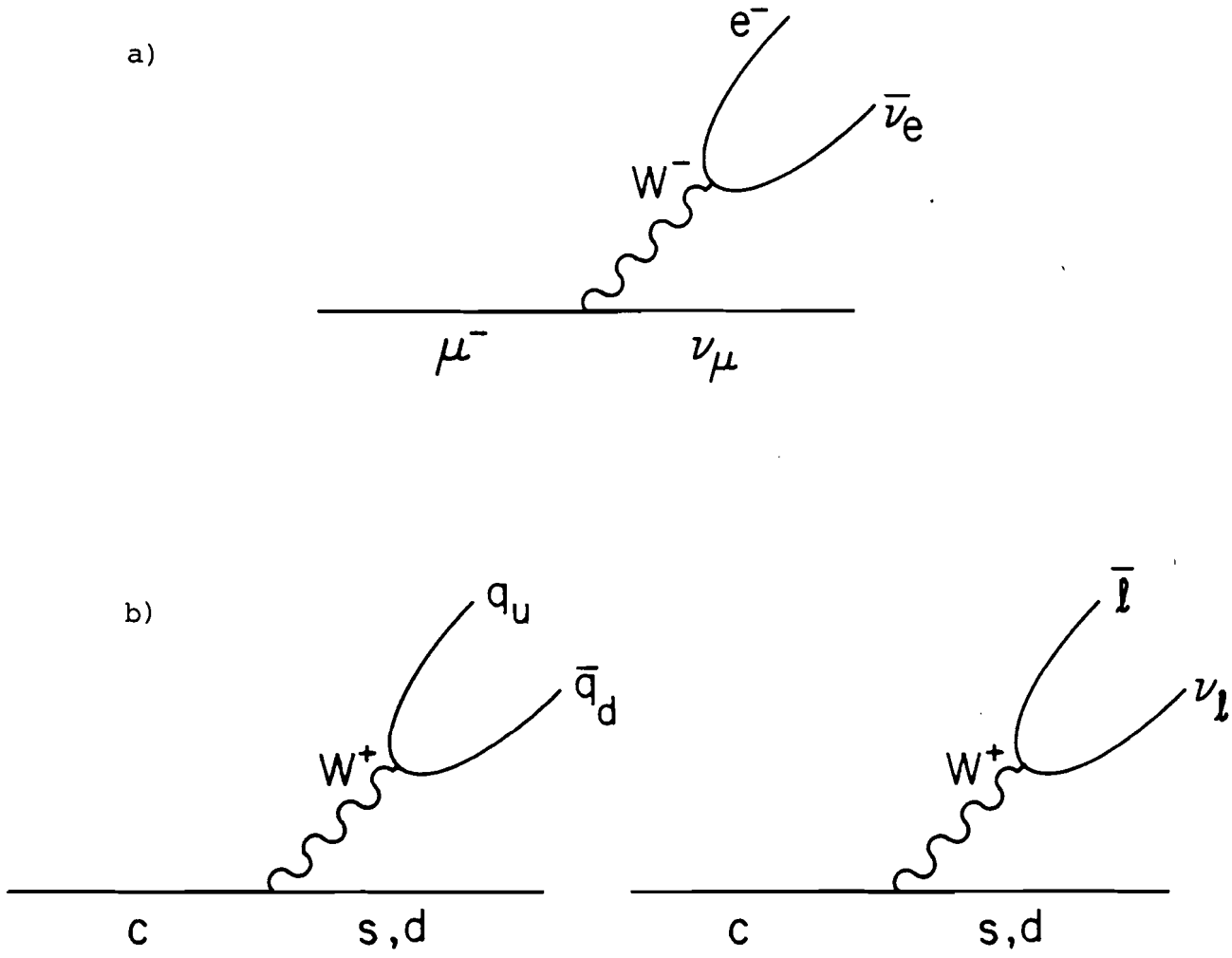

Figure 6. a) Muon decay. b) Decay of the charm quark.

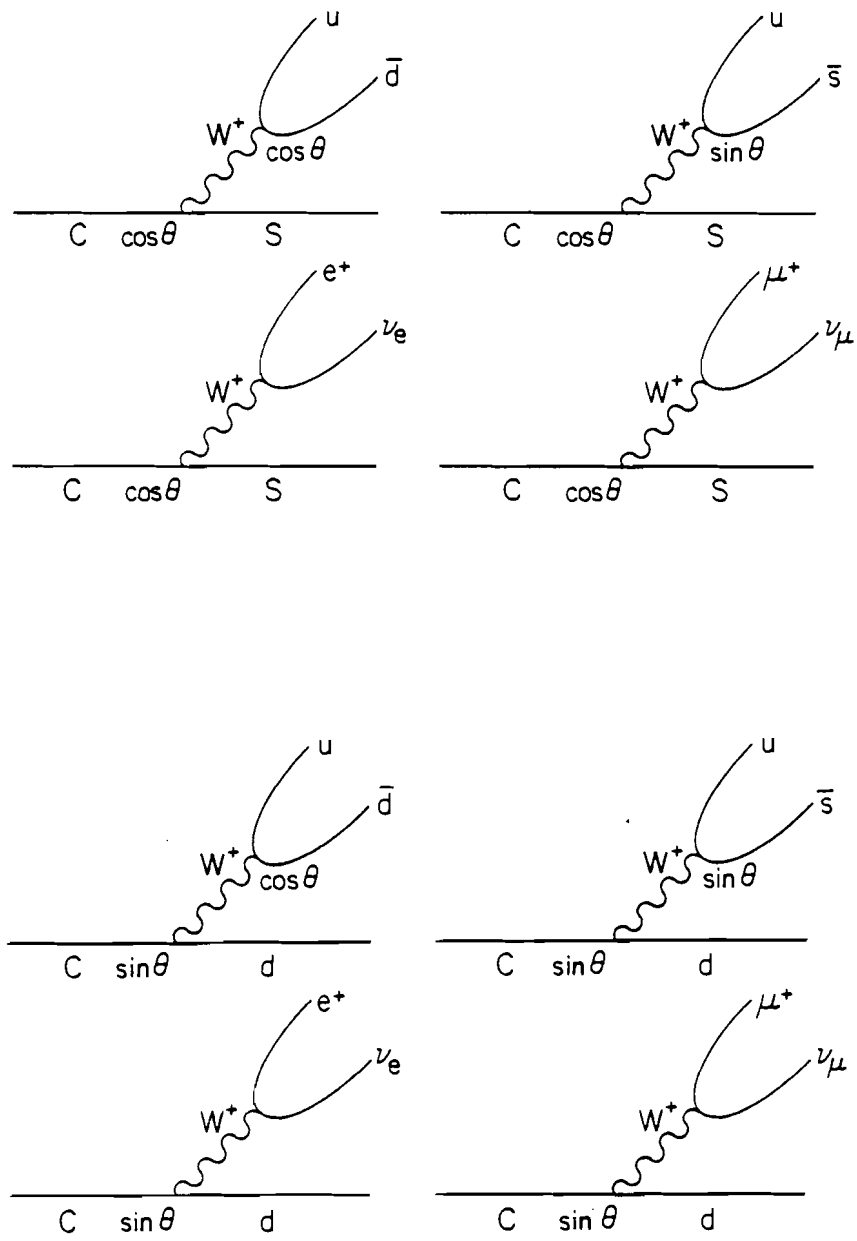

Figure 7. Spectator decays of the charm quark.

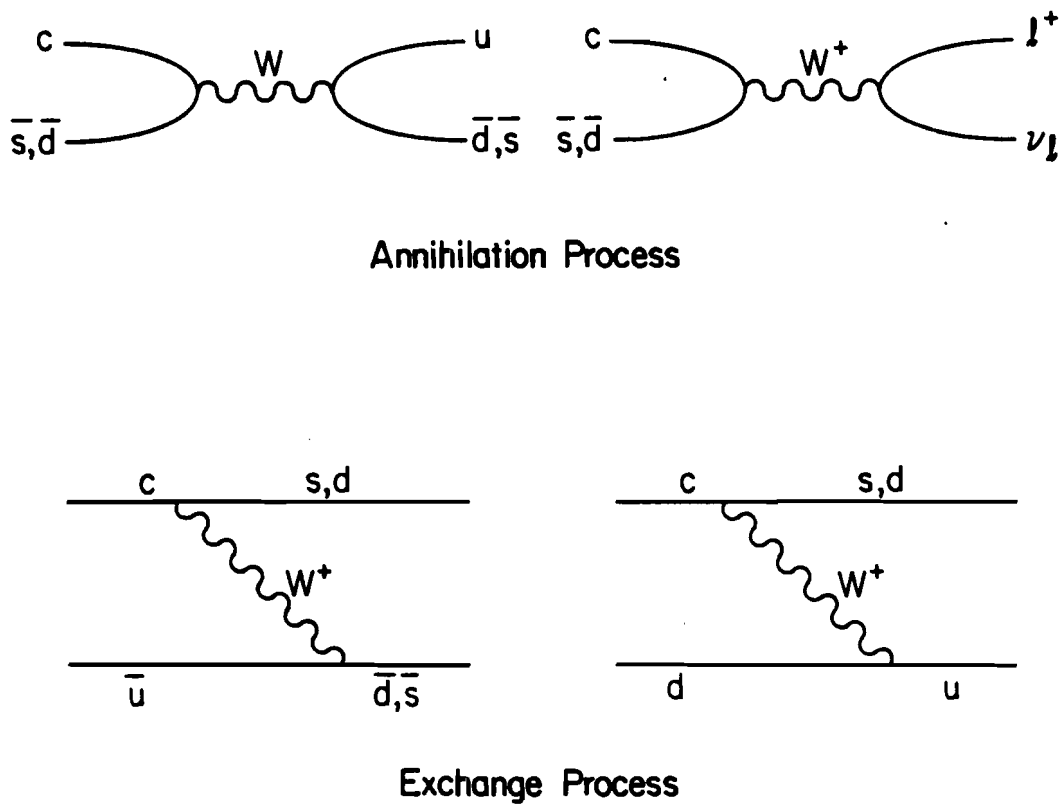

Figure 8. Alternative charm decay mechanisms.

charm quark along with an $\bar{s}$ or $\bar{d}$ antiquark annihilate to form a W^+, which then decays to leptons or noncharmed quarks. The exchange process is that in which a $W^{\pm}$ is exchanged between two quarks, both of which change their flavour in the process.

The annihilation process will enter into our discussion of the $D^{\pm}$ and $F^{\pm}$ lifetimes. However, for both the D^o and the Λ_c^+, there is no $\bar{d}$ or $\bar{s}$ with which the charm quark can annihilate. The exchange diagram can be applied to the decays of Λ_c^+ and D^o. In comparing the decay rates of different charmed particles, one must also consider the effects of quark mixing. Processes which occur with strength $\cos \theta_c$ will be enhanced or "Cabibbo-favoured" relative to those which occur with strength $\sin \theta_c$ which will be "Cabibbo-suppressed". Summing up the effects of these alternative diagrams, the D^o, $F^{\pm}$, and Λ_c^+ may all decay through Cabibbo-favoured exchange or annihilation diagrams. For the $D^{\pm}$ on the other hand, the annihilation process is a Cabibbo-suppressed decay, so the $D^{\pm}$ should decay primarily through the spectator quark model.

The alternative processes of annihilation and exchange are not quite as simple as stated above. Strong corrections are necessary. In particular, one must include in the annihilation diagram the effect of gluons which may be radiated by the quark

in the same manner as an electron radiates a photon. Inclusion of these removes the inhibition that would otherwise be caused by a combination of angular momentum conservation and the left-handed weak charged current.

2.3 Decays of Charmed Particles (High Mass States)

The higher mass states, the D^{+*}, the F^{+*}, and the Σ_c and Σ_c^* will first undergo strong or electromagnetic decay. (Strong processes occur approximately 10^{12} times and electromagnetic processes approximately 10^{10} times more quickly than weak processes at these energies.) These occur through the emission of a pion or photon, leading to the ground states, D^+, F^+, and Λ_c^+, which then decay weakly in the manner discussed above.

In terms of observing charm decays with techniques such as nuclear emulsion, this means that the decay of the higher mass charmed particle occurs at (or extremely close to) the primary (production) vertex, and the observed decay length is that of the weakly decaying ground state.

3. EQUIPMENT

The predicted charmed particle lifetimes of approximately 10^{-13} seconds correspond to decay lengths from a few to several thousand microns. At the time this experiment was being designed (1976), the only detector capable of achieving this resolution was nuclear emulsion.[1] Any charged particle passing through nuclear emulsion will leave a visible track. Neutral particles do not leave any visible tracks. Although this implies that the emulsion is 100% efficient in detecting charged particles, it also allows the emulsion to become quickly blackened with tracks of irrelevant particles. To avoid this problem the emulsion was placed in a neutrino beam. Only the charged particles related to events in which a neutrino has reacted in the emulsion, the beam associated background, and cosmic ray particles will produce visible tracks. In addition, previous experimental evidence [Benvenuti, 1975] suggested that approximately 10% of all neutrino interactions would produce charmed particles.

All of the charged decay particles can be observed in the emulsion, and the decay lengths of both the charged and neutral

---

[1]Recent developments in bubble and streamer chambers and in solid-state detectors have produced detectors of comparable resolution [Bellini, 1982].

parent particles can be measured. However, scanning the entire emulsion volume for interactions becomes prohibitively expensive and time consuming. In addition, the emulsion provides particle identification only for slow particles with β appreciably less than 1. Therefore a downstream electronic detector (spectrometer) was used in conjunction with the emulsion. The detector is shown schematically in Figure 9. Tracks of charged particles were reconstructed which enabled prediction of the neutrino interaction vertex. The detector was required to cover a large solid angle (high acceptance) and successfully track almost all particles entering it (high efficiency). Two sets of drift chambers on either side of a wide-aperture magnet measured the three-momenta of charged particles.

A plastic sheet covered on both sides by thin layers of emulsion was placed on the downstream face of the emulsion target. This fiducial sheet, which was changed every two to three days during the experiment, served as a high-resolution, low-background detector, to link the spectrometer tracks to the main emulsion tracks. Tracks reconstructed from the spectrometer could be easily found in the fiducial sheet and then followed back into the emulsion target. This increased the efficiency of vertex finding by approximately 50% as compared to that for simple volume scanning, and was also of great value in the charm decay search.

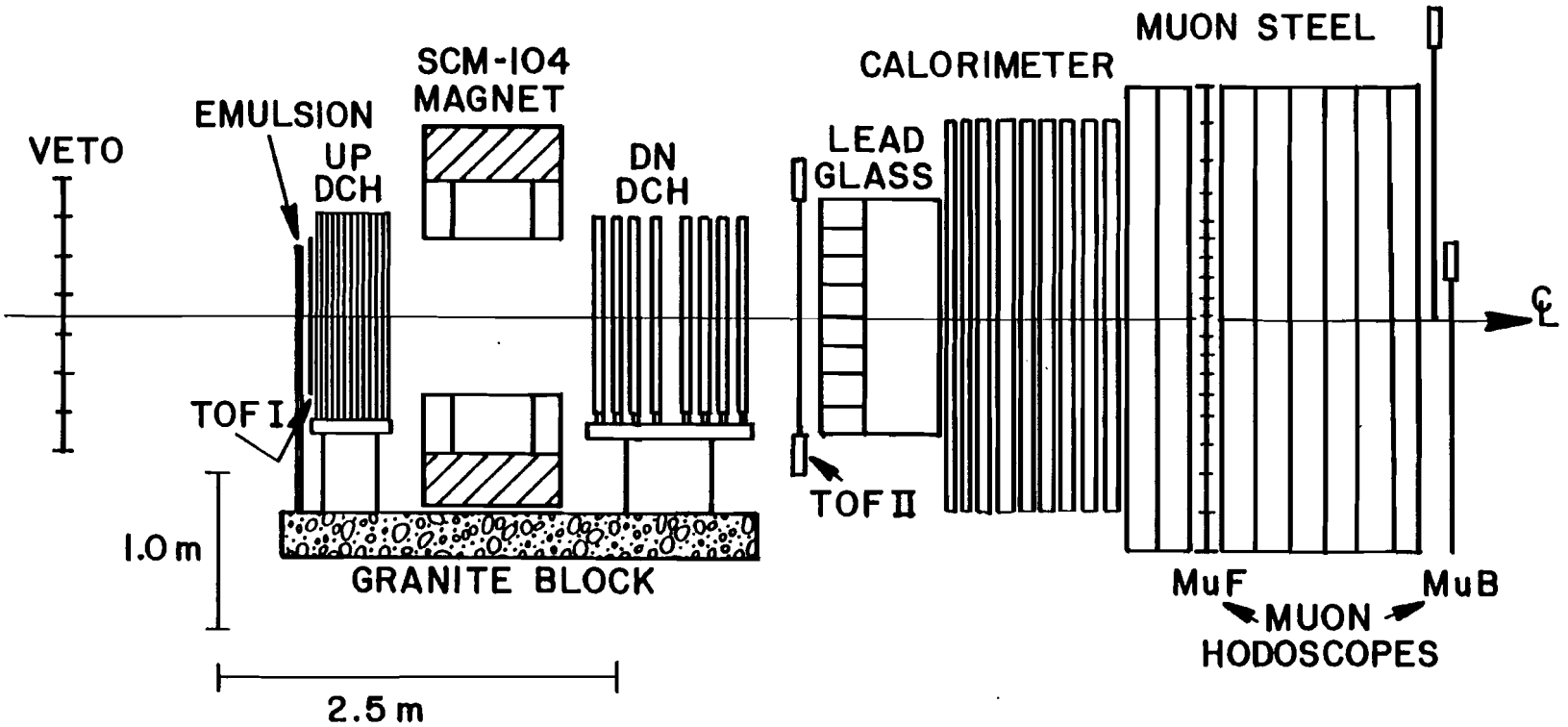

Figure 9. Side view of the E531 apparatus.

To completely reconstruct a decay vertex and identify the decaying charmed particle it is necessary to identify all of the decay particles and measure their momenta. Charged particles were tracked by the drift chambers in conjunction with the magnetic field of the wide-aperture magnet. The identification of some of the charged hadrons was accomplished through the time-of-flight system. Electrons were identified by the lead glass system and muons by their penetration of a steel absorber. The existence of neutral secondaries was inferred using the lead glass array and the hadron calorimeter.

Knowledge of the position of the downstream spectrometer relative to the emulsion was crucial in order to locate the events in the emulsion. An extensive optical survey of the apparatus was done before and after the taking of data. In addition, position and temperature sensors were attached to the apparatus at numerous points to calibrate the effects of thermal expansion.

3.1 Neutrino Beam Line

The protons were extracted in a fast spill mode at the end of each 7 second machine cycle and transported to the neutrino production target by a conventional magnetic beam line.

Approximately 1.5 x 10^{13} protons per spill were incident upon the neutrino production target, a 30 cm long (one interaction length) piece of beryllium oxide, located 954 m upstream of Experiment 531 (Figure 10). Charged pions and kaons are among the particles produced when the protons hit the BeO target. These pions and kaons decay primarily through the processes

$$K^+ \rightarrow \mu^+\nu_\mu \quad \text{and} \quad \pi^+ \rightarrow \mu^+\nu_\mu \quad ,$$

in the 410 m long decay space following the target. A single pulsed magnetic horn located 30 m into the decay space was used to focus positively charged particles which had production angles greater than 1.8 mrad and thus increase the neutrino flux. (During 2.5% of the data-taking period, the polarity of the horn was reversed to obtain an antineutrino beam.)

For this experiment (in order to avoid blackening of the emulsion) it was necessary to minimize the flux of background muons. The closeness of the experiment to the neutrino production target and the lack of sufficient steel shielding meant that intolerably high muon fluxes, 6000 μ/m^2/pulse, were recorded when the protons were accelerated to 400 GeV (the usual operating energy of the accelerator). By decreasing the proton energy to 350 GeV, the muon flux was reduced to approximately 500 μ/m^2/pulse, while the neutrino event rate decreased by only about 26%.

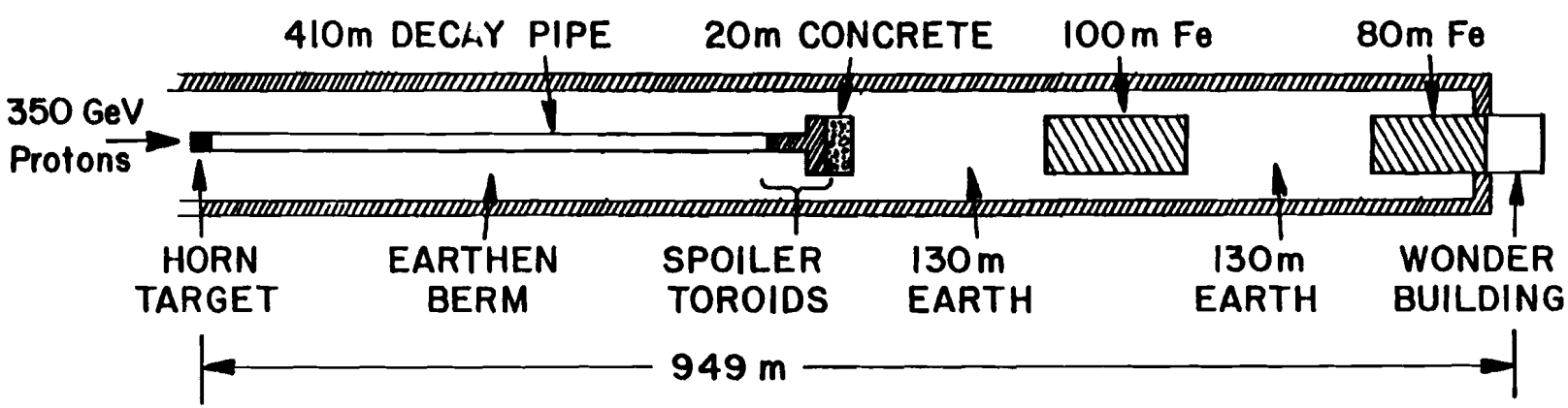

Figure 10. The Fermilab neutrino beam line.

After one month of taking data, 18.3 m of additional concrete shielding was installed, further reducing the muon flux by a factor of two. A system of toroidal sweeping magnets (the muon spoiler system), which had been installed upstream of experiment 531, was not used until very late into the running period because it greatly increased the muon flux at the 15-foot bubble chamber, situated 512 m downstream of experiment 531, which was taking data simultaneously.

The energy spectrum of reconstructed ν interactions is shown in Figure 11. The peak energy is at 25 GeV. This spectrum was obtained by unfolding the effects of the acceptance and resolution of experiment 531 from the observed energy spectrum of 2022 neutrino-induced interactions. The energy of the incident neutrino is calculated by summing the energy of the muon, the energy of the charged particles, and the energy of the lead glass system and the calorimeter, which cannot be attributed to charged particles.

3.2 Emulsion

The emulsion target was composed of 23.6 liters of Fuji ET-7B nuclear emulsion, which had been melted, poured and cut into very thin sheets or pellicles. The emulsion sheets were packaged

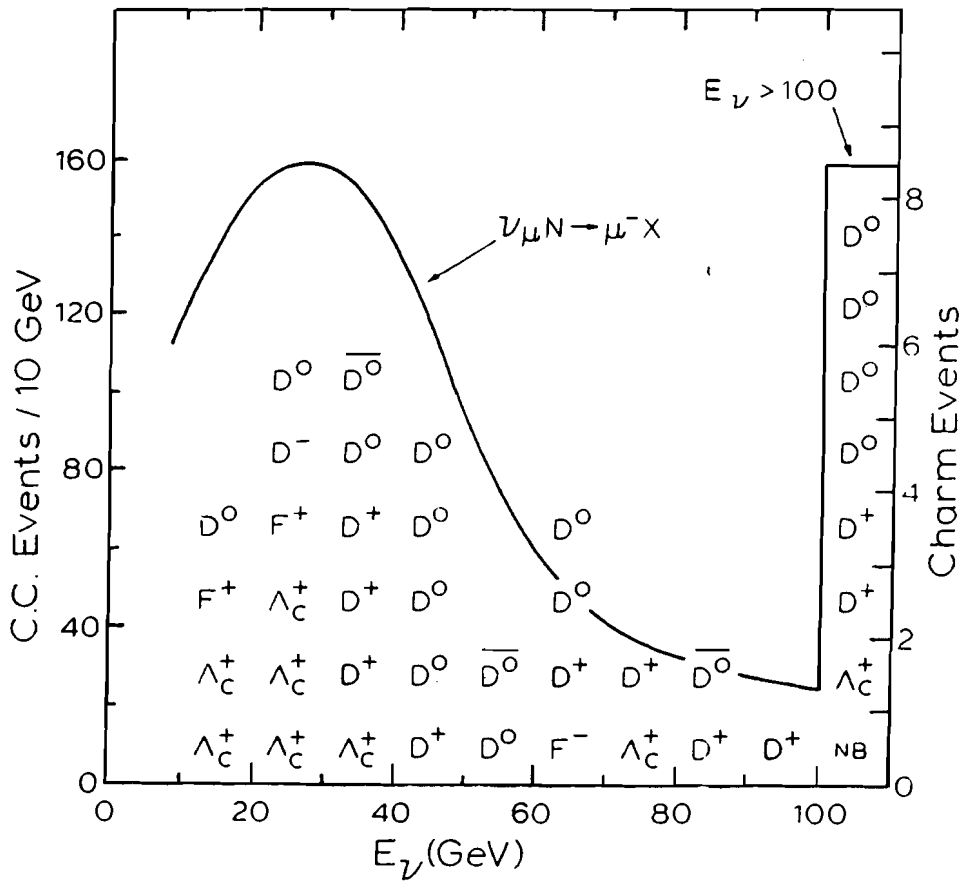

Figure 11. The neutrino energy spectrum, shown by the solid curve, for reconstructed charged current events. Also shown is the distribution of the neutrino energy for the charm decay candidates.

TABLE 1. Chemical composition of Fuji ET-7B emulsion.

Element	Percentage by Weight
Iodine	1.31
Silver	46.5
Bromine	33.7
Sulfur	0.4
Oxygen	4.3
Nitrogen	2.7
Carbon	7.4
Hydrogen	0.92

into modules which were placed on an aluminium and hexcell support frame (Figure 12). The sheets of emulsion were placed in the beam line with two different orientations: vertical and horizontal. Each vertical emulsion module contained 68 sheets. Each sheet was composed of a 12 cm x 9.5 cm x 70 μ polystyrene base coated on both sides with 330 μ of emulsion. The plane of the emulsion sheets was perpendicular to the beam direction. The horizontal emulsion modules were placed so that the beam line was incident parallel to the emulsion sheets. These pellicles were 5 cm x 14 cm x 600 μ sheets of solid emulsion. There were 188 sheets in each of the horizontal modules. (Figure 13). A total of 29 vertical modules and 13 horizontal modules were exposed during the data-taking period, although only 27 vertical and 12 horizontal modules were in place at any one time. (Three modules were removed midway through the data-taking period for

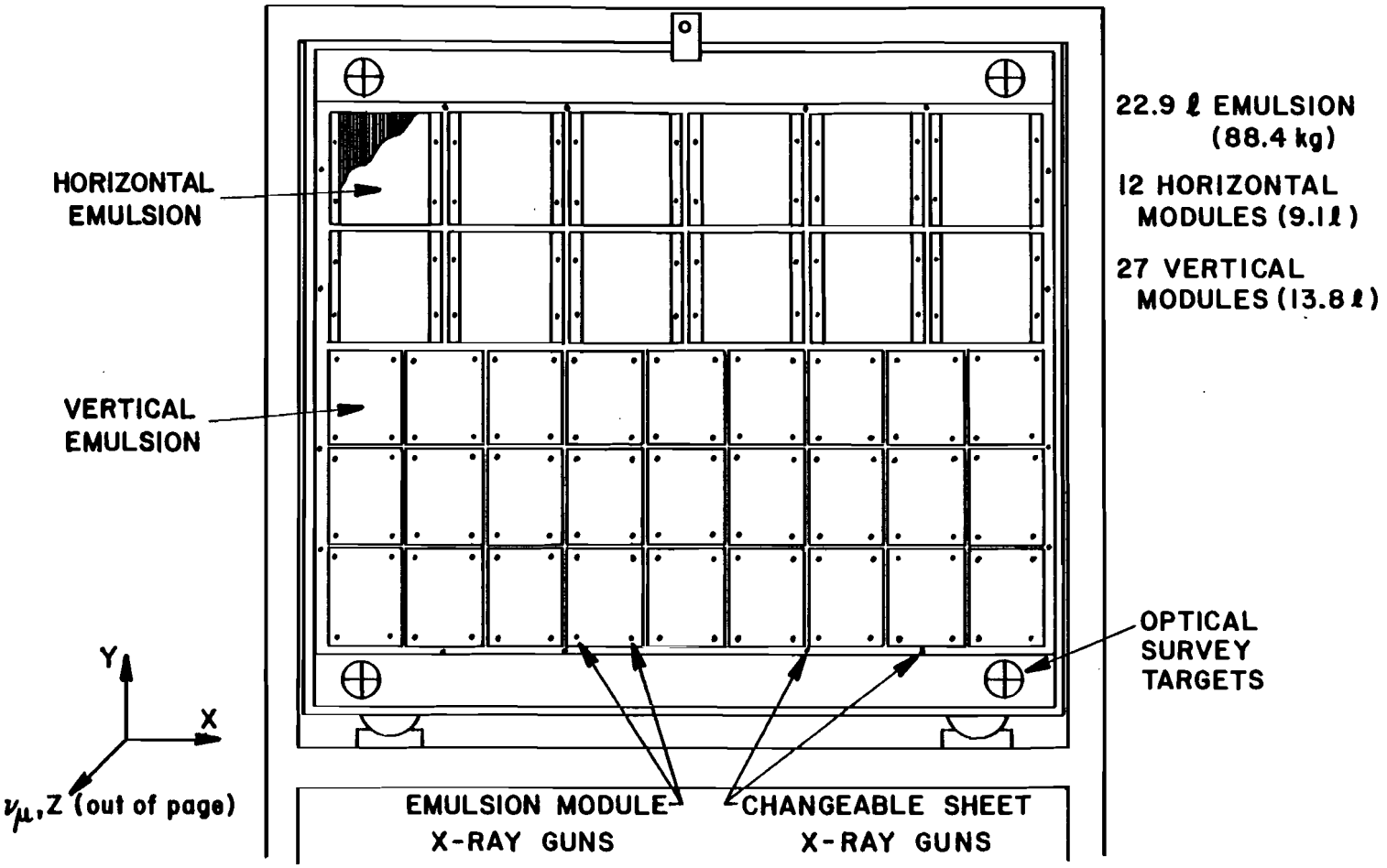

Figure 12. Placement of the emulsion in the beam line.

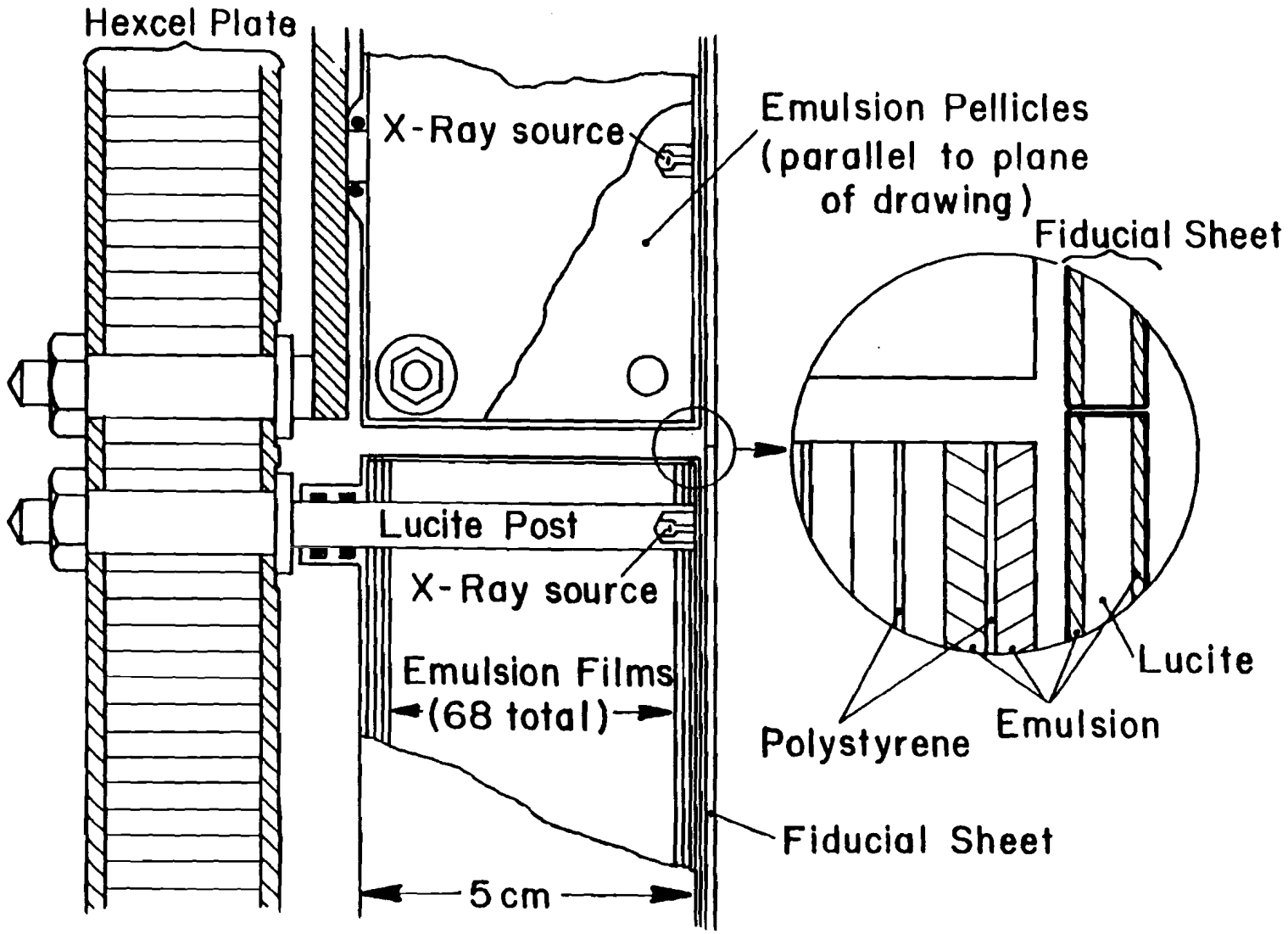

Figure 13. The emulsion. Top: horizontal emulsion module. Bottom: vertical emulsion module.

examination and replaced with new modules.) The emulsion modules were wrapped in polylaminated paper and mounted on four posts, the external portions of which were used to mount the modules onto the precision aluminium frame.

The fiducial sheet was immediately downstream of the target. This sheet consisted of a 91.5 cm x 80 cm x 800 μ lucite base coated on both sides with 75 μ of emulsion. The fiducial sheet was used to couple tracks reconstructed by the spectrometer with those in the emulsion target. It was changed every two to three days during the taking of data. The position of the target emulsion relative to that of the fiducial sheet was determined through the use of small, collimated ^{55}Fe X-ray sources embedded in the posts of the emulsion modules. The tracks reconstructed by the spectrometer were first located in the fiducial sheet then followed back into the vertical emulsion sheets with an efficiency of 0.96 $\pm$ 0.02. This method of following tracks back into the emulsion is technically more difficult with the horizontal modules, owing to the distortion near the edges of the pellicles that occurs during drying, and was therefore used only sparingly.

A set of small individually wrapped pellicles, identical in construction to the fiducial sheets, was placed on the upstream face of the emulsion target frame. These were removed one at a

time, at regular intervals during the data-taking period, and processed immediately. These integrating emulsion pellicles enabled a reliable check of the muon flux through the emulsion target.

The emulsion modules were supported by an accurately machined solid aluminium and aluminium hexcell frame. The frame provided adequate support strength and at the same time represented minimal additional matter in which neutrinos could interact. This frame was attached to aluminium supports which allowed the frame and the emulsion to be temporarily displaced during the installation and removal of the fiducial sheet. One corner of the frame was fixed while the others were free to move in case of expansions and contractions. Such motion was monitored by a system of linear variable differential transformer (LVDT) monitors which were mounted to the frame. The LVDT monitors had a spatial resolution of 15 μ.

The temperature of the emulsion was maintained at $10\pm2^{\circ}C$ by a closed circuit air conditioning system. The frame for the emulsion and the support frames of the upstream and downstream drift chambers were placed on a solid 3.5 ton granite optical bench in order to minimize the shifting of the emulsion with respect to the drift chambers, which could have prevented a successful search for the neutrino-induced events in the emulsion.

3.3 Anti-coincidence Counter

An array of scintillators, the anti-coincidence counter, was placed 1.3 m upstream of the emulsion target. This counter was used to prevent data collection resulting from incident charged particles, for instance muons, in the beam line. The array consisted of 7 scintillation counters, each 25.4 cm x 178 cm, placed horizontally such that the area in the beam was 3.1 m^2. An Amperex 56AVP phototube was placed on each end of the seven scintillators. The efficiency of the anti-counter was 0.89±0.01.

The timing of the anti-counter relative to TOF I was extremely critical on account of the proximity of the two. Charged particles emitted in the backward direction from a neutrino interaction vertex could trigger the anti-coincidence counter thereby vetoing the event (backscatter). Using time spectra accumulated for neutrino interactions, it was determined that 15 % of the neutrino triggers would have been vetoed, had the timing of the anti-counter been poorly adjusted. A LeCroy 824 octal mean timer was used to remove time jitter resulting from the variable position of the hits in the anti-counter.

3.4 Time of Flight

The Time of Flight (TOF) system had two purposes: It was used to trigger data collection and in the identification of particles by measuring the flight times of charged particles.

TOF I was a single piece of Pilot F scintillator 92 cm x 74 cm x 0.95 cm, located 7.6 cm from the downstream face of the emulsion target. The light was transmitted through curved light guides to 12 RCA 8575 phototubes (Figure 14).

TOF II consisted of 16 narrow counters (7.0 cm x 150.0 cm x 2.5 cm) and 14 wide counters (10.2 cm x 150.0 cm x 2.5 cm) arranged in a vertical hodoscope with the wider counters further from the centre of the beam (Figure 15). The array was 2.84 m downstream of the emulsion target. The narrow counters were overlapped by 0.6 cm and the wide counters by 0.2 cm. All counters were constructed with Pilot F scintillator, which has an attenuation length of 1 m, and were viewed at both ends by Amperex XP-2230 phototubes.

The signals from the time-of-flight counters were split so that $\frac{4}{5}$ was discriminated and input to LeCroy 2228A TDC units set at 50 ps/count. The remaining $\frac{1}{5}$ of the signal was input to LeCroy 2249A ADC units which were set at 0.25 pC/count. High

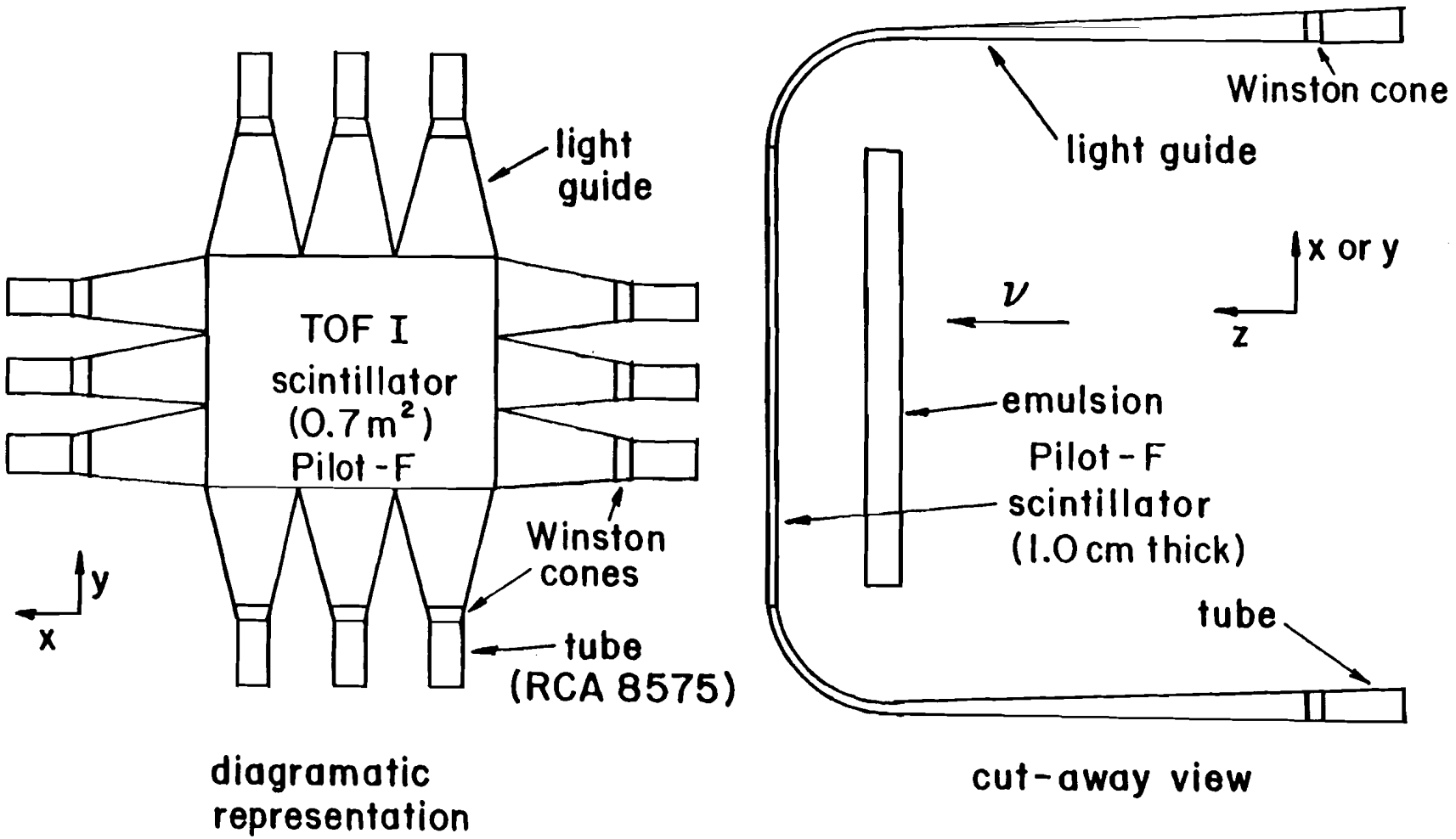

Figure 14. Time of Flight I Counter.

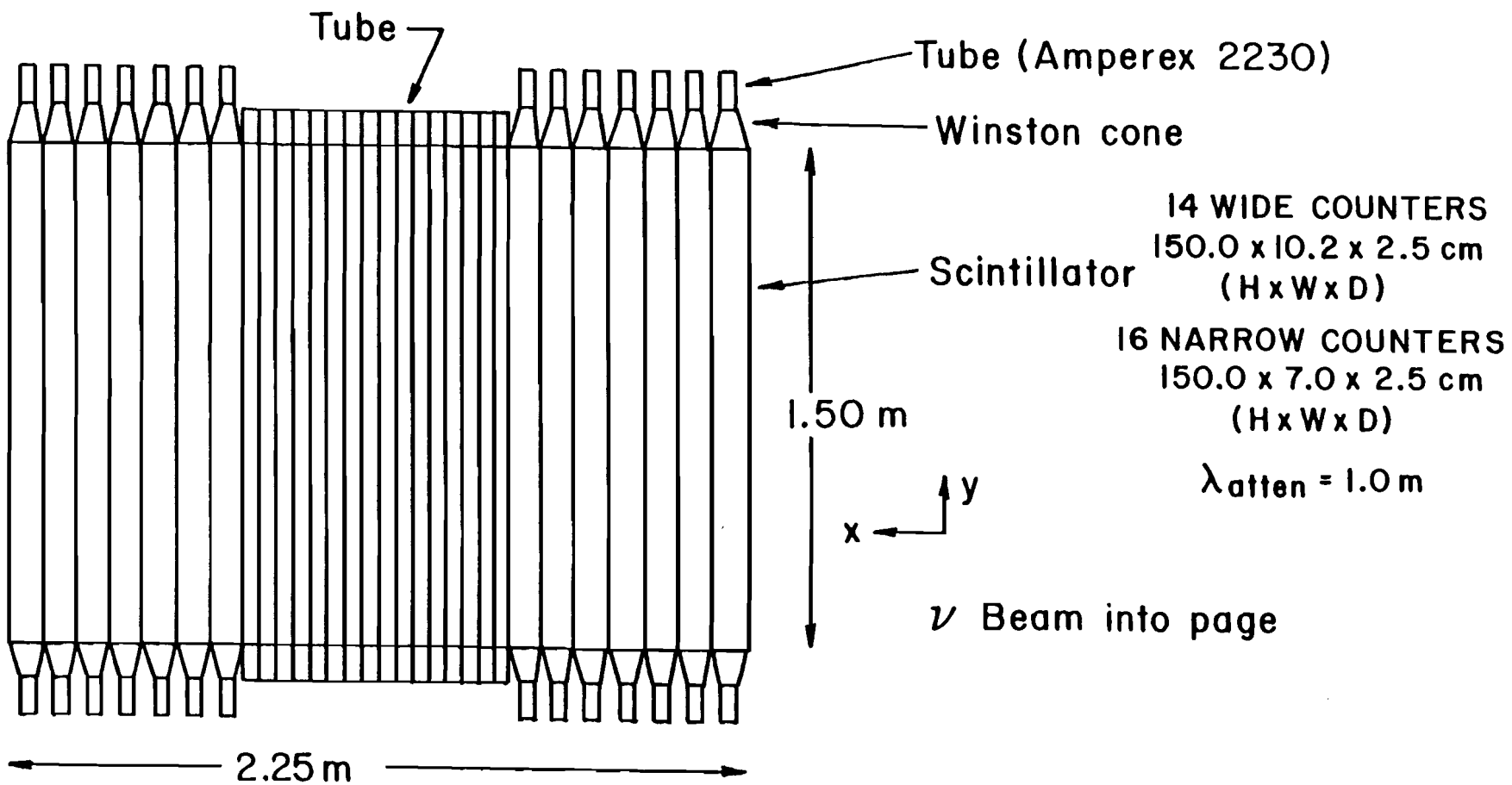

Figure 15. Time of Flight II Counter.

voltage to the tubes was supplied by LeCroy R24 H4032 units which constrained the drift in the voltage on each tube to less than 1 V. During the data collection portion of this experiment the voltages of all counters were maintained constant to this precision.

The stability of the time-of-flight counters was monitored through the use of a nitrogen laser system. The ultraviolet laser light was focused on a block of scintillator, which reemitted visible light that was transmitted through a system of fibre optics to the centre of each TOF II paddle and to the TOF I light guides.

The time-of-flight system was calibrated using data for 2 x 10^5 muon tracks which were accumulated during the data-taking period. The muon trigger system required that the pulse height from TOF I be equivalent to at least one minimum ionizing particle and that there be at most one particle detected by TOF II. For calibration purposes, the muon trigger data was reduced to satisfy the requirements that there be only a single reconstructed track and that the TOF I pulse height be restricted to one minimum ionizing particle.

The time resolution obtained for TOF I was 350 ps for neutrino-induced events using a fitted start time. The time

resolution of TOF II was 100 ps for the narrow counters and 150 ps for the wide counters. Several factors contributed to the poor resolution of the TOF I counter: inefficient light collection by the phototubes and the size (5 cm in diameter) of track clusters associated with neutrino interactions, which corresponds to a time jitter of 300 ps.

3.5 Drift Chambers

The purpose of the drift chambers was to track charged particles emanating from the neutrino interaction vertex and to measure the deflection of these particles by the magnetic field. Two sets of drift chambers were used, one group upstream of the large aperture magnet, the other group immediately downstream of the magnet.

3.5.1 Upstream Chambers

The twelve identical upstream chambers were grouped in four sets of three. Each set measured an x, u, and v coordinate for an individual track, where the u chambers were rotated clockwise 60° (looking downstream) with respect to the x chambers and the v chambers 60° counterclockwise (Figure 16). In order to resolve the left-right ambiguity inherent in drift chambers, the

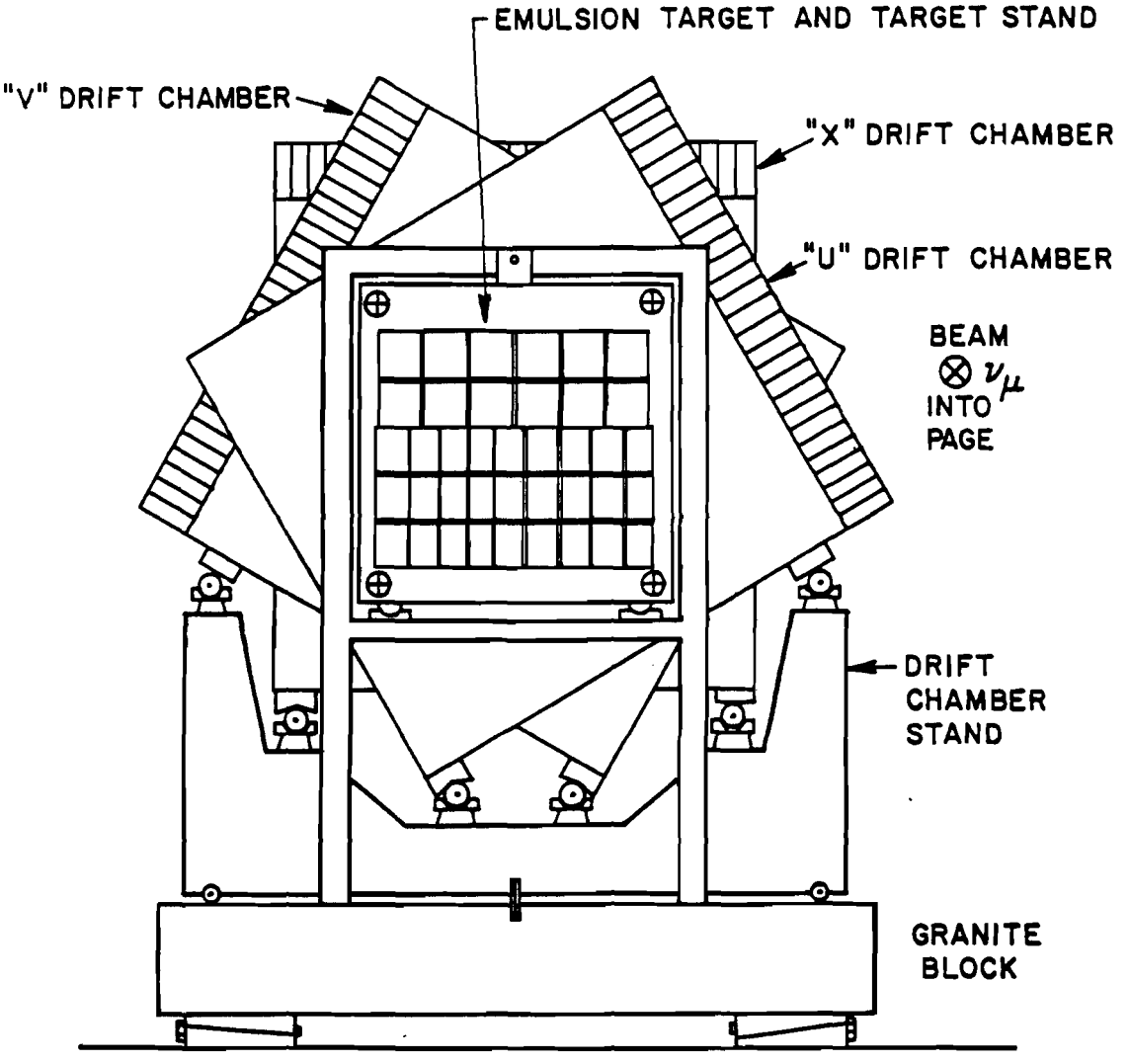

Figure 16. Placement of the upstream drift chambers in the beam line.

alternate sets of chambers had the position of their sense wires shifted by one half of a cell size. The judicious choice of arrangement and orientation maximized the information obtained for individual tracks. The first chamber was positioned 15 cm from the downstream face of the emulsion target. The distance between chambers was 4.66±0.02 cm.

Each chamber contained 32 gold-plated, 20 μ diameter, tungsten sense wires at a tension of 50 g. The sense wires were maintained at zero voltage. The cell size of the chambers was 4 cm. The cells were divided with field-shaping wires (Figure 17). These wires and the cathode plane wires were 75 μ diameter copper-plated beryllium strung with 200 g tension. The separation between the cathode planes was 6.35 mm and the spacing between neighbouring cathode wires was 2 mm. The active area of each chamber was 128 cm x 132 cm.

The frames were constructed of G-10 (fibreglass). Aluminized mylar windows (25 μ aluminium on 50 μ mylar) on the exterior of the chambers served both to shield the chamber from RF noise and to contain the gas. The gas used was a 50% argon - 50% ethane mixture.

An electric field of 700 V/cm was provided with the normal operating voltages of -3100 V (V_{max}) on the drift wires and the

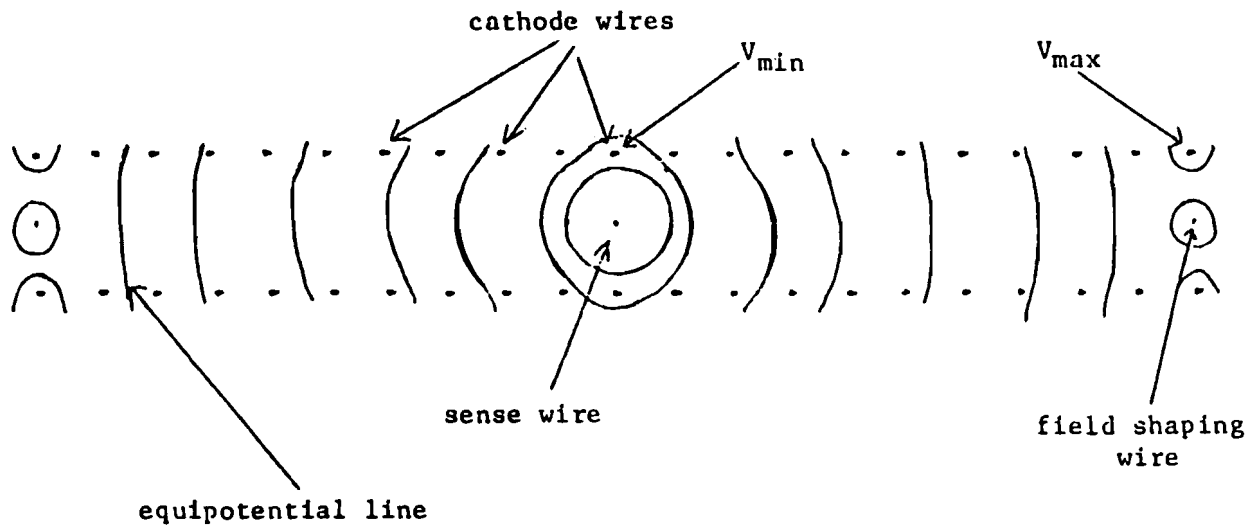

Figure 17. One drift cell in cross-section. The equipotentials are marked with solid lines. Cell size is 5.08 cm and cathode to cathode spacing is 6mm.

cathode wires furthest from the sense wires, and -1700 V (V_{min}) on the cathode wires adjacent to the sense wires. A voltage divider board (simply a chain of resistors) provided intermediate voltages to the remaining cathode wires.

3.5.2 Downstream Chambers

Eight large drift chambers were positioned in sets of four downstream of the magnet. These were arranged as: x, v, u, x' and x, v', u', x', where the prime (') denotes that the sense wires have been shifted by one half of a cell size. As opposed to the upstream chambers which received their orientation simply by rotating the entire chamber, the downstream chambers were constructed with inherent orientations. The u chambers had wires rotated 10.6° clockwise from the vertical and the wires of the v chambers were rotated 10.6° counterclockwise. The separation of neighbouring chambers was 5 cm except for the two innermost chambers which were separated by 16 cm.

The x chambers each contained 40 sense wires of 25 μ diameter, gold-plated tungsten wire spaced 5.08 cm apart. Between the sense wires lay field shaping wires of 75 μ diameter copper-plated beryllium. The sense wires were strung at a tension of 60 g and the field shaping wires at a tension of 120 g. The cathode planes were constructed of mylar foil 62.5 μ

in thickness upon which flattened 125 μ diameter copper wire had been laminated. The resulting copper strips were 400 μ wide and 25 μ thick. The frames were constructed of G-10 . The chambers were covered with aluminized mylar gas windows. A brass u-channel around the perimeter of the chamber completed the RF-shielding.

The u and v chambers were the same as the x chambers in all respects except that these chambers contained 43 and 44 sense wires respectively. The perpendicular distance between neighbouring sense wires was again 5.08 cm. The position of the sense wires in all of the downstream chambers was within 25 μ during the construction of the chambers. The active area (X x Y) for all of the downstream chambers was 203.2 cm x 118.1 cm.

The sense wires were maintained at 0 V, separated from ground by 10 KΩ resistors. The nominal operating voltages for the downstream chambers were V_{max} = -3700 V and V_{min} = -1800 V, which provided a drift voltage of 750 V/cm. A cross-section of a drift chamber cell is shown in Figure 17.

During the course of the experiment however, internal electrical problems developed on some of the chambers necessitating lower operating voltages. The same argon-ethane mixture as that for the upstream chambers was used.

Extensive tests of prototypes for the downstream chambers were carried out in the Fermilab test beam [Pitman, 1979]. Several topics were studied:

- The feasibility of the new technique of using copper-clad mylar foils as cathode planes;
- The relative merits of various gases;
- Suppression of cross-talk between neighbouring sense wires; and
- The dependence of pulse height on the direction of the track.

3.5.3 Drift Chamber Electronic Data Collection System

The amplifiers and the drift chamber data collection system were designed at the Ohio State University. Attached to each drift chamber sense wire was a fast amplifier and discriminator which amplified the signals by a factor of 100, while shaping the signal pulses to eliminate the ringing at the tail end of the pulses. This was necessary to optimize track resolution and to avoid cross-talk between wires. Pulses were then discriminated and converted to standard NIM levels (700 mV) with a variable threshold discriminator. During the experiment the threshold was set to 15 mV. Typical pulse heights for minimum-ionizing particles were 100 mV at the input of the discriminator and pulse widths varied from 20 to 40 ns. The NIM level pulses were input

to a drift chamber readout system where time digitization occurred. Pulses from each sense wire were input to separate time recorder channels, which had the capability of storing up to 16 drift chamber signals (hits) separated by at least 1.5 ns. The trigger for the readout system was supplied by the TOF system during the data-taking period and internally during testing of the system. When the trigger occurred, the trigger pulse was distributed to several time encoders into which pulses from up to 20 time recorders were fed. The sense wire discriminator output pulses determined time intervals in the time encoders that were stored in the local memories. The time recorders then resumed data collection. Thus information for multiple events could be recorded during each neutrino spill. At the end of the spill, the drift chamber data was read into the online computer through a CAMAC interface.

3.5.4 Calibration of Drift Chambers

During the experiment, data was also recorded for events known as muon triggers. These were taken while the magnet was both on and off and provided data for 2×10^5 muons, which was used as input, along with the survey data, for the drift chamber tuning program. The data were divided into short time periods, approximately 10 runs long, and analysed. Variations in such

parameters as wire positions and the drift velocity of electrons in the argon-ethane gas were studied. Inadvertent rotations or translations of a chamber with respect to the others could be diagnosed. (The amount of movement of the chambers was found to be less than 125 μ, which agreed with that monitored by the LVDT system.)

The spatial resolution of the drift chamber system based on data from the entire run was 125 μ. The resolution with which two adjacent tracks through the same drift chamber cell could be separated was 1.8$\pm$0.3 mm. This resolution was calculated based on time correlation studies of tracks from neutrino events.

3.6 Magnet and Momentum Measurements

Placed between the two groups of drift chambers was a wide-aperture SCM-104 magnet, which in conjunction with the drift chambers was used to determine the momenta of charged particles. The dimensions of the interior aperture were 2.1 m x 1.02 m x 0.8 m. Since the magnetic field was highly non-uniform, the measurement of an extensive field map representing 43,000 data points taken between the two pole faces was imperative. The central magnetic field was 5 KG. Throughout the experiment the current supplied to the magnet was 2400$\pm$12 A.

The bending of charged tracks in the magnetic field, made possible the calculation of the momenta of the charged particles. The bend angle,

$$\theta = \frac{0.03\int B\cdot dl}{p} \tag{16}$$

where p is the component of the momentum perpendicular to B, the magnetic field. At a current of 2400 A, $\langle\int B\cdot dl\rangle = 6.2$ KG·m. The momentum resolution for charged particles passing through the magnet can be calculated using the equation, derived from (16),

$$\frac{\Delta p}{p} = \frac{p\Delta\theta}{0.186}, \tag{17}$$

where θ is measured in radians and p is measured in GeV/c. The spatial resolution of 125 μ in the drift chambers yields an angular resolution of 0.6 mrad, giving $\Delta p/p = 0.005p$. However, to properly calculate the momentum resolution one must include the effects of multiple scattering which occurs in all materials such as mylar, aluminium, and air, traversed by the particles in the spectrometer. In order to minimize this effect, a bag of helium was placed in the aperture of the magnet during the data-taking run. The resolution for the 20 chamber system becomes:

$$\frac{\Delta p}{p} = \sqrt{(0.009)^2 + (0.005p)^2} \tag{18}$$

The momentum resolution was considerably worse for tracks which were at such wide angles that they did not pass through the magnetic field and reach the downstream chambers. For those tracks whose angles were less than 300 mrad,

$$\frac{\Delta p}{p} = 0.35p \ . \tag{19}$$

For tracks with angles between 300 and 600 mrad,

$$\frac{\Delta p}{p} = 0.5 \ . \tag{20}$$

Finally, for tracks with angles greater than 600 mrad,

$$\frac{\Delta p}{p} = 0.75 \ . \tag{21}$$

The momentum for these upstream only tracks was calculated from their bending in the fringe field of the magnet.

3.7 Lead Glass

The function of the lead glass blocks was to measure electromagnetic energy by collection of Cerenkov radiation produced by the charged particles of electromagnetic showers produced by electrons, positrons or photons which showered in the blocks. Using pulse heights from the photomultiplier tubes

coupled to the lead glass blocks, the presence of correlated pairs of photons resulting from π^0 decay could be inferred.

Sixty-eight lead glass blocks, all 19 x 19 cm^2 in cross-section, were arranged in a rectangular array nine blocks wide and eight blocks high with the four corners missing (Figure 18). Positioned in the centre of the array were the eight "long" blocks, 35.6 cm (12.5 radiation lengths) long, which were composed of SF2 lead glass. The remainder of the array was filled with "short" blocks, 30.5 cm (10.5 radiation lengths), made of F2 lead glass. A 12.7 cm diameter EMI 9815 phototube was glued to the end of each block.

The signals from the lead glass blocks were first amplified by a factor of 10 and then split in the ratio 1:13. The smaller fraction of the signal was input to an ADC unit set at 0.25 pC/channel, which was used to measure electromagnetic shower energy of neutrino events. The larger part of the signal was input to another ADC unit, set at 1.0 pC/channel, which recorded the pulse height for relativistic, non-interacting particles (in this case, muons). The energy attributed to photons and electrons is equal to the total energy detected minus the energy due to charged non-interacting particles.

The gains of the phototubes were initially set equal through

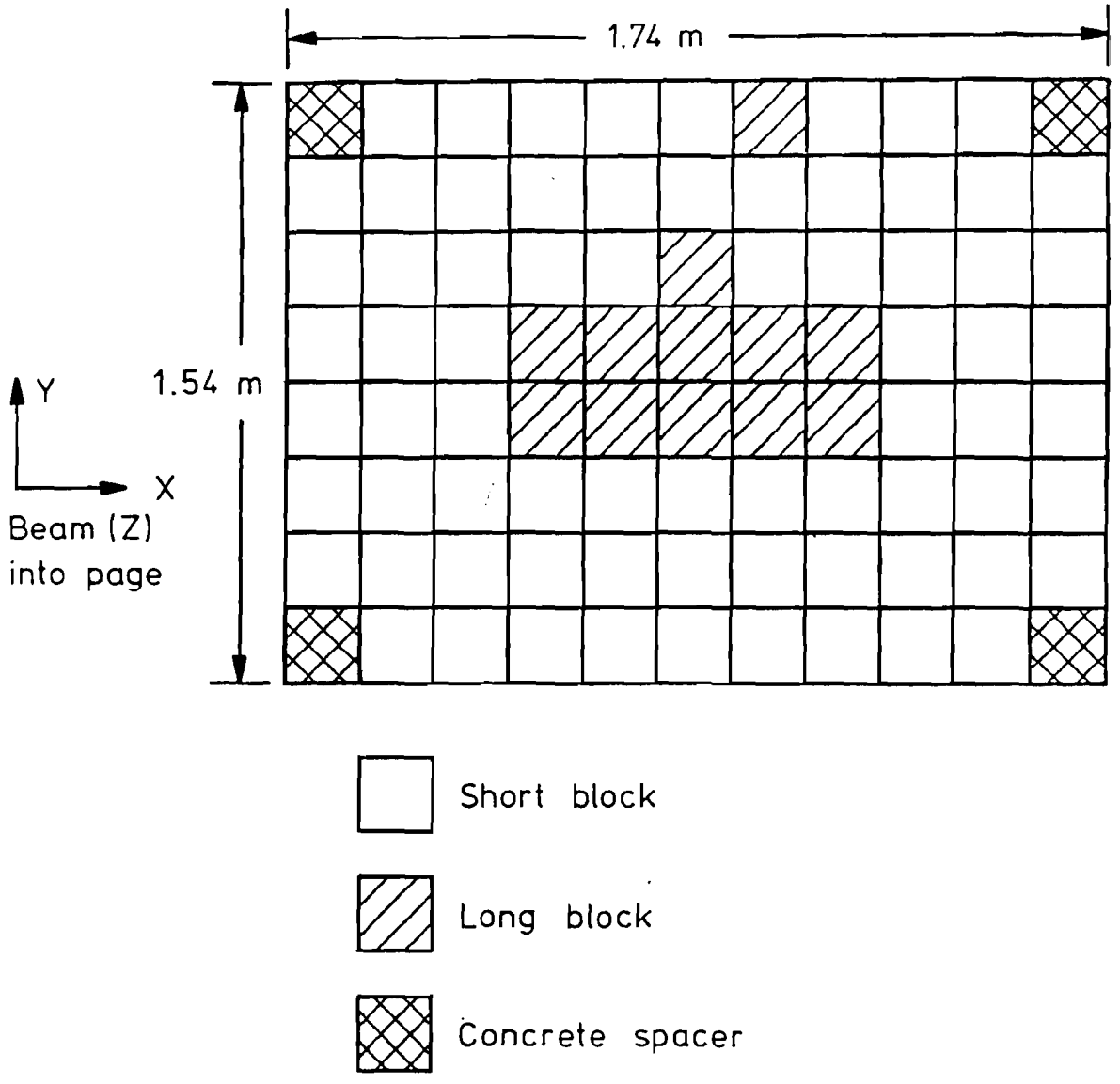

Figure 18. The lead glass array.

the use of a neon flasher. The flasher light was transmitted to the front of each lead glass block through fibre optics. During the experiment the flasher was pulsed between every neutrino spill and new calibration data recorded. The gain of the phototubes was set such that the maximum energy per block which could be measured was 35 GeV.

The calibration of the lead glass blocks was based primarily on tests performed in the Fermilab M5 beam line. One long and one short block were placed in both electron and charged hadron beams with energies ranging from 5 to 30 GeV. The average energy responses obtained for non-interacting particles incident upon the entire faces of the blocks were:

$$E_{short} = 333 \pm 15 \text{ MeV, and}$$
$$E_{long} = 397 \pm 13 \text{ MeV.}$$

These energies are 15% less than those obtained when restricted to the case of non-interacting particles incident upon only the centre of the blocks. The energy resolution obtained was

$$\frac{\Delta E}{E} = \frac{0.15}{\sqrt{E}} \tag{22}$$

Based on studies performed for Fermilab Experiment 25 using the long lead glass blocks, the pulse height for a photon was 5%

less than that of an electron of equal energy [Egloff, 1979]. For π^0 with energy less than 4 GeV, the probability of both photons entering the same lead glass block was only 1%. The probability of both photons entering the same block increased to 30% for π^0 with energy approximately 10 GeV.

3.8 Hadron Calorimeter

The hadron calorimeter was designed to provide a crude measurement of hadronic energy associated with neutrino-induced events. The calorimeter consisted of five planes of scintillator counters interleaved with planes of 10 cm thick steel (Figure 19). The cross-sectional area of the planes was 3 m x 2.44 m. Each plane consisted of 4 counters, 1.3 cm thick of NE110 or NE114 scintillator. Attached to the top of each scintillator was a light guide, a Winston cone, and an Amperex 58DVP phototube.

The signals from the calorimeter were split in the ratio 1:7. Similarly to the lead glass system, the smaller fraction of the signal was used to record hadronic energy for neutrino interactions and the larger portion was used to measure the pulse height of minimum-ionizing particles. Both components were input to 1024 channel ADC units set at 0.25 pC/channel.

Since the calibration of the calorimeter in the neutrino

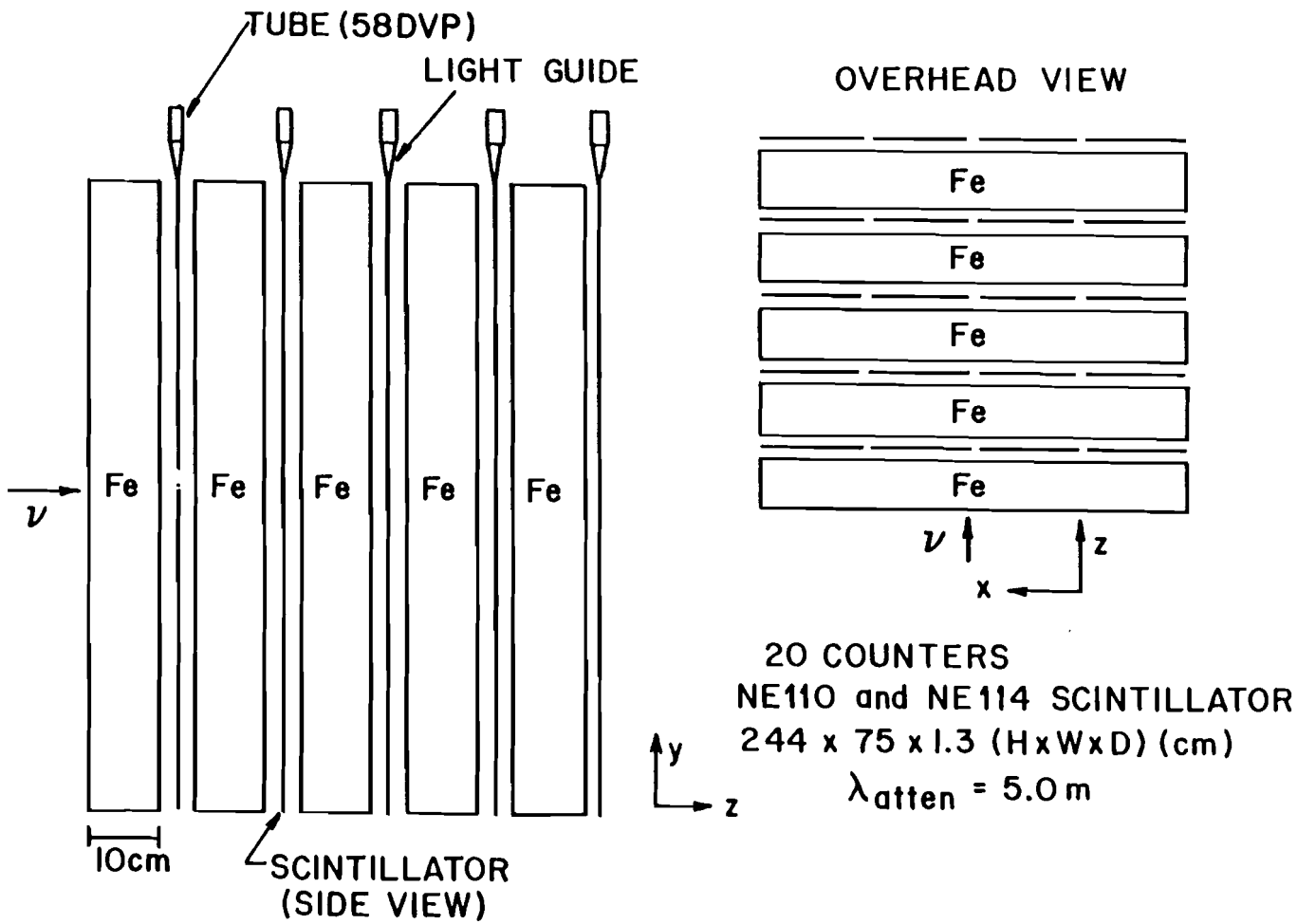

Figure 19. The hadron calorimeter.

beam was not possible, we used the previously obtained result from a similar calorimeter [Bodek, 1975],

$$\frac{dE}{E} = \frac{1.1}{\sqrt{E}} \tag{23}$$

The mean energy deposited by each minimum ionizing track in the calorimeter was equivalent to 2.08 GeV of hadronic energy. The maximum energy which could be measured by an individual calorimeter paddle was 13.7 GeV.

3.9 Muon Identification Counters

The purpose of the muon counters was to identify muons by range. This was achieved using two planes of scintillators, shown in Figure 20, which were embedded in steel after 1.2 m and 2.3 m respectively, corresponding to muon energies of 1.9 and 3.4 GeV. The front plane of counters consisted of two vertical columns each containing 18 scintillators oriented horizontally. The dimensions of the 10 innermost counters were 10.2 cm x 1.52 m x 1.27 cm, those of the next four were 20.3 cm x 1.52 m x 1.27 cm, while the outermost four counters had dimensions 27.9 cm x 1.52 m x 1.27 cm. On the outside ends were light guides, Winston cones, and Amperex 56 AVP phototubes. The second plane contained 40 scintillators, similar to the ones in the first

plane, but oriented vertically in two horizontal rows. At the tops of the scintillators were the light guides, Winston cones, and Amperex 56 AVP phototubes. The signals from the muon counters were split such that $\frac{2}{5}$ was input to an ADC unit and $\frac{3}{5}$ to a TDC unit.

Calibration of the muon counters was achieved using the 2 x 10^5 muon triggers for which a single track was reconstructed in the drift chambers and for which only one TOF II paddle had fired. From these data we calculated the relationship between the position along the counter and the time of arrival of the photomultiplier pulse to obtain a spatial resolution of 12.9 cm. The X-Y position of muon candidates in the muon counters was predicted by the downstream drift chambers. A candidate was identified as a muon if its position was within 2.5 standard deviations of the predicted location. The most credible muons were those which were detected by both the front and the back muon planes.

The efficiency with which muons were detected in both banks of counters was 89%. The detection efficiencies for the single planes were 95±1% (front) and 94±1% (back). Part of the inefficiency results from geometry and the fact that small gaps existed in the scintillator planes.

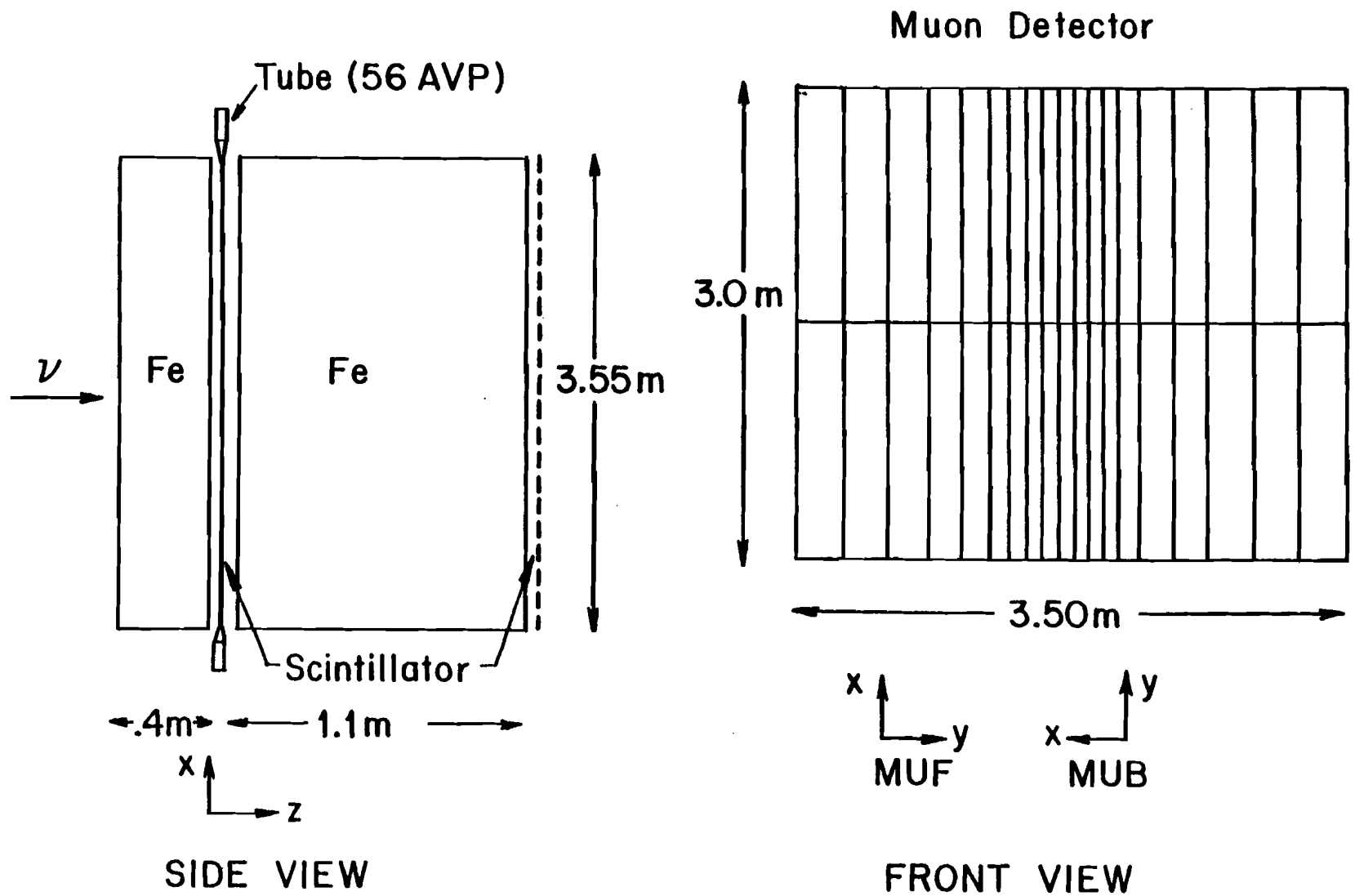

Figure 20. The muon detector.

The detection of muons is important for several reasons:

- To determine whether the neutrino interaction was a neutral or charged current interaction;
- To differentiate between μ^- and μ^+ and thus determine whether the incoming particle was a neutrino or an antineutrino;
- To detect muons from the semi-leptonic decay of charmed particles.

We measured the ratio of $\frac{\bar{\nu}_\mu}{\nu_\mu}$ charged current interactions to be 0.066 ± 0.020.

3.10 Data Acquisition

Throughout the experiment, four triggers were used to enable the logging of data: the neutrino trigger and three calibration triggers -- the muon, flasher/laser and sensor triggers.

The requirements for the neutrino trigger were that there be no charged particle passing through the veto counter, that the pulse height of TOF I be greater than or equal to that of two minimum ionizing particles and that there be at least two tracks passing through TOF II. In addition it was required that the neutrino trigger occur during the fast beam spill, which was achieved by a gate timed to include the beam spill. This gate was triggered by the background muons associated with the neutrino

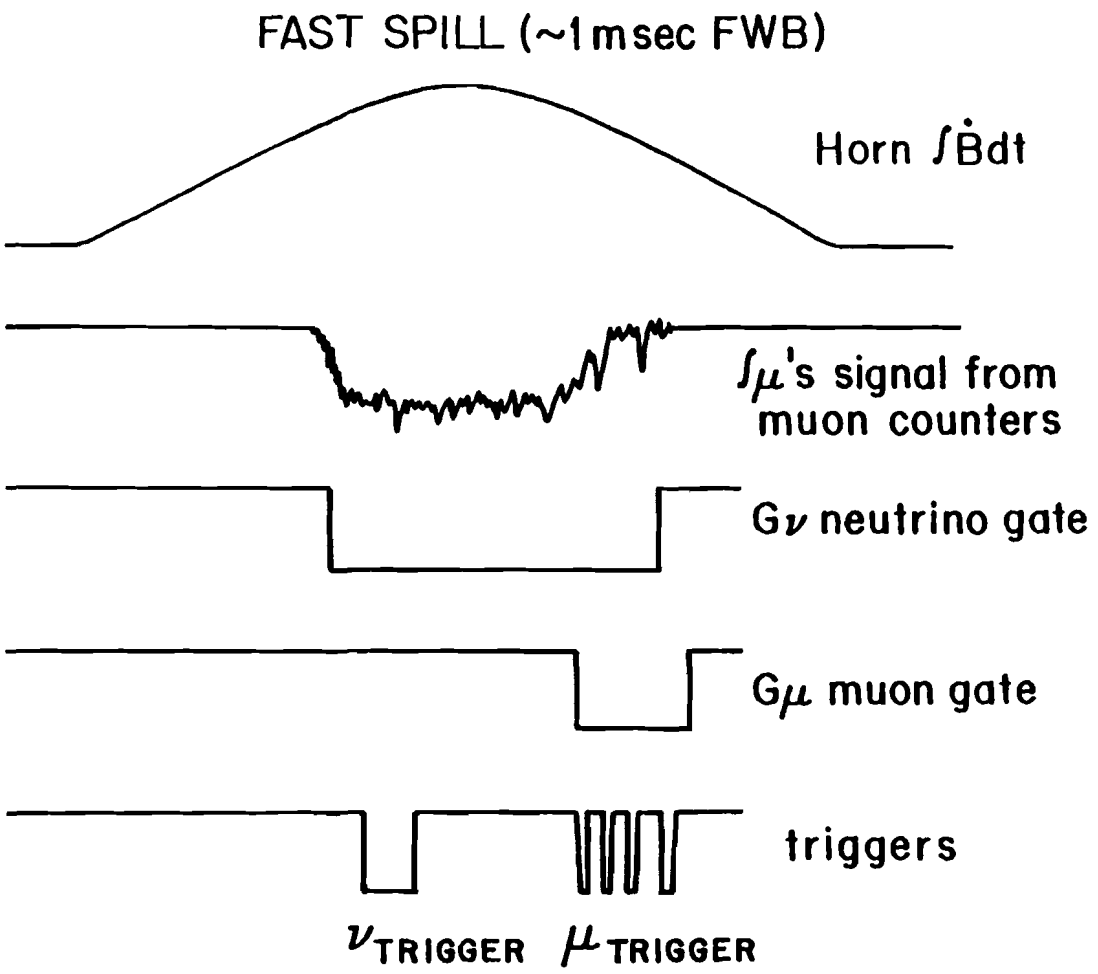

Figure 21. The relative timing of the triggers.

beam. This method of gating the electronics was preferred to one using timing signals of the accelerator, since the latter fluctuated intolerably. The relative timing of the neutrino spill and the various triggers is shown in Figure 21.

The data was read into the computer once per neutrino spill. This process of reading and clearing the ADC units took approximately 5 ms, compared to the neutrino spill length which was 1 ms long. Thus, if two triggers occurred during the same spill, for instance two neutrino triggers or a muon trigger followed by a neutrino trigger, the counter information (except for that of the drift chambers, which was stored in the local drift chamber readout memory) for only the first trigger would be recorded. To maximize the number of neutrino triggers recorded, muon triggers were accepted only in the last 0.05 of the neutrino spill. Since the muon flux was relatively high, ample muon triggers were still recorded. The other requirements of the muon trigger were that the pulse height of TOF I be equivalent to that of one or more minimum-ionizing particles and that there be one and only one track passing through TOF II.

In order to record lead glass pulses from several muon triggers per spill, a separate "sub-trigger" was used involving individual TOF II counters and columns of calorimeter paddles. This was done to ensure that all parts of the apparatus would

have a sufficient sample of muon data for calibration purposes. Since the muons are primarily positively charged, they are deflected to the beam-right side by the magnetic field.

The purpose of both the laser/flasher and sensor triggers has been discussed in previous sections. The only logical requirement for both these triggers was that the triggers occur once between every neutrino spill.

Data from the ADC units and TDC units and the drift chamber readout were recorded onto magnetic tape, using a Data General Eclipse Computer. The online program both recorded data and monitored all the experimental apparatus during data-taking. Audible alarms were set off if failures of important things, such as the drift chamber voltage supplies, the gas supply to the drift chambers, or the magnet power supply, were detected. In addition, every readout channel of each piece of apparatus could be accessed, both as the data was being taken and after the run. A separate program, CHIMP, histogrammed the pertinent data following the termination of the run, allowing the user to check for equipment malfunctions (e.g. faulty drift chamber amplifiers and inactive channels of the electronics).

4. RESULTS

Data-taking for experiment 531 took place from 18 November 1978 until 7 February 1979. During the 1250 hours of running time, 183 magnetic tapes were recorded. The events were produced by an integrated flux of 7.33×10^{14} neutrinos passing through the emulsion target ($1.7 \times 10^{15}\ \nu/m^2$), which resulted from a total of 7.2×10^{18} protons incident on the neutrino beam production target.

The data included approximately 68,000 neutrino triggers, 140 antineutrino triggers, 9×10^5 muon triggers for calibration, and the flasher/laser and sensor triggers. Thus about one neutrino trigger per seven machine cycles (ν spill) and ~2 muon triggers/spill were taken. The cycle time of the accelerator was 7 seconds long for most of the run.

Due to the inefficiency of the anticounter (11±1%), most of the events recorded as neutrino triggers resulted from charged particles, mainly muons, incident upon the apparatus. Approximately 1/30 of the neutrino triggers resulted from neutrino interactions in the emulsion target and support plate.

The mean live time of the neutrino trigger was 79%, resulting from a 73% live time during the beginning of the run

when the muon flux was extremely high, a 79% live time following the installation of additional shielding in the berm, and an 82% live time towards the end of the experiment when the toroidal sweeping magnets were in use.

4.1 Reconstructed and Calculated Neutrino Event Samples

Two methods were used to calculate the expected number of neutrino interactions to be observed in the emulsion volume. The first method extrapolated the number of neutrino interactions found by experiment 545, which took data during the early part of the same running period. This experiment used the Fermilab fifteen-foot bubble chamber, filled with deuterium and with a target mass of 2184 Kg. After corrections of about 20%, the experiment reported ~ 12,000 charged current neutrino events [Hanlon, 1981], based on an integrated flux of 2.9×10^{18} protons on the neutrino target. The number of events expected for experiment 531 may then be calculated:

$$N_{531} = \frac{m_{531}\ (n_p)_{531}\ \mathrm{flux}_{531}}{m_{545}\ (n_p)_{545}\ \mathrm{flux}_{545}}\ N_{545} \cdot (1.32) \cdot (1.05) \qquad (24)$$

where N is the number of events; m_{E531}, the mass of the emulsion target, is 122±5 Kg; n_p is the number of protons incident on the neutrino target, which for E531 was 7.2×10^{18}; and $\frac{\mathrm{flux}_{531}}{\mathrm{flux}_{545}}$, the ratio of the neutrino flux per incident proton at the Wonder

Building to that at the bubble chamber was a factor of 2.4±0.24. The factor of 1.32 represents the inclusion in E531 of neutrino-induced neutral current events. The factor 1.05 accounts for the additional events induced by antineutrinos.

Several factors contribute to losses in the number of events expected to be observed on the emulsion. There were short periods for which data-taking was disabled although the accelerator was running: during the changing of the fiducial sheet and during the changing of magnetic tapes, in between runs. Also for a very small portion of the running time, the neutrino horn was focused, intentionally, such that the majority of beam particles were antineutrinos. The cross-section for antineutrinos on nucleons is a factor of two less than that for neutrinos. It is estimated that these factors decrease the expected number of events by 10%.

Based on Monte Carlo studies, the reconstruction efficiency of the spectrometer is approximately 65%. The spectrometer is particularly inefficient at low energies ($E < 10$ GeV) since at these energies there are not always at least two tracks through the downstream drift chambers, as required by the neutrino trigger and by the reconstruction programs to calculate the vertex locations. Thus the number of events expected using this method of calculation is 2549±500.

The second method of calculating the expected event yield used a Monte Carlo simulation. Input to this was the energy spectrum for the Fermilab wide band neutrino beam, which has been calculated by S. Mori [Mori, 1979]. However, there are severe discrepancies between the Mori calculated spectrum and the observed neutrino spectrum, in particular at low energies [Hanlon, 1980]. A neutrino energy spectrum, $S_\nu(E)$, which has been modified to agree with the data of E545 was used in the integration:

$$N = m \int_0^{350} \sigma_\nu(E) S_\nu(E)\, dE, \tag{25}$$

where N is the number of neutrino events, m is the target mass, and the cross sections for neutrino and antineutrino scattering are given by

$$\sigma_\nu(E) = 0.63 \times E \times 10^{-38}\ \mathrm{cm}^2/\mathrm{nucleon/GeV} \text{ and} \tag{26}$$

$$\sigma_{\bar{\nu}}(E) = 0.3 \times E \times 10^{-38}\ \mathrm{cm}^2/\mathrm{nucleon/GeV}. \tag{27}$$

We obtain 1927±480 as the predicted number of neutrino and antineutrino events in the emulsion.

The reconstruction of neutrino interactions occurring in the emulsion was achieved by reconstructing tracks using the information from the drift chambers. A discussion of the various

vertex reconstruction programs is given in section 5. The final, most complete pass through the data yielded 2285 candidates for neutrino interactions in the target region. This sample was reduced to 2022 candidates, after elimination of predictions outside the fiducial emulsion volume.

4.2 Emulsion Processing

The processing of the emulsion modules took place at the University of Ottawa over a three month period after the data-taking run. The fiducial sheet and the integrating sheets were processed at Fermilab during the data-taking period. The processing procedures were different for the vertical and horizontal modules and for the integrating and fiducial sheets [Ushida, 1983].

The vertical modules could be processed immediately as the emulsion was already mounted on lucite backing. Before the horizontal emulsion could be processed, it was necessary to stick the pellicles to gelatin-coated lucite. Four per cent of the emulsion was rendered unusable due to blistering during this process. The thickness of both the vertical and the horizontal emulsion sheets shrank by a factor of 2 during processing.

To facilitate the measurement of tracks, the emulsion was

marked in several ways to obtain both local and relative coordinates. The sides of the sheets in the horizontal modules were marked with an X-ray gun at Argonne National Laboratory prior to processing. The horizontal sheets were imprinted with a 500 μ x 500 μ optical grid which had been stuck to the lucite. During the construction of the vertical emulsion modules the emulsion-coated sheets had four holes punched near the corners. The holes were used for mounting the sheets during exposure and also later to determine a local coordinate system. The position of the fiducial sheet relative to the emulsion target was determined by small ^{55}Fe sources, embedded in the support posts of the emulsion modules, which produced marks on the fiducial sheets.

The grain density, a measure of the emulsion quality, was excellent:

$28.4 \pm 0.7/100\,\mu$ horizontal emulsion modules,
$31.3 \pm 1.2/100\,\mu$ vertical emulsion modules,
$32.3 \pm 1.2/100\,\mu$ fiducial sheets.

The grain density of freshly-poured emulsion is $40/100\,\mu$. Grain density is usually determined by following charged tracks through the emulsion and counting the number of exposed silver granules, which appear as black dots. The above measurements were made by following electrons which resulted from the decays of stopping

muons. Measurements were also made to study the effects of fading of the exposed silver grain over the period prior to processing. For the target modules the amount of fading was 10% for the three month period the modules were in the beamline. The variations from one pellicle to another were less than 3%.

5. DATA ANALYSIS

5.1 Neutrino Event Reconstruction Programs

Two independent neutrino event reconstruction programs were used to predict the locations of neutrino-induced interactions, which were later searched for in the emulsion. A program was developed at the University of Toronto, which was used in the early stages of the data analysis. Later the emulsion was scanned chiefly using predictions of a program written at the Ohio State University.

Toronto Program

The first step in this program was to obtain an estimate of the vertex location. This was accomplished by making histograms of the x, u, and v intercepts at the point $z = 0$, which corresponds physically to the upstream face of the emulsion, of line segments which had been reconstructed using any two drift chamber hits from a particular view. The following step was the reconstruction of up-to-down tracks, which began with the fitting of downstream segments. The technique employed was to first require 3 or 4 collinear hits in the downstream x chambers then to search for consistent u and v chamber hits. The downstream segments thus constructed were projected to the centre of the

magnet. Upstream segments were searched for with the constraints that the segment lie within 2.5 cm of the vertex and within 0.65 cm of the point at the magnet mid-plane. The line segments were reconstructed by requiring 3 or 4 hits in a particular view and then combining these with hits from the other two views. Acceptance of upstream track segment candidates was based on the chi-squared per degree of freedom (CHISQ/DF) of the track and the number of hits used.

More than one upstream track segment were retained for a given downstream segment. To obtain the up-to-down tracks, quintic spline fits were executed in which five track parameters were fitted: dx/dz and dy/dz, the x and y intercepts at z=0, and the inverse of the momentum. By taking a least squares fit to a common vertex for all of the reconstructed tracks, the estimate of the vertex location was refined.

Ohio State Program

The most important feature of the Ohio State program was that two "passes" were made on every event, the first being primarily to reconstruct the track of the muon or an energetic hadron. Muons could be identified by penetration of the first or both of the planes of muon counters. Tracks were reconstructed in a manner similar to that of Toronto program. The downstream

and upstream segments were reconstructed individually and then joined. A trial vertex was obtained by taking the intersection point of high momentum tracks with that of the muon. Other tracks were searched for, including those which bent in the fringe field of the magnet, although no upstream-only tracks were reconstructed. If no other tracks than that of the muon or energetic hadron could be found, the process was repeated. The start time of the event and one or more vertices were then fitted using the reconstructed tracks, weighting them according to the momentum, the chi-squared, the number of hits used and the muon identification.

The approach of the second pass was similar to that of the first, the differences being that the fitted start time and vertex location(s) were used as input data. Tracks which had been reconstructed the first time were retained with the possibility of ameliorating such tracks.

Figure 22 shows the distribution of the number of tracks reconstructed in the events. The mean number of tracks reconstructed in an interaction was 4.8. For all the charged current interactions, it was estimated using Monte Carlo techniques that 71% of the interactions were reconstructed. For neutrino energies greater than 10 GeV, 80±10% of the events were reconstructed and for neutrino energies greater than 20 GeV, this

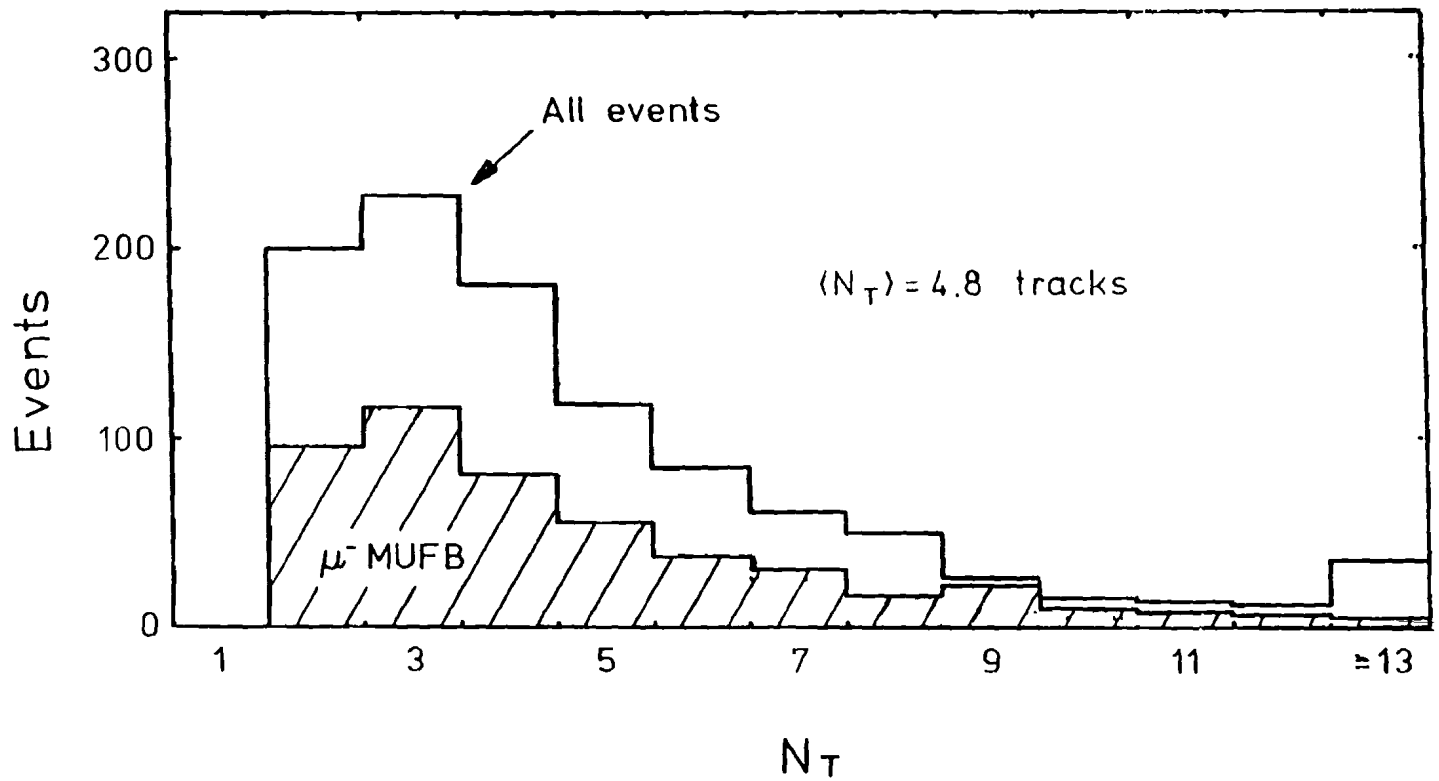

Figure 22. Number of tracks reconstructed per event by the event reconstruction program. The shaded area represents those events which have an identified muon.

number increased to 90±10%. These efficiencies include the trigger efficiencies along with the program reconstruction efficiencies, evident from the dependence of the efficiency upon the energy of the neutrino. (The program reconstruction efficiency is estimated to be greater than 95%.) For low energy events, the particles are emitted at wide angles and there are not always two up-to-down tracks, necessary for reconstruction of the event.

5.2 Search for Neutrino Events in the Emulsion

For both the horizontal and the vertical modules, fiducial cuts were made to exclude regions which were plagued by distortions. This included a margin near the edges and around the post holes of 3 mm for the horizontal modules and 2.5 mm for the vertical modules. Additional cuts were made for the horizontal modules to exclude regions of G-10. These cuts in the volume to be searched reduced the number of predicted events by 12% for the horizontal modules and 13% for the vertical modules.

Two techniques were used in the search for events predicted to occur in the emulsion target: volume scanning and track followback. The vertical emulsion pellicles were scanned using only the track followback technique. The horizontal emulsion

pellicles were primarily volume scanned although some attempts were made to use the followback technique. The conventional technique, volume scanning, involves the scanning of a volume of emulsion centred around the predicted vertex.

A volume 320 mm^3 (4 mm x 4 mm x 20 mm) surrounding the predicted vertex in the horizontal emulsion was scanned. This method was 51±2% efficient at finding events. The method of volume scanning was less efficient for events occurring in the upstream and downstream portions of the horizontal modules since these are regions of distortion. Due to multiple scattering, the resolution decreases for tracks originating at the upstream face of the emulsion. This effect is more pronounced for low momentum events.

Another disadvantage of volume scanning is that events with black tracks resulting from recoil nuclear fragments are found more easily than white stars (events which have no dark tracks), thus creating a scanning bias.

The followback technique was used primarily for the vertical emulsion modules. Tracks which were reconstructed by the downstream spectrometer were initially searched for in the fiducial emulsion sheet. Due primarily to the low background in the fiducial sheet these tracks were found 96±2% of the time.

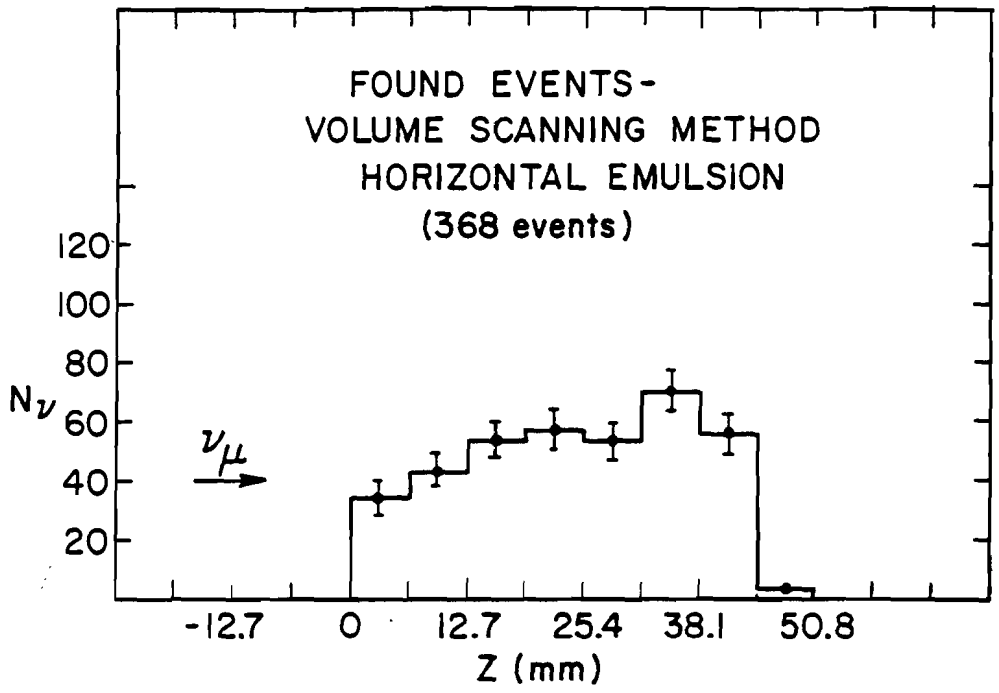

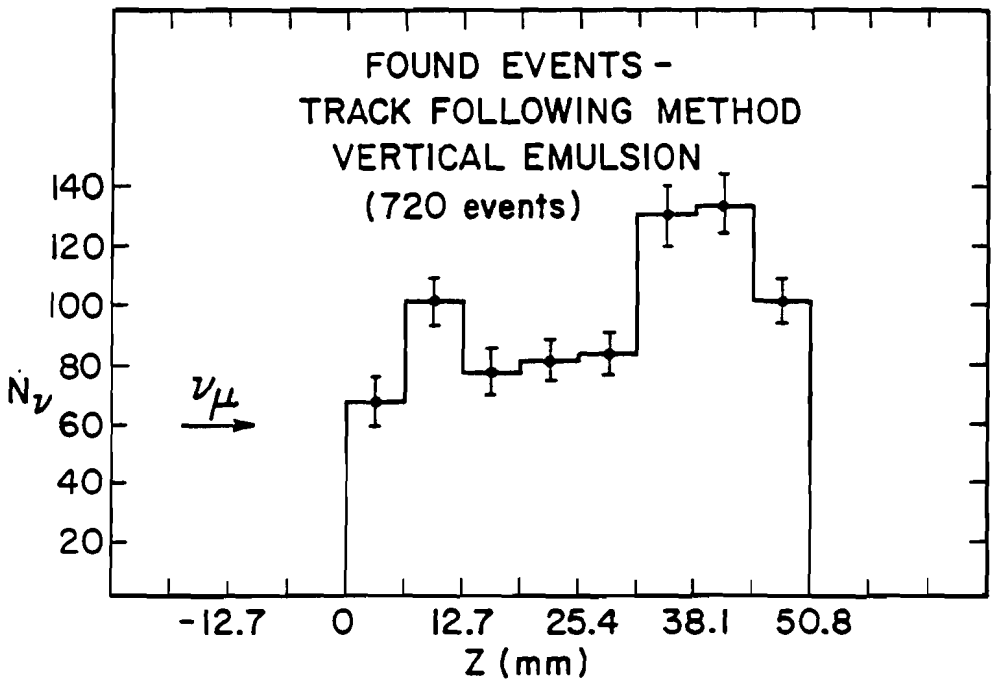

Figure 23. Z-Coordinates of found events in the emulsion target.

The "fiducial sheet" tracks were then followed back into the emulsion modules with an efficiency of 90±2%. The efficiency for finding vertices was thus 87±2%. The number of found events as a function of the position in the emulsion target is shown in Figure 23.

Discrepancies between the counter predictions and the location of actual events found in the emulsion are larger than those differences which can be attributed to the surveying resolution. These differences which are not fully understood are:

$$< \Delta x > = 235\ \mu;\ < \Delta y > = 645\ \mu,\ \text{and} < \Delta z > = -75\ \mu.$$

The distributions of the predicted and actual coordinates are shown in Figure 24. These distributions are for all vertical and horizontal events, independent of the method in which the events were searched for. The widths of the distributions are:

$$\sigma_x = 370\ \mu,\ \sigma_y = 290\ \mu,\ \text{and}\ \sigma_z = 1.4\ \text{mm}.$$

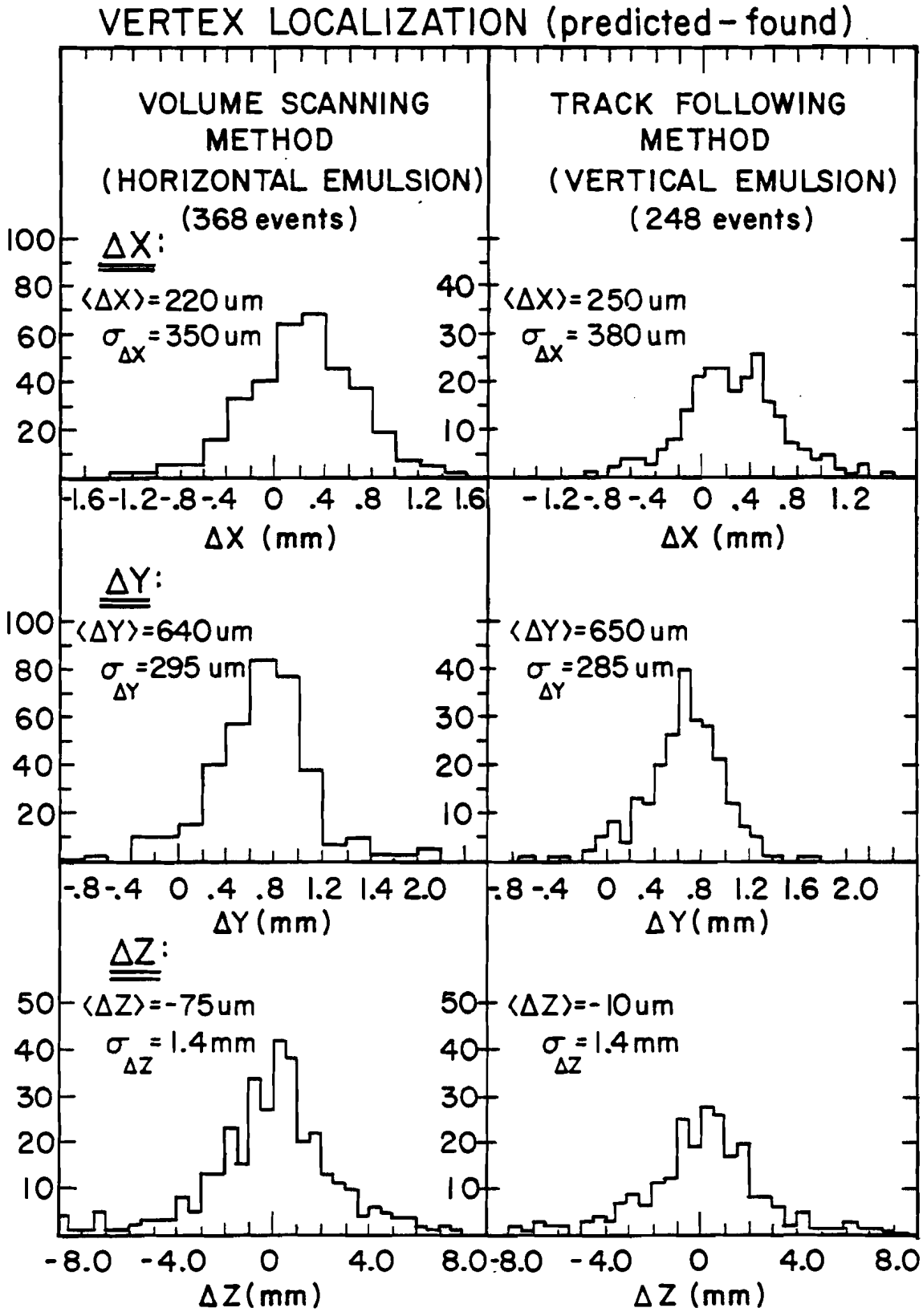

Figure 24. Differences between predicted and found vertex coordinates.

5.3 Search for Charged Decays

5.3.1 Horizontal Emulsion Modules

Decays of charged particles were searched for by following tracks which satisfied certain criteria for at least 6 mm or until the track left the emulsion module. The criteria were that both the x and y slopes relative to the beam direction ($\frac{dx}{dz}$ and $\frac{dy}{dz}$) be less than 365 mr, the differences in the slopes measured in the emulsion and those measured in the spectrometer be less than 15 mr, and the relative ionization of the track be less than 4. The efficiency for finding charged decays at a given distance was calculated by taking the number of tracks followed for that distance divided by the number of charged tracks followed. Figure 25 shows the efficiency for following charged tracks with various angles as a function of the distance followed.

5.3.2 Vertical Emulsion Modules

For the vertical emulsion modules two methods were used to search for decays of charged particles: the track following method and the scanback method. The track following method involved following charged tracks for at least 6 mm with certain criteria imposed: that $\frac{dx}{dz}$ and $\frac{dy}{dz}$ be less than 200 mr, and that the differences between the slopes measured in the emulsion and

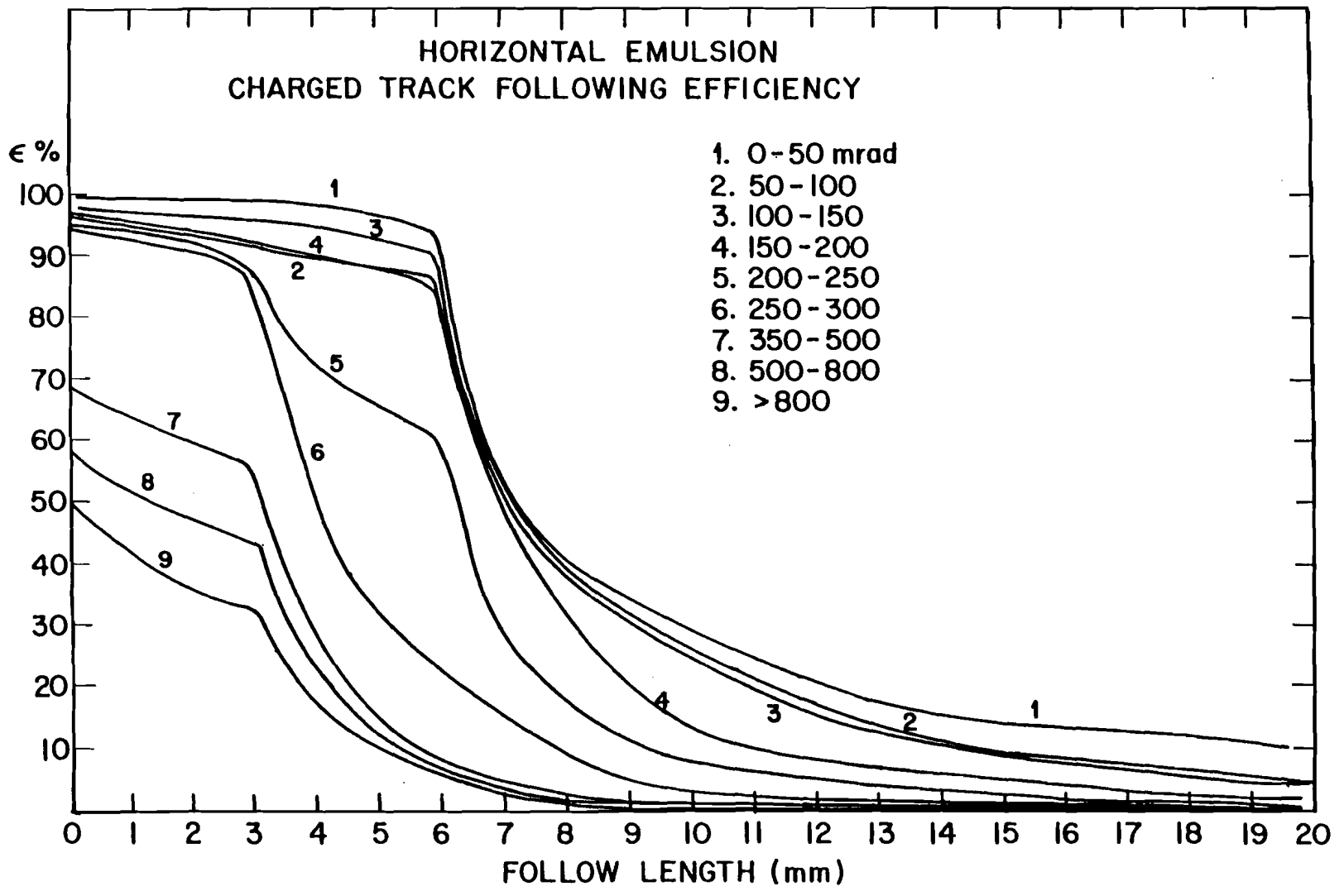

Figure 25. Track following efficiency as a function of the distance followed for tracks of various angles.

the slopes measured by the spectrometer be less than 15 mr. The scanback method was identical to the track followback method used to locate the primary vertex. (For the same reason the scanback method was not implemented for the horizontal emulsion modules.) Tracks reconstructed by the spectrometer, which had momenta greater than 700 MeV/c, whose projections lay within 2.0 mm of the primary vertex, and which had not been initially located in the emulsion, were searched for in the fiducial sheet. The tracks were then scanned back to their points of origin, which was often the site of a gamma conversion or nuclear interaction.

For distances less than 6 mm the scanning efficiency for charged decays in the vertical emulsion modules was the same as that for the horizontal emulsion modules, since the same technique, track following, was used.

The efficiency for the scanback technique could be determined from the knowledge of the number of charged tracks which had been reconstructed by the spectrometer. For a single charged track, the efficiency for finding the track on the fiducial sheet was $\epsilon_{cs} = 96 \pm 2\%$. The efficiency for finding the decay could then be expressed as

$$\epsilon = \frac{1}{N}[\sum_k n_k \, \epsilon_{cs}{}^k], \tag{28}$$

where $N = \sum n_k$ and n_k is the number of events of a particular geometry with k reconstructed tracks. For charged decays the only decay geometry considered was that of three charged decay particles (trident). There were significant differences in the scanning efficiencies dependent on the energy of the event. For event energies less than 10 GeV, the decay tracks were less likely to be reconstructed by the spectrometer since the particles were emitted at wide angles. Using equation 28, the efficiencies obtained were

$$\epsilon = 0.70^{+0.15}_{-0.10} \ (P_{charm} < 10 \text{ GeV/c}) \text{ and} \tag{29}$$

$$\epsilon = 0.998^{+0.002}_{-0.030} \ (P_{charm} > 10 \text{ GeV/c}), \tag{30}$$

which averaged to

$$\epsilon_{\text{charged scanback}} = 0.8 \pm 0.1. \tag{31}$$

5.4 Search for Neutral Decays

5.4.1 Horizontal Emulsion Modules

Only the volume scanning method was used to search for decays of neutral particles in the horizontal emulsion modules.

The volume scanned was a cylinder of radius 200 μ and length 1000 μ downstream of the production vertex.

The efficiency for volume scanning was deduced from the efficiency for volume scanning of e^+e^- pairs produced in neutrino interactions. The number of e^+e^- pairs found may be compared to the number expected from the conversion of π^0 in the emulsion, which is approximately 2 per neutrino interaction. This efficiency was expressed as

$$\epsilon(z) = 0.7 - 0.0006z \tag{32}$$

where z, the distance between the gamma conversion point and the primary vertex, is between 10 and 1000 μ.

Although the process of volume scanning for neutral charm decays is identical to that for an e^+e^- pair, the e^+e^- pair should be more visible since the two tracks initially lie on top of each other to effectively create a 2x minimum-ionizing track. In contrast the divergent tracks from the charm decay vertex will only be those of minimum-ionizing particles. Thus the efficiency for finding e^+e^- pairs is an upper limit to the efficiency for finding charm decays.

5.4.2 Vertical Emulsion Modules

Decays of neutral particles in the vertical emulsion modules were searched for by the methods of volume scanning and scanback. The volume scanning method involved the scanning of a volume $600\,\mu \times 600\,\mu \times 1000\,\mu$.

The scanback method was the same as that used for the charged decays. This method was particularly useful for events in which the decay vertex had been found first and mistakenly identified as a primary production vertex having no black recoil tracks. Using the scanback technique the primary vertex could be located. The method of determining the scanning efficiency for the volume scanning technique was the same as that for the horizontal emulsion modules, that is, a calculation based on locating the points of e^+e^- conversions.

The scanning efficiency for finding neutral decays by the scanback method could be calculated using equation 28. Three charged particle geometries were observed for the neutral decays: two-prong, four-prong, and six-prong. The overall efficiency for the finding of neutral decays by scanback, which was obtained by taking a weighted average of the efficiencies for two-, four-, and six-prong decays, was $\epsilon = 93.8\%$. In general the charm decay candidates which were produced with low momentum were the

baryons. Apart from one event which is consistent with a neutral baryon hypothesis [Errede, 1981], all of the neutral decays resulted from the decay of a charmed meson whose momentum was generally greater than 10 GeV/c. Thus for the neutral scanback technique there is no dependence upon the parent momentum.

5.4.3 Overall Scanning Efficiencies

The scanning efficiency at each distance was obtained by combining the efficiencies for each of the scanning techniques used at that distance, weighted by the number of events found by each technique. Although the emulsion scanned at the University of Ottawa and Korea University was of the vertical type, it was not scanned by the scanback technique and it is therefore included in the average of the scanning efficiencies for horizontal modules at distances greater than 30 μ.

For the horizontal emulsion modules both the charged and neutral scanning efficiencies were simply the volume scanning efficiency in each region. The charged scanning efficiency for the vertical modules included efficiencies for both the track following and scanback techniques. The neutral scanning efficiency for the vertical emulsion modules encompassed the efficiency for volume scanning and for the scanback technique. The charged and neutral scanning efficiencies are shown in

TABLE 2. Summary of Emulsion Scanning

Computer predictions of ν events	2022
ν events found	1248
Scanning efficiency	69%
Charged track followed (including muons)	34.8 m
Nuclear interactions found	89
Single-prong events	48
e^+e^- pairs	199
Vees (strange particles)	4
Neutral charm candidates	21
Charged, multi-prong, charm candidates	22
Charged, single-prong, charm candidates	5

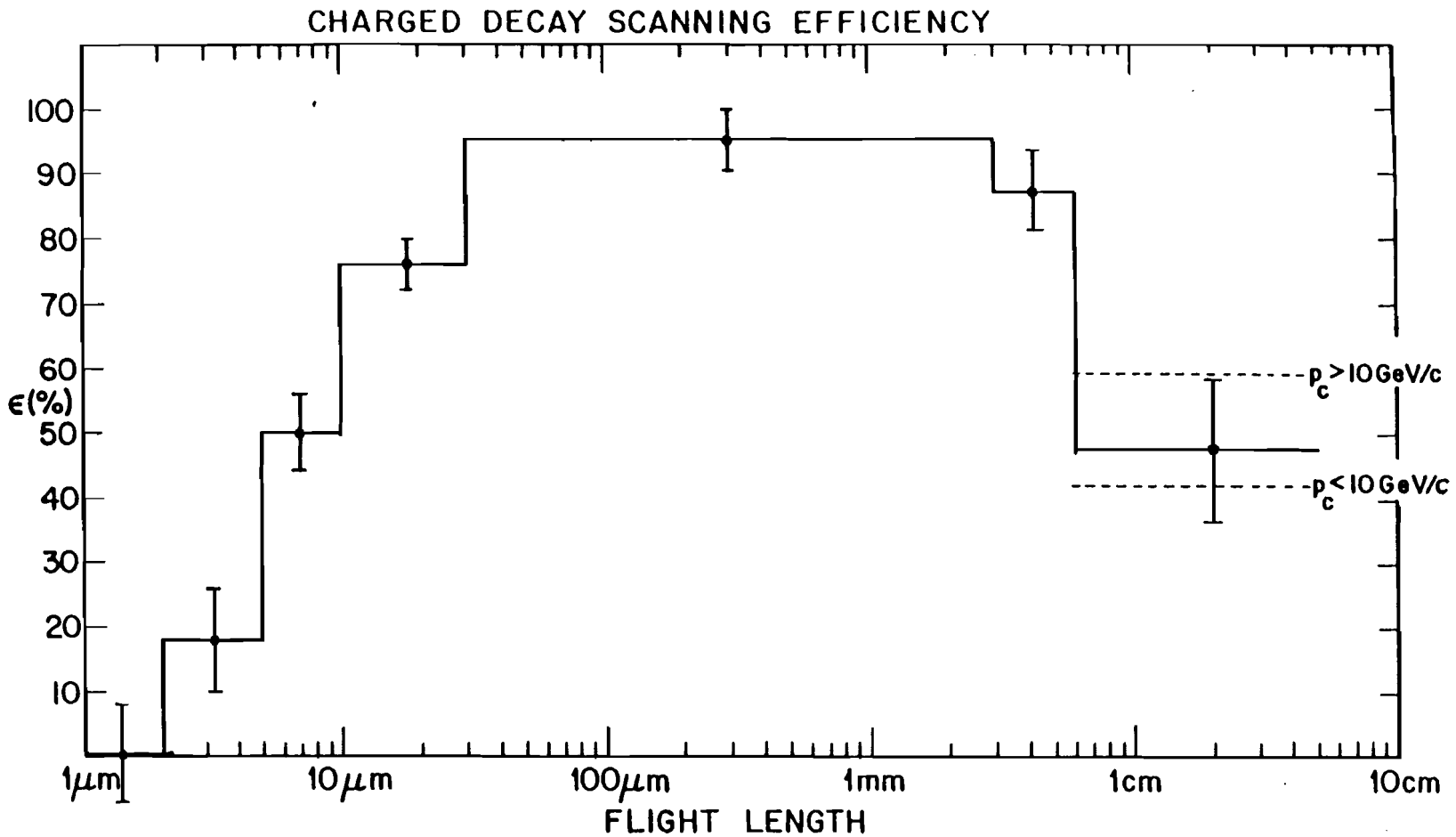

Figure 26. Charged Scanning Efficiency as a function of the Flight Length.

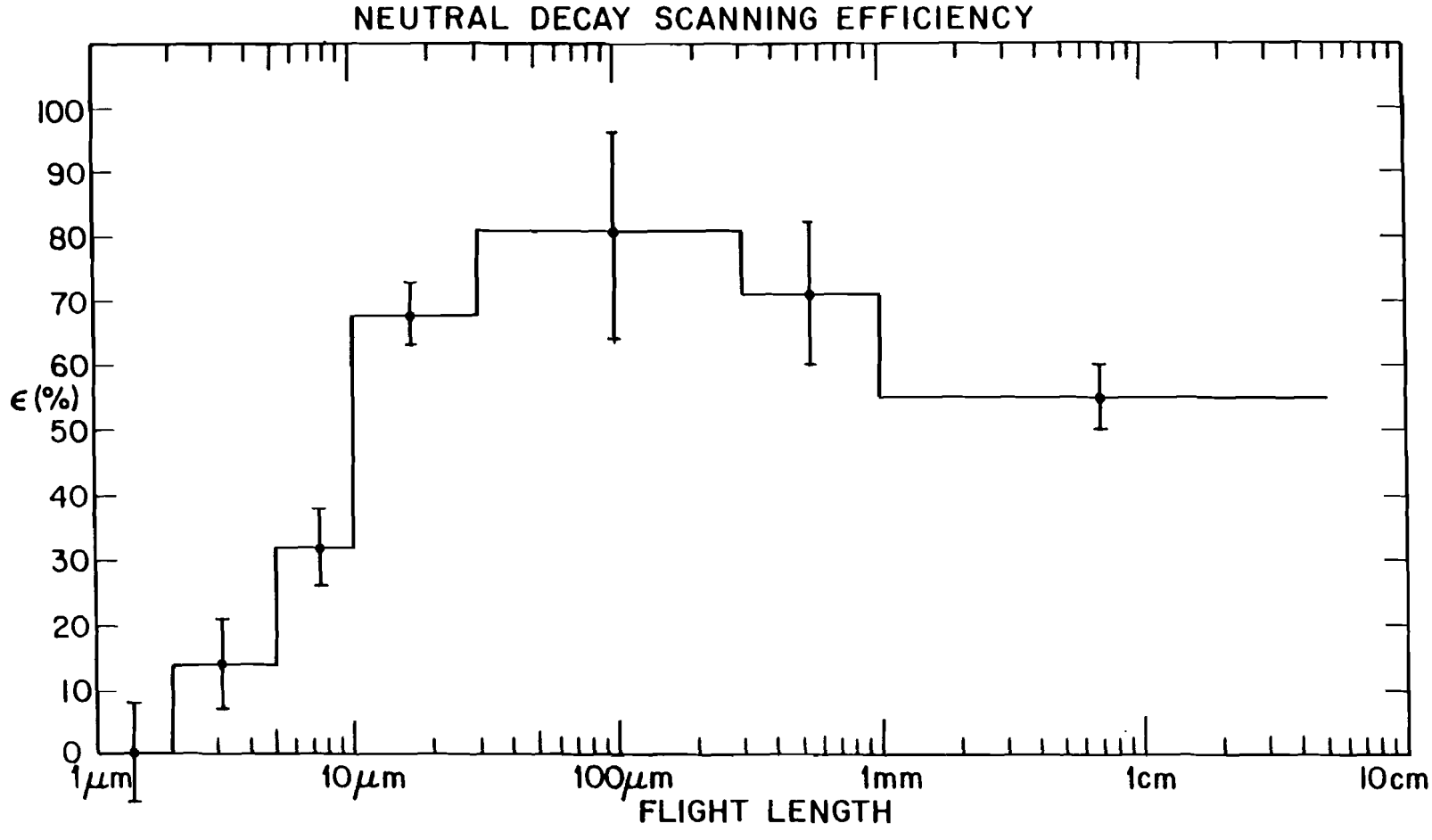

Figure 27. Neutral Scanning Efficiency as a function of the Flight Length.

Figures 26 and 27. The scanning efficiency is not a constant over the entire length of the emulsion. At short distances the efficiency is quite low because of nearby tracks obscuring decays. The efficiency depends upon the diameter of the primary vertex which is given by

$$D = 0.25(N_h + N_s/2) + 1.80, \text{ for } D \geq 3\,\mu, \tag{33}$$

where N_s is the number of minimum ionizing tracks and N_h is the number of black recoil tracks. For distances less than $3\,\mu$, two tracks cannot be resolved.

At large distances, the efficiency is also low because the scanback technique was possible only for the vertical emulsion modules.

5.5 Backgrounds to Charm Decays

The background to the multi-prong charm decays can be calculated using the number of nuclear interactions which are observed. Of the 89 nuclear interactions, 5 events do not have black recoil tracks, but are identified as nuclear interactions because they are not charge-conserving. (In four of the events one minimum-ionizing track becomes two tracks, while in the fifth event a minimum-ionizing track appears from nowhere.) Since the

emulsion is betweeen 0.9 and 1.4 percent hydrogen, one expects to find 2.3±1.8 events which are hydrogen interactions, which always appear as non-charge-conserving. Thus there are 2.7 events, which result from a charged or neutral particle interacting with a bound proton in the emulsion. The number of protons and neutrons in the emulsion is roughly equal. Thus one would expect the same number of interactions occurring with neutrons, which, in contrast, appear as charge-conserving.

Using the data of 79 of the nuclear interactions, the relative number of events, N, as a function of the number of minimum-ionizing particles in the event, n_s, is [Bailey, 1983]:

$$\frac{dN}{dn_s} \alpha e^{-0.48n_s}. \tag{34}$$

The fraction of multi-prong interactions ($n_s \geq 2$) is $0.4^{+0.3}_{-0.1}$. The number of background, multi-prong interactions is 0.4 x 2.7 = $1.1^{+0.2}_{-0.6}$ events for all energies. If one considers only events with momentum greater than 4 GeV/c, the expected number of background events is 0.2.[2] This is calculated using the empirically derived (from all hadrons with momentum greater than 1 GeV/c) relation

---

[2]All but one of the charged, charmed, multi-prong events (549-4068) have momentum greater than 4 GeV/c.

$$\frac{dn}{dp} \alpha\ e^{-0.4p}, \tag{35}$$

where n is the number of hadrons with momentum p.

The number of single prong or kink events found in the emulsion is 47, of which 40 are not charm events [Ushida, 1981]. Using primarily a transverse momentum cut, the number of events which would simulate charm decay is estimated to be 0.3.

Of the 47 kink events, 4 are fitted as decays of charmed particles. Of the 43 remaining events, two-thirds arise from incident positively charged hadrons, which we use to estimate a background to the number of charmed decays.[3] The number of single prong events as a function of the transverse momentum at the kink vertex is

$$\frac{dn}{dp} \alpha\ e^{-9p_{\perp}} \tag{36}$$

If one considers only single prong events which have transverse momentum greater than 0.5 GeV/c, the number of expected

---

[3]The charmed decays are primarily positively charged. An estimate of the total number of single prong background events is obtained by correcting the positive-only number, on the basis of the $\bar{\nu}$ flux.

background events is 0.3 events.[4]

5.6 Analysis of Events with Short Decays

Events which contained multi-prong decays and single tracks which were observed to kink were analysed using computer programs at Fermilab and the University of Toronto. For these events, the scanning of the emulsion provided the decay lengths, the slopes (dx/dz and dy/dz) for all observed charged primary and secondary tracks, and the slopes of the decaying parent. It was also possible to obtain ionization and $p\beta$ measurements for charged tracks found in the emulsion, although this was not routinely done.

The analysis of charm decay candidates proceeded in two stages. The initial step was the reconstruction and momentum analysis of the event. Once this had been accomplished, the kinematic fitting of the events, in which the identity of the decaying particle was searched for, was possible.

At the University of Toronto, the analysis of the charm candidates was performed using a VAX 11/780 computer system. The

---

[4]One of the five single-prong, charm events (671-7015) has transverse momentum less than 0.5 GeV/c.

reconstruction of the tracks of charged particles using the drift chamber hits and the general visual analysis of the data contained by the lead glass system and the hadron calorimeter was done using the program PSANAL2. Reconstruction of π^{o}s was accomplished with the program PIGAM and, if necessary, the kinematic fitting program TESTKIN. The overall kinematic fitting of the event in which a particular decay hypothesis was assumed was done using TESTKIN in the case of constrained fits. For fits which could not be constrained, that is, events containing unobserved neutral decay particles (neutrinos and π^{o} and K^{o} which missed the lead glass or calorimeter), zero-constraint calculations were performed using the program ZEROC.

Several data files were used as input for the charged track fitting program PSANAL2. All of the emulsion data (dx/dz and dy/dz for all of the decay and production tracks, the decay length, and dx/dz and dy/dz for the decaying parent) were manually transferred to the file CHARMING1.DAT after being received from Japan via TELEX. The spectrometer data for each charm candidate event was transferred from the magnetic tape recorded during the data-taking run to a disk file CHARMALL.DAT by a program which selected events by their run and record number. Data files containing the measurements of the magnetic field and the results of the drift chamber tuning program, which

provided drift chamber tuning parameters (most importantly the drift velocity as a function of time), were also used.

PSANAL2 was capable of running in both non-interactive (automatic) and interactive modes. In general, the program was first used in the automatic mode to search for tracks. The method used was to first reconstruct downstream track segments using the drift chamber hits. Such segments could be found easily since only about half of the charged tracks for any particular event reached the downstream chambers. Also, because the downstream tracks were usually well-separated, few spurious permutations were possible. In contrast, the upstream drift chambers were usually filled with many closely-spaced hits, making it difficult to disentangle overlapping tracks. Once the downstream segment had been reconstructed, it was projected through the magnet gap to the emulsion vertex. Drift chamber hits in the upstream chambers within 2.54 cm of the projection were searched for and if found were combined with the downstream hits in a refit of the entire track. Fits for tracks which had a CHISQ/DF larger than 6.0 were discarded. The results of the attempted and successful track reconstructions (both the up-to-down and downstream-only) were compiled in the output file PRINT.DAT.

At this point the results of the track reconstruction were

manually compared with the emulsion data. The information for tracks whose angles corresponded well with those in the emulsion were retained for later sessions with PSANAL2.

In the interactive mode it was possible to select various hits in an attempt to find up-to-down or up-only tracks, guided by the visual appearance of the hits and the slopes of the emulsion tracks. It was not possible to interactively fit downstream-only track segments nor did an interactive routine exist for the kinematic fitting of Vees, that is, neutral particles which decayed in the drift chambers or in the magnet gap. Along with the upstream and downstream drift chambers in all three views, visual displays of the TOF II counters, the calorimeter counters which contained signals, and of the entire lead glass array could be made on both a Tektronix scope terminal and on paper copies.

The identification of the charged particles was done by several means. The identification of a charged particle as a muon was done within the PSANAL2 program, using the criterion that a signal be observed in the muon counters within 2.5 standard deviations of the point predicted by the downstream drift chamber track. Every charged track was examined to see if it satisfied this criterion.

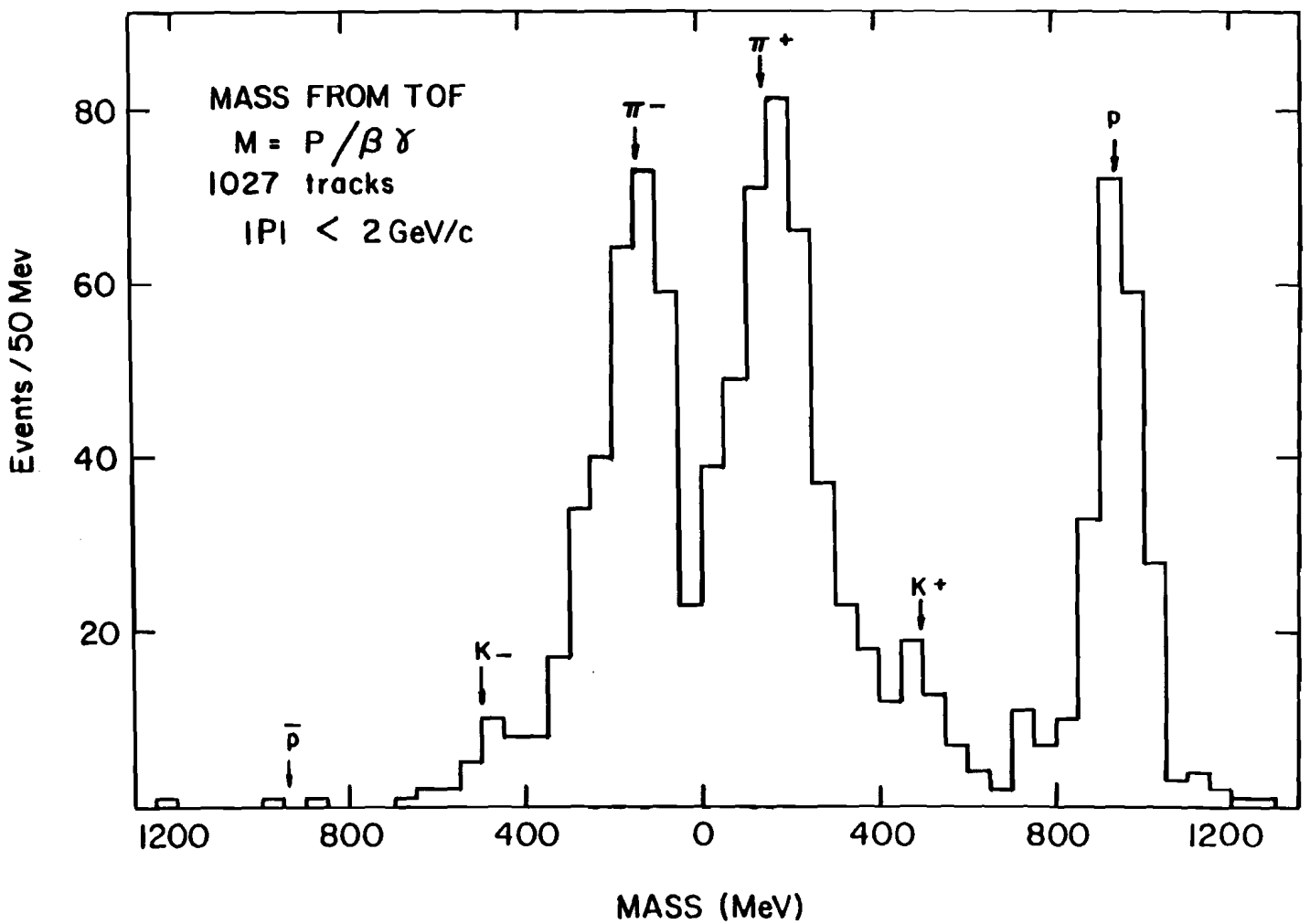

Figure 28. The mass spectrum found using time-of-flight.

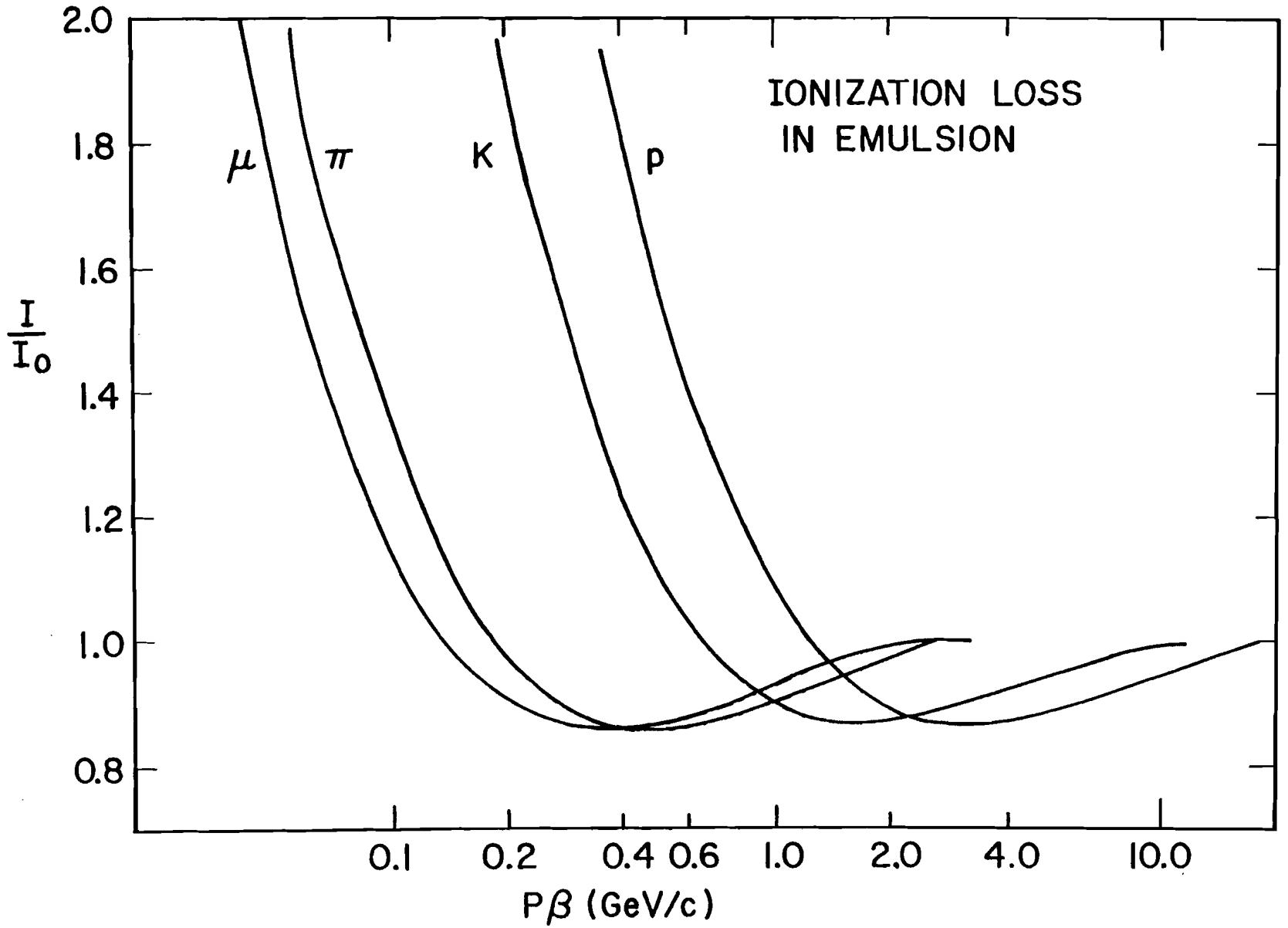

Figure 29. Relative ionization loss in emulsion as a function of $p\beta$ for various particles.

The identification of a charged particle as an electron or positron was done manually after the examination of the lead glass system. Particles which deposited energy in a lead glass block approximately equal to their momentum measured using the drift chambers, were considered to be electrons. (In fact the measurement of the energy deposited in the lead glass should be the more accurate since it included the energy of the photons radiated by the electron or positron through the bremsstrahlung process.)

Charged particles not identified as a muon or as an electron were considered to be hadrons. For particles with momenta greater than 700 MeV/c and less than 5 GeV/c hadron identification was possible using TOF and emulsion measurements. Pions could be distinguished from kaons up to 2.5 GeV/c and kaons could be separated from protons up to 5 GeV/c at the 90% confidence level. Figure 28 shows the mass spectrum observed using TOF. The relative ionization loss in the emulsion versus $p\beta$ for several charged particles is shown in Figure 29.

The next stage in the process involved an analysis of the lead glass system. Paper copies of the output of the program PSANAL2 were manually examined. The invariant masses of candidates for π^0s were calculated using all possible permutations of the lead glass blocks in which was deposited

energy not associated with incident charged particles. Candidates within one standard deviation of the π^0 mass were retained for later kinematic fitting. Isolated blocks which could not be used to form π^0s were later used in the invariant mass calculations of the systems $F^* \rightarrow F\gamma$ and $D^* \rightarrow D\gamma$.

The hadron calorimeter was also examined manually. Energy deposited in the calorimeter which could not be attributed to that of incident charged hadrons was considered as evidence of neutral hadrons. In this regard, it was useful to refer back to the drift chambers for evidence of a K^0. It was not usually possible to measure the angles and momenta of K^0 although such was possible if the hadron shower started in the lead glass array, which had much finer angular resolution.

Having reconstructed charged and neutral particles from both the primary and secondary vertices, the overall kinematic fit of the decay could be accomplished. The hadronic masses used in the kinematic fit were based on TOF identifications when these were available. When a particle was not identified at the 90% confidence level (because it was too energetic or it did not pass through the TOF II paddles) separate calculations were performed for every possible hadron particle identification. If several of the decay particles were unidentified, the analysis of the event became much more tedious because of the additional hypotheses.

Two programs were used in the kinematic fitting -- TESTKIN and ZEROC.

TESTKIN was used for constrained fits, that is, in cases where the number of independent equations describing the decay exceeded the number of unknown parameters. For a kinematic fit performed on one decay vertex, all of the variables are linked by 4 independent equations of momentum and energy conservation. The program, TESTKIN, was also capable of simultaneously fitting two vertices, in which case there are eight independent equations of momentum and energy conservation.

In order to perform a constrained fit it was necessary to know the angles (dx/dz and dy/dz), the momentum, and the mass for each decay particle. These parameters could either be constants, as is the case with the masses, or measured parameters which could be shifted slightly during the fitting. In general the constrained fitting proceeded in two steps. Initially, a 2-constraint fit was performed in which the mass and the momentum of the parent were calculated. Then a 3-constraint fit was carried out in which the only quantity to be fitted by the program was the momentum of the parent. The mass of the parent was assumed to be that of a D^o (1863 MeV/c^2), $D^{\pm}$ (1868 MeV/c^2), $F^{\pm}$ (2030 MeV/c^2), or Λ_c^+ (2285 MeV/c^2). Usually Cabibbo-suppressed decay modes were not used in the 3-constraint fits.

The confidence level for the 3-constraint fit indicated how well the event could be kinematically fitted when a particular parent and decay mode were forced upon it. Only those hypotheses for which the 3-constraint confidence level was greater than 1% were retained.

ZEROC performed zero-constraint calculations of momentum and mass for events containing unobserved neutral secondaries (neutrinos, neutrons, K^o, and π^o, which could not be reconstructed). In this case the four independent equations of momentum and energy conservation are balanced by four unknown quantities -- the momentum of the decaying particle and the momentum, dx/dz and dy/dz of the unobserved neutral particle. A particular parent mass must be assumed in order to solve the equations. ZEROC also allowed one to step through a range of parent masses from which one could generate a parabola-shaped, -1-constraint curve of the mass of the particle versus its momentum. This curve was used to indicate the minimum mass which the decaying particle could have for a particular decay mode. In general there are two momentum solutions for the zero-constraint calculation (the two points at which a horizontal line crosses the parabola). For events for which the minimum of the -1-constraint curve is at the mass of the assumed parent, there is only one solution. For some events, in particular those with

missing π^o or K^o, it was possible to eliminate one of the solutions because the angles and momentum predicted for the K^o or π^o were ruled out by the spectrometer.

If the decay contained a muon or electron, the existence of a neutrino was necessary for lepton conservation. In addition, the neutrino could be used to balance the transverse momentum at the decay vertex. For these events, the only possible method of analysis was with ZEROC, since the neutrino was never observed.

Other events were initially analysed for charged only decay modes. Transverse momentum imbalance at the decay vertex and a fitted mass far below that of the known charmed particles, yet too high for a strange particle, usually necessitated the addition of at least one neutral secondary. (Four of the neutral decay candidates were in fact consistent with the decay of strange particles.) This neutral secondary could be a π^o, reconstructed using the lead glass, or a K^o or n, inferred from the hadron calorimeter.

For those events containing π^o candidates, constrained kinematic fits for the decay could often be made, since the angles and the momentum of the π^o had usually been calculated. Each fit using TESTKIN assumed a particular decay hypothesis. If the event contained more than one π^o candidate, separate two-

vertex fits (the charm decay and the π^o decay) were performed using the different possibilities in order to minimize the chi-squared of the fit.

Constrained fits could not be made immediately for events which contained K^o and n, since the coarseness of the hadron calorimeter was so great that it was useful mainly as an indicator of the presence of neutral hadrons rather than as a detector which measured angles and momenta. Zero-constraint calculations were made for all possible decay modes. The results of these calculations, in particular the predicted angles and momentum of the missing K^o could then be compared to the spectrometer data. Often a K^o decay in the drift chambers could be manually reconstructed or at least pieced together if evidence in the form of downstream segments existed. Or, the hadron shower could have begun prematurely in the lead glass since the blocks were 2/3 of an interaction length. Thus, angles and momenta for the K^o could be estimated and then used as input for a constrained fit for the charm decay.

Several other calculations were made in order to improve the interpretations of the events. The existence of excited states $D^{\pm *}$, $F^{\pm *}$, and Σ_c and Σ_c^* was systematically searched for in each event using energy observed in the lead glass (which had not already been used in the fit of the ground state charmed

particle) to construct π^0 and γ. The invariant masses of pairs of the charged and neutral decay particles were calculated in order to observe evidence of resonant states such as K^* and η.

Associated with each decay hypothesis is the proper decay time of the event, which is calculated using the formula

$$t = \frac{L}{\beta\gamma c} = \frac{Lm}{pc}, \tag{37}$$

where L is the decay length, p is the momentum, m is the mass and c is the speed of light.

The interpretations of events as either Λ_c^+ or $F^\pm$ could be easily made. A proton or Λ^0 in the decay products signified a baryon parent hypothesis. In the case of the $F^\pm$, the minimum mass of each of the events, that is, an all-pion hypothesis is too high to be consistent with the mass of the D^+. For these reasons the charged particle data sample has been divided into three categories -- Λ_c^+, $F^\pm$, and $D^\pm$/ambiguous -- for the purpose of the lifetime calculations.

6. LIFETIME AND MASS CALCULATIONS

The method of maximum likelihood [Frodesen, 1982] may be used to estimate an unknown parameter u, from a set of n measurements $x_1,\ldots,x_n$. Given the probability density function $f(x_i|u)$, the likelihood function

$$\mathcal{L}(u) = \prod_{i=1}^{n} f(x_i|u), \tag{38}$$

where $\mathcal{L}(u)$ represents the joint probability of the observations for a fixed u. The best estimate for the parameter u is that which maximizes $\mathcal{L}(u)$.

For a particle decaying with lifetime, τ, and an exponential decay distribution, the probability density function, assuming all measurements of the decay time, t_i, are equally likely, is given by

$$f(t_i|\tau) = \frac{1}{\tau} e^{-t_i/\tau}. \tag{39}$$

If the detection efficiency, $\epsilon(l_i)$, for the decay lengths, l_i, is not constant, the density function becomes

$$f(t_i|\tau) = \epsilon(l_i)\frac{1}{\tau}\frac{e^{-t_i/\tau}}{A_i(\tau)}, \tag{40}$$

where $A_i(\tau)$ is a normalization factor given by

$$A_i(\tau) = \int_0^\infty \frac{1}{\tau}\, \epsilon(\frac{t}{t_i} l_i)\, e^{-t/\tau} dt. \tag{41}$$

The normalization factor, $A_i(\tau)$, is necessary to insure that

$$\int_0^\infty f(t_i|\tau)dt = 1. \tag{42}$$

The likelihood function is thus given by

$$\mathcal{L}(\tau) = \prod_{i=1}^{N} f(t_i|\tau) \tag{43}$$

$$= \prod_{i=1}^{N} \epsilon(l_i)\frac{1}{\tau}\frac{e^{-t_i/\tau}}{A_i(\tau)}. \tag{44}$$

The best estimate of the lifetime, τ, is that which maximizes $\mathcal{L}(\tau)$ $(\mathcal{L}_{max})$. The one standard deviation (68.3% confidence level) limits on the lifetime may be calculated by finding the values of τ for which $\mathcal{L}(\tau) = e^{-0.5}\mathcal{L}_{max}$. The two standard deviation (95.4% confidence level) limits are those τ values for which $\mathcal{L}(\tau) = e^{-2}\mathcal{L}_{max}$.

6.1 The $F^{\pm}$

The four events shown in Table 3 were fitted as decays of the $F^{\pm}$. A photomicrograph of one of the events appears in Figure 30. The minimum masses exclude $D^{\pm}$ interpretations for the first

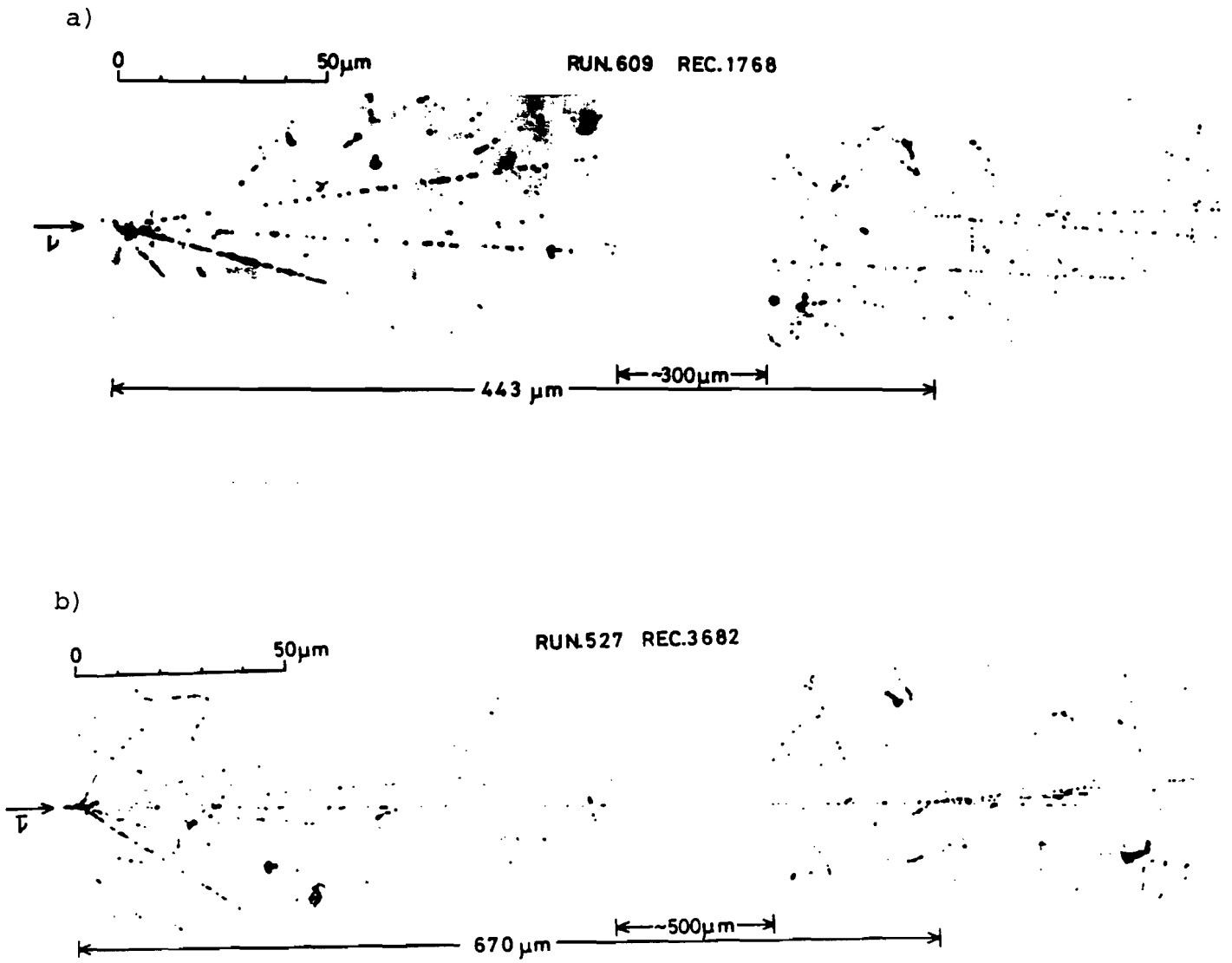

Figure 30. a) A photomicrograph for a neutral charm decay.
b) A photomicrograph for event 527-3682, an F decay candidate.

three events. The events are discussed individually in the Appendix.

Using the method of maximum likelihood, the $F^{\pm}$ lifetime is determined to be $1.9^{+1.3}_{-0.7} \times 10^{-13}$ s. The average $F^{\pm}$ mass, 2057±38 MeV/c^2, was found by fitting a Gaussian distribution to the Gaussian ideograms of the masses of the four $F^{\pm}$ events, as shown in Figure 31. The solid line represents the sum (normalized) of the four individual Gaussian ideograms. The dashed line is the Gaussian fit to the data. The lifetime changes to 2.0×10^{-13} seconds if the last, low momentum event is not considered.

TABLE 3. Fitted $F^{\pm}$ Decays

Event Number	Decay Length (μ)	Decay Hypothesis	2-C Mass (MeV/c^2)	P_{charm} (GeV/c)	Decay Time (10^{-13} s)
527-3682	670±4	$F^- \to \pi^-\pi^-\pi^+\pi^0$	2021±60	12.4±0.3	3.65±0.09
597-1851	130±11	$F^+ \to K^+\pi^-\pi^+K^0$	2082±71	8.8±0.2	1.00±0.09
638-9417	153±8	$F^+ \to K^+K^-\pi^+\pi^0$	2077±51	6.1±0.1	1.69±0.09
671-7015	65±5	$F^+ \to K^+K^0$	2048±112	2.9±0.1	1.57±0.10

Figure 32 shows the Gaussian ideograms for the masses of all events for which Cabibbo-favoured $F^{\pm}$ decay modes were possible. These are the decay modes $K^+K^-(n\pi)$, $K^+K^0(n\pi)$, $K^-\bar{K}^0(n\pi)$, and $(n\pi)$, where $(n\pi)$ stands for any number of charged and neutral pions.

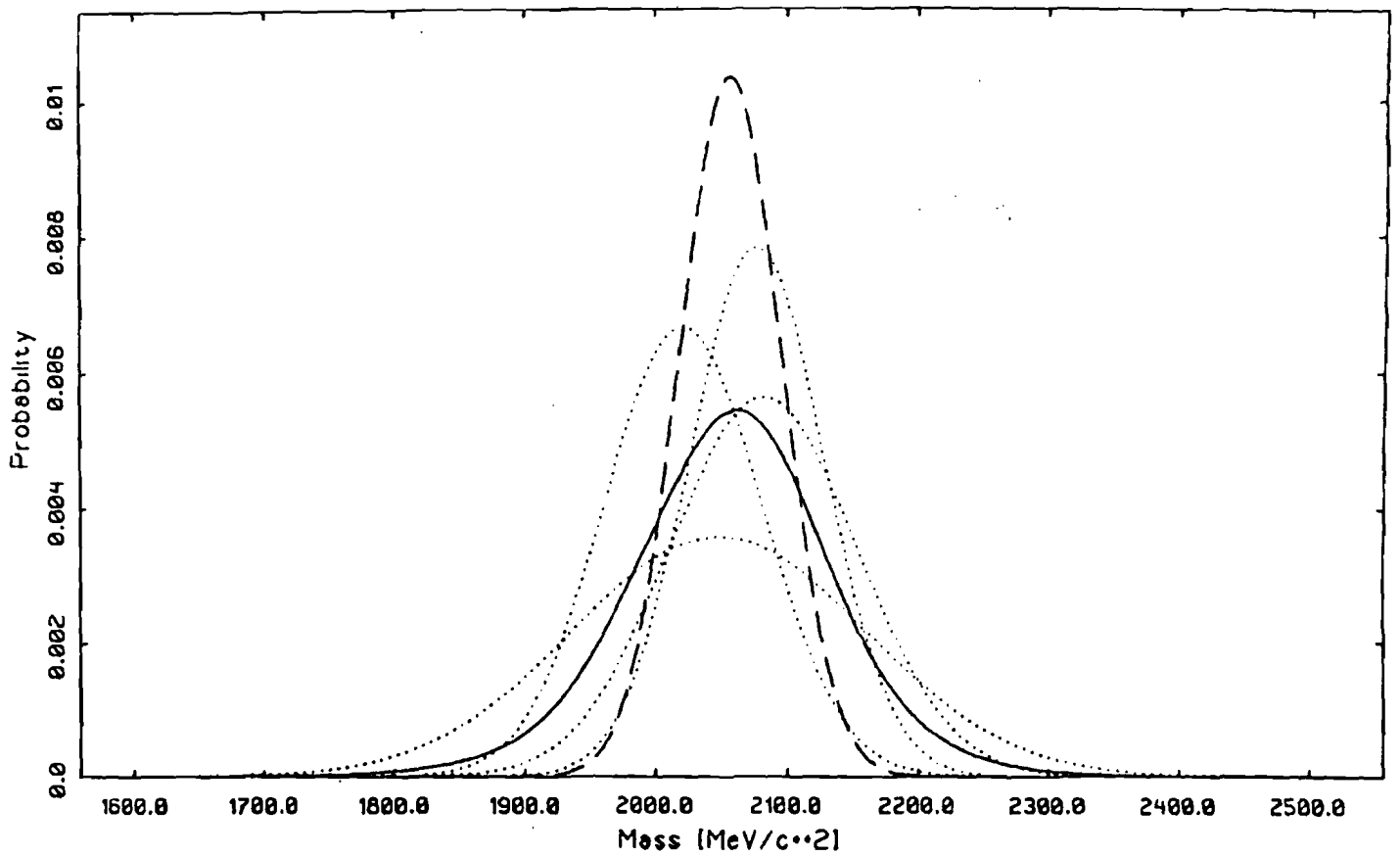

Figure 31. Gaussian ideograms for the four fitted $F^{\pm}$ events, shown by dotted lines. The solid curve is the sum (normalized) of the four dotted lines. The dashed line is the Gaussian fit to the four entries, which has a mean of 2057 MeV/c^2, a standard deviation of 39 MeV/c^2 and a CHISQ of 0.64. The peak of the solid curve is at 2064 MeV/c^2.

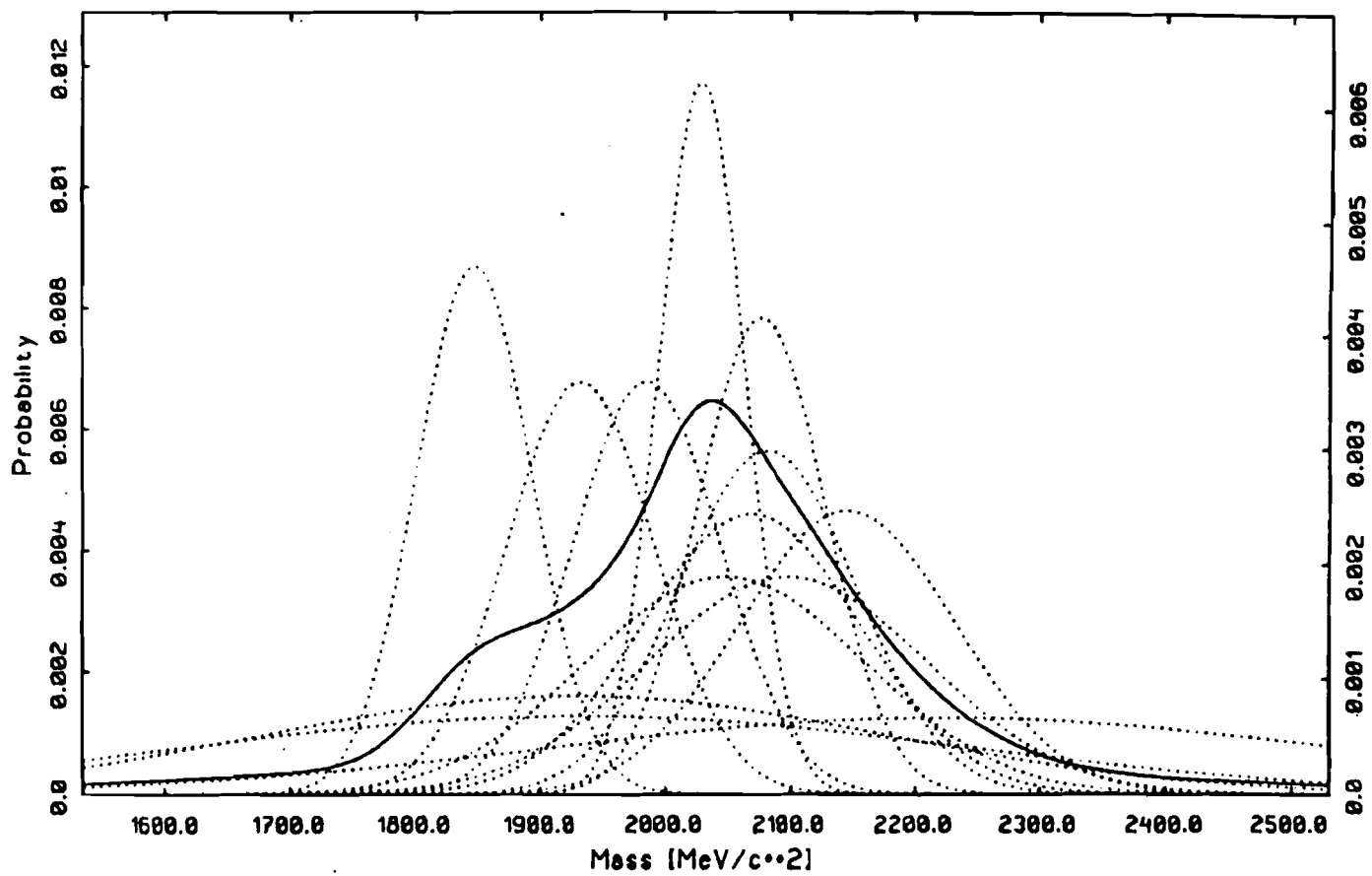

Figure 32. Gaussian ideograms of the 2-C masses for all events with Cabibbo-favoured $F^{\pm}$ decay modes. The solid curve is equal to a constant times the sum of dotted entries. The peak occurs at 2037 MeV/c^2.

Most of these events, which have multiple acceptable decay hypotheses, are discussed later as part of the $D^{\pm}$ sample. The solid line in the figure represents the normalized sum of the 13 individual ideograms. The peak of this distribution appears at 2039 MeV/c^2. There is also a less pronounced peak occurring at approximately 1850 MeV/c^2. This may be interpreted as the mass of the $D^{\pm}$ for its Cabibbo-suppressed decay modes.

F^* Production

TABLE 4. Summary of F^* Production

Event	F^* Mass (MeV/c^2)	Q^2 (GeV^2)
527-3682	2163±21	2.69±0.11
597-1851	no candidate	6±3.5
638-9417	2136±23 2124±23	9.57±0.82
671-7015	2155±35	0.10±0.03

Table 4 gives the $F^* \rightarrow F\gamma$ candidate masses, where the mass of the F has been constrained to be 2030 MeV/c^2, and the Q^2 values for the four F events. The average F^* mass is 2151±14 MeV/c^2. Q^2 is the standard scaling variable for lepton reactions:

$$Q^2 = -(p_\ell - p_\ell')^2$$

where p_ℓ is the 4-momenta of the incident lepton, in our case the ν_μ, and p_ℓ' is the 4-momenta of the final state lepton, the μ^- for charged current interactions.[5] For charged current interactions, Q^2 is a measure of the momentum transferred through the W^+, which is emitted by the ν_μ, to the target nucleus which then becomes part of the final hadronic system.

Along with the usual mechanism for neutrino charm production in which the W^+ interacts with a valence or sea quark of the target nucleus to produce charm, it is expected [Gaillard, 1975] that diffractive production of charm should contribute significantly to the rate for F^* production. In this mechanism, the W^+ itself "decays" into a $c\bar{s}$ pair, to which it couples with strength $\cos\theta_c$. The $c\bar{s}$, which is produced with $J^P = 1^-$, is an F^* which decays electromagnetically to $F\gamma$. For such a process, the momentum transferred to the hadronic system, Q^2, should be small, since the target quarks are not struck by the W^+.

Based on the small sample size, it is difficult to conclude how significant the contribution of diffractive production is to

---

[5]For event 597-1851, the Q^2 value is an estimate, since the μ^- is not observed.

F^* production. Two of the F^* events have relatively low Q^2, although the interpretation of event 671-7015 as the decay of a charmed particle is subject to some doubt because of its low momentum. The ratio of $F:F^*$ production (at the primary vertex) is expected to be 1:3 on the basis of spin counting. The data is in agreement with this ratio -- three of the four F events are consistent with the decay $F^* \rightarrow F\gamma$.

6.2 The Λ_c^+

The eight decay candidates shown in Table 5 have been identified as Λ_c^+. Each of these events, which are discussed individually in the Appendix, has an identified baryon in the decay products.

The lifetime of the Λ_c^+ obtained by the maximum likelihood method is $2.3^{+1.0}_{-0.7} \times 10^{-13}$ s.

The invariant masses of all possible $\Lambda_c^+\pi$ combinations are shown in Table 6 and plotted using Gaussian ideograms in Figure 33. Most events contribute more than one ideogram, since each event can have several $\pi^\pm$ or π^0. Both the $\Lambda_c^+\pi^+$ (Figure 34) and the $\Lambda_c^+\pi^-$ (Figure 35) plots show two-peak structures which contribute to the two prominent peaks of Figure 33. These plots do not change significantly if the data is restricted to only

TABLE 5. Λ_c^+ Decays

Event Number	Decay Length (μ)	Decay Hypothesis	Fitted Mass (MeV/c^2)	P_{charm} (GeV/c)	Decay Time (10^{-13} s)
476-4449	27.7±2.8	$\Lambda_c^+ \to \pi^+\pi^- p(K^o)$	0-C	4.65	0.45±0.05
498-4985	180±5	$\Lambda_c^+ \to \Lambda^o\pi^+\pi^-\pi^+$	2274±44	8.30	1.65±0.05
499-4713	366±6	$\Lambda_c^+ \to \Sigma^o\pi^+$	2220±25	3.97	6.99±0.14
549-4068	20.6±2.0	$\Lambda_c^+ \to p\pi^+K^-(\pi^o)$	0-C	1.7 2.6	0.92±0.09 0.60±0.06
602-2032	283±5	$\Lambda_c^+ \to p\pi^-\pi^+(K^o)$	0-C	3.3 6.4	6.51±0.12 3.36±0.06 (4.48±1.4)
610-4088	221±4	$\Lambda_c^+ \to \pi^+\pi^+\pi^-(\Lambda^o)$	0-C	6.4	2.62±0.05
650-6003	40.6±2.0	$\Lambda_c^+ \to \pi^+\pi^+\pi^-(\Lambda^o)$	2135±75	5.77	0.53±0.30
567-2596	175±5	$\Lambda_c^+ \to p(K^o)$	0-C	6.2	2.1±0.1

pions which have up-to-down tracks. However, for both the $\Lambda_c^+\pi^+$ and $\Lambda_c^+\pi^-$ plots, it is possible to eliminate one of the peaks by excluding, in each case, one of the events.[6] Figure 36 shows the invariant mass plot for this subset (4 events) of the data.

Several theoretical papers [de Rujula, 1975; Lee, 1977; Copley, 1979] have addressed the topic of charmed baryon masses.

---

[6]For the $\Lambda_c^+\pi^+$ case this is accomplished by eliminating the 2446±5 entry; for the $\Lambda_c^+\pi^-$ case, the entries for event 567-2596.

TABLE 6. $\Lambda_c^+\pi$ Invariant Masses (MeV/c^2)

Event	$\Lambda_c^+\pi^+$	$\Lambda_c^+\pi^-$	$\Lambda_c^+\pi^0$
476-4449	2444±28	2488±26*	2590±49
	2919±41	2506±28*	2720±58
	2451±29*	2497±23*	
	2424±25		
	3470±846*		
499-4713	2494±16		
549-4068	3448±30		
	2543±31*		
567-2596	2499±15	2473±13	
		2550±13	
		2558±22	
610-4088			
650-6003	2728±80	2763±83	
	2430±83		
498-4985	2496±9*	2911±39	
	2446±5	2611±30*	
602-2032			

*up-only tracks for the pion

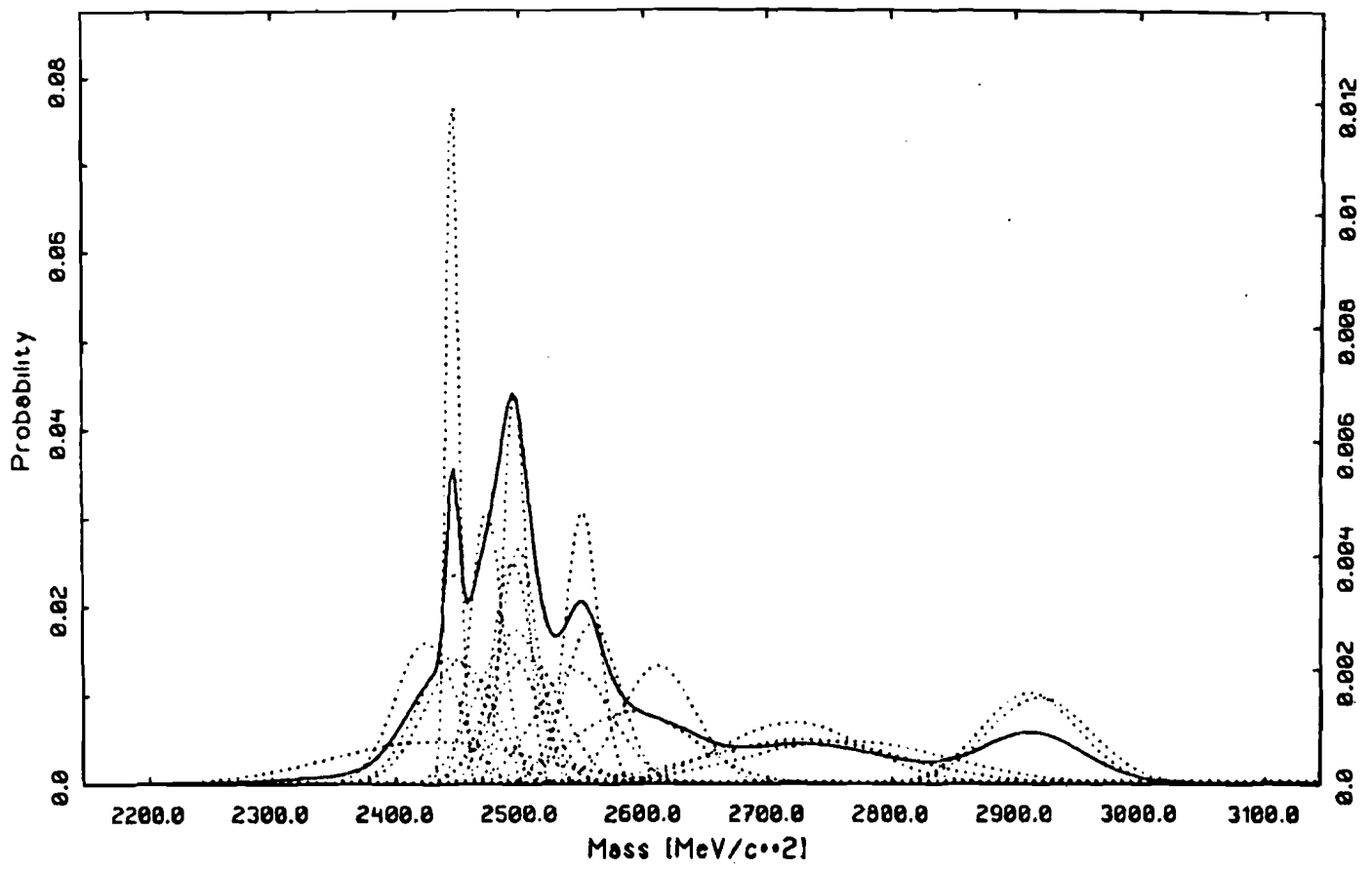

Figure 33. Gaussian ideograms for the invariant masses of all $\Lambda_c^+ \pi$ combinations. Each Λ_c^+ may contribute more than one entry. The solid line is equal to a constant times the sum of the dotted entries.

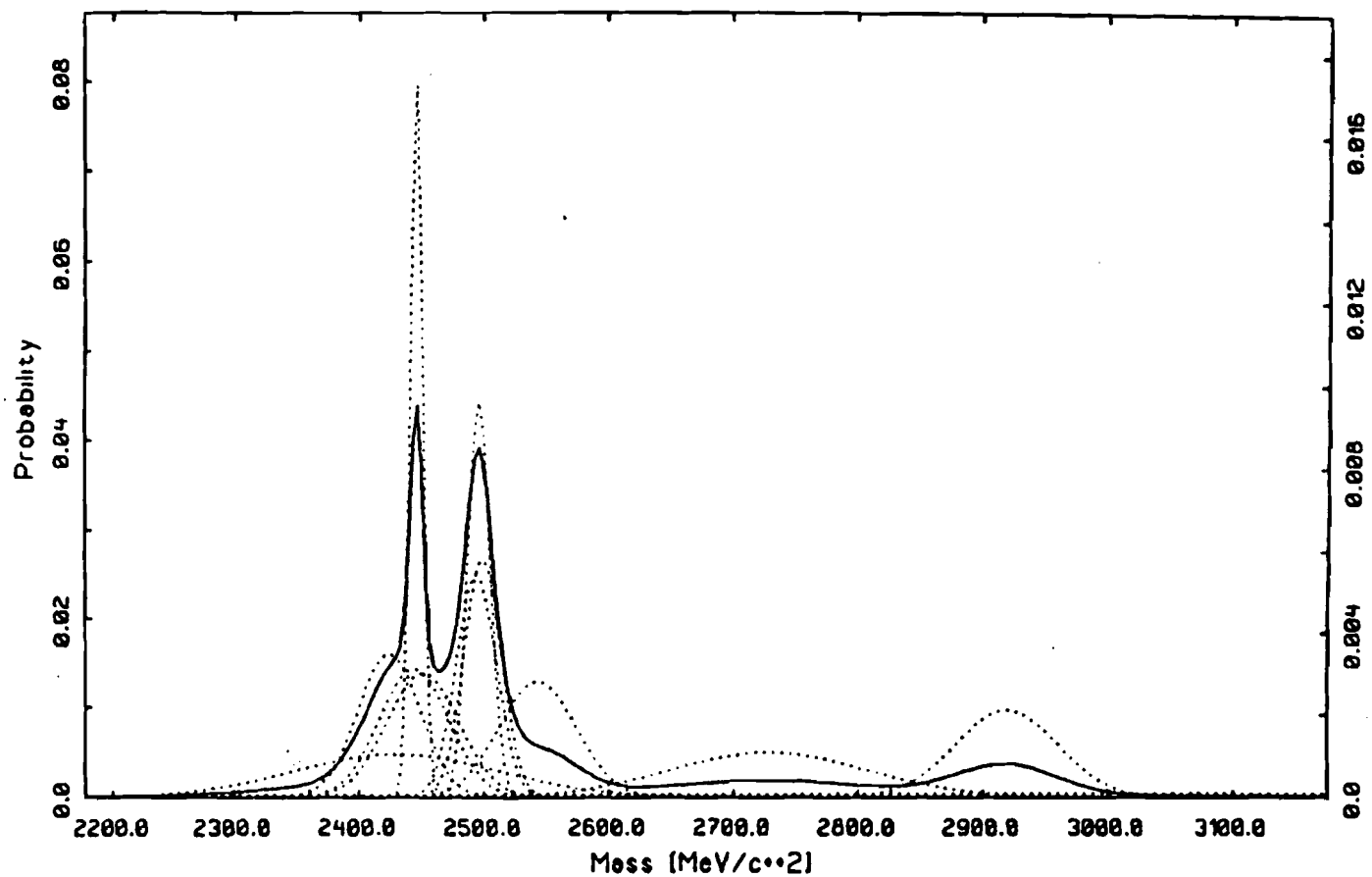

Figure 34. Gaussian ideograms for the invariant masses of all $\Lambda_c^+ \pi^+$ combinations.

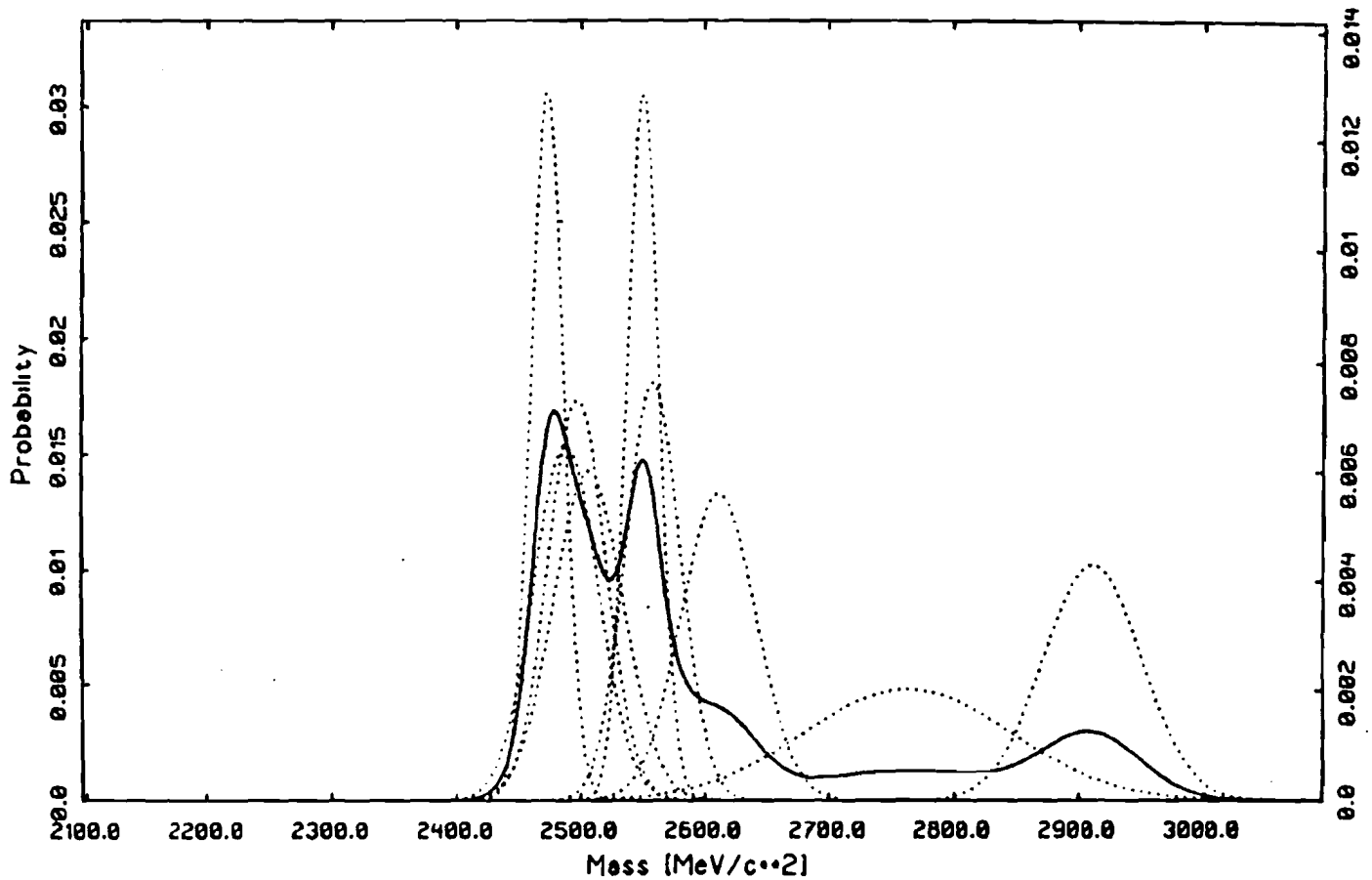

Figure 35. Gaussian ideograms for the invariant masses of all $\Lambda_c^+ \pi^-$ combinations.

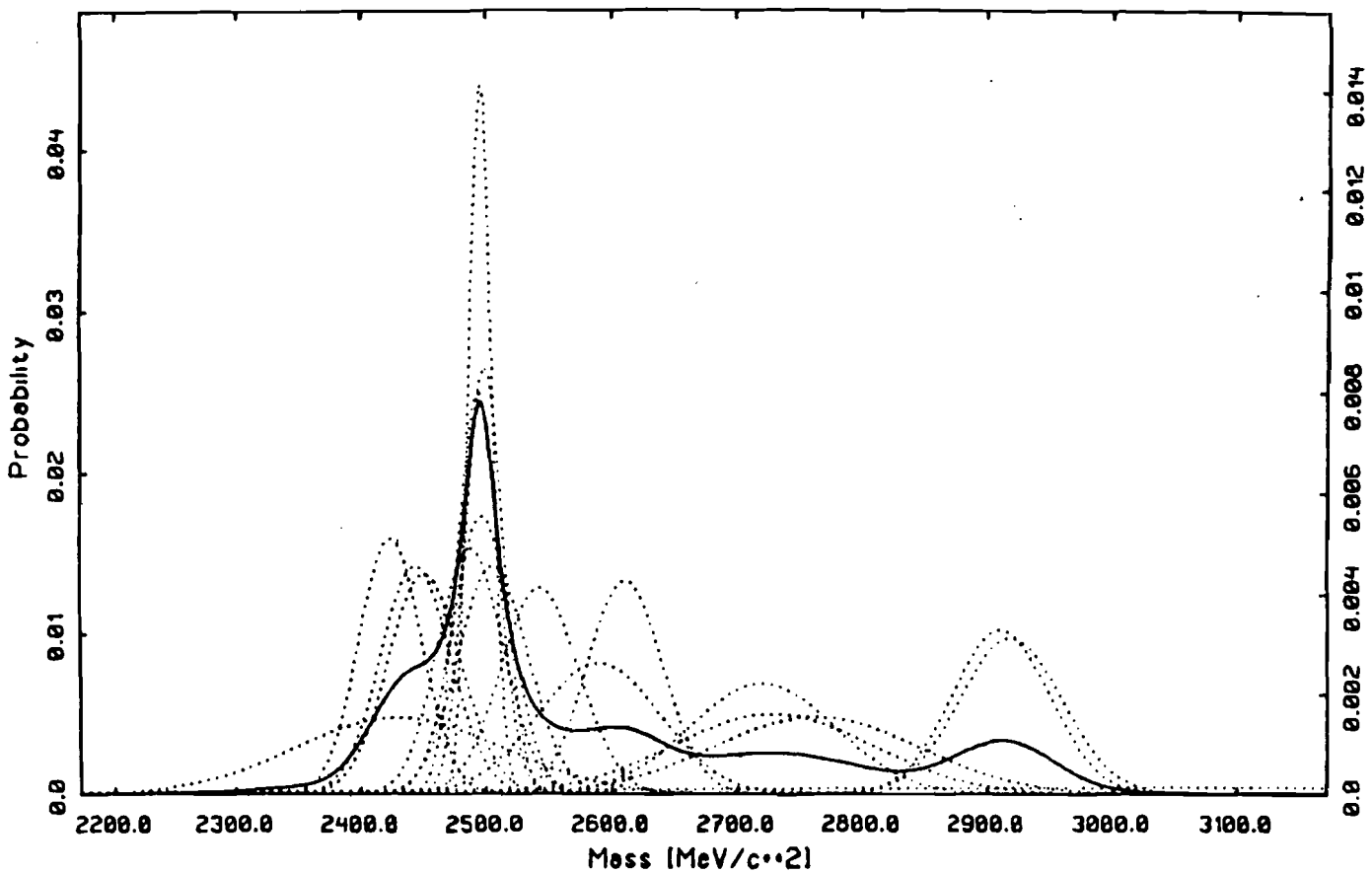

Figure 36. Gaussian ideograms for the masses of a restricted set of $\Lambda_c^+\pi$ combinations. The data plotted represents entries for four Λ_c^+ events. The peak is at 2495 MeV/c^2.

These predict the masses of the Σ_c triplet and the Σ_c^* triplet to be separated by about 60 MeV/c^2 and to be approximately 2500 MeV/c^2. Both the Σ_c and the Σ_c^* are expected to decay to the Λ_c^+ by emission of a pion.

The evidence for the existence of these two charmed baryon states is not compelling, given that one of the invariant mass peaks can be made to disappear by a small restriction to a subset of the data. The existence of at least one charmed baryon with mass ~2495 MeV/c^2 and which decays strongly to the Λ_c^+ is evident. Six of the Λ_c^+ events are consistent with there being such a higher-mass baryon state, which is to be expected, since on the basis of spin counting the ratios of primary production of $\Lambda_c^+:\Sigma_c:\Sigma_c^*$ are 1:3:6 [Campbell, 1980]. Since the latter two decay to the Λ_c^+, only 1 Λ_c^+ of every 10 observed should not be the decay product of a higher-mass charmed baryon.

6.3 The $D^{\pm}$

The $F^{\pm}$ and Λ_c^+ candidates in the charged decay sample are well identified, either by the presence of a baryon in the decay products, or because the minimum mass of the parent excludes a $D^{\pm}$ hypothesis. The remaining 11 charged charm candidates have multiple decay hypotheses. These events are shown in Table 7 and

TABLE 7. Summary of $D^{\pm}$ decays.

Event	Decay Length (microns)	Decay Hypothesis	$p_{F/\Lambda}$ (GeV/c)	p_D (GeV/c)
493-1235	2203	$D^+ \to \pi^+\pi^+\pi^-(K^0)$ $F^+ \to \pi^+\pi^+K^-(K^0)$ $\Lambda_c^+ \to \pi^+\pi^+K^-(n)$	11.5	11.0
512-5761	457	$D^+ \to K^-\pi^+\pi^+\pi^0$ $F^+ \to K^-K^+\pi^+\pi^0$	10.3	10.3
522-2107	13600	$D^+ \to \pi^+\pi^+K^-\pi^0$ $F^+ \to K^+\pi^+K^-\pi^0$ $\Lambda_c^+ \to p\pi^+K^-\pi^0$	24.8	23.7
529-0271	2547	$D^+ \to \pi^+\pi^0(K^0)$ $F^+ \to K^+\pi^0(K^0)$ $\Lambda_c^+ \to p\pi^0(K^0)$	30.2	48.5
533-7152	5246	$D^+ \to \pi^+\pi^0(K^0)$ $F^+ \to K^+\pi^0(K^0)$ $\Lambda_c^+ \to \pi^+(\Lambda^0)$	34.0	42.0
546-1339	2150	$D^+ \to \pi^-\mu^+\pi^+(\nu_\mu)$ $F^+ \to K^-\mu^+K^+(\nu_\mu)$	15.5	16.5
547-3192	185	$D^+ \to \pi^+\pi^+K^-$ $F^+ \to \pi^+\pi^+\pi^-\pi^0$	10.8	9.4
580-4508	2307	$D^- \to e^-\pi^-K^+(\nu_e)$	9.2	9.2
598-1759	1802	$D^+ \to K^-K^+\pi^+\pi^0$ $\Lambda_c^+ \to K^-p\pi^+\pi^0$	18.1	17.7
656-2631	570	$D^+ \to \pi^+K^-\pi^+$ $F^+ \to K^+K^-\pi^+$ $\Lambda_c^+ \to pK^-\pi^+$	32.6	34.2
663-7758	13000	$D^+ \to \pi^+K^-e^+(\nu_e)$ $F^+ \to K^+K^-e^+(\nu_e)$ $\Lambda_c^+ \to pK^-e^+(\nu_e)$	113.5	123.5

discussed individually in the Appendix. Since a large fraction of this sample is expected to be $D^{\pm}$ decays, a 2-dimensional maximum likelihood calculation was performed on this sample in order to extract both the lifetime of the $D^{\pm}$, τ_D, and the fraction of the sample which is $D^{\pm}$, f_D.

The sample is considered to be of two parts: A significant fraction should be $D^{\pm}$ with the corresponding lifetime τ_D and a contaminant part containing $F^{\pm}$ and Λ_c^+ decays with the respective lifetimes 2.0 and 2.3 x 10^{-13} s. This type of analysis can be performed because the $D^{\pm}$ lifetime is different from the lifetimes of the $F^{\pm}$ and Λ_c^+.[7]

The 2-dimensional likelihood function is given by

$$\mathcal{L}(\tau,f) = \prod_{i=1}^{N} \int_0^{\infty} \left[f\epsilon(l_i)\frac{e^{\frac{-m_D l_i}{p_i^D c\tau}}}{A_i^D(\tau)} + (1-f)\epsilon(l_i)\frac{e^{\frac{-m_X l_i}{p_i^X c\tau_X}}}{A_i^X(\tau_X)} \right] e^{\frac{-(t-\tau_X)^2}{\sigma_X^2}}\, dt, \tag{45}$$

---

[7]This was expected since the usual maximum likelihood method yields a lifetime of 12.0 x 10^{-13} s for this sample. The usual method does not, however, address whether the sample is consistent with one parent species.

where m_D = 1868 MeV/c^2, is the mass of the $D^{\pm}$; m_X = 2160 MeV/c^2, is the average of the masses of the $F^{\pm}$ and Λ_c^+; l_i is the decay length for event i; p_i^D is the momentum of event i when interpreted as a $D^{\pm}$; p_i^X is the momentum of event i when interpreted as an $F^{\pm}$ or Λ_c^+; $\tau_X = 2.15 \times 10^{-13}$ s, is the average of the measured $F^{\pm}$ and $\Lambda^+{}_c$ lifetimes; $\sigma_X = 1.8 \times 10^{-13}$ s, is the error in the measured $F^{\pm}$ and Λ_c^+ lifetimes; and the A_i are the normalization constants given by

$$A_i^D = \int_0^{\infty} \frac{1}{\tau_D} (z_D') e^{-t'/\tau_D} dt' \text{ and} \tag{46}$$

$$A_i^X = \int_0^{\infty} \frac{1}{\tau_X} (z_X') e^{-t'/\tau_X} dt'. \tag{47}$$

The integration in Equation 45 is performed in order to take into account the fact that the $F^{\pm}$ and Λ_c^+ lifetimes are measured quantities and as such have errors associated with them. It is assumed that the spread in the measured $F^{\pm}$ and Λ_c^+ lifetimes is Gaussian.

The possible decay hypotheses and averages of the momenta for D and F/Λ interpretations for each of the 11 events are given in Table 7. Using these data the likelihood function, $\mathcal{L}(\tau,f)$ was calculated. A plot of the surface is shown in Figure 37. A contour plot of the surface is shown in Figure 38. The maximum,

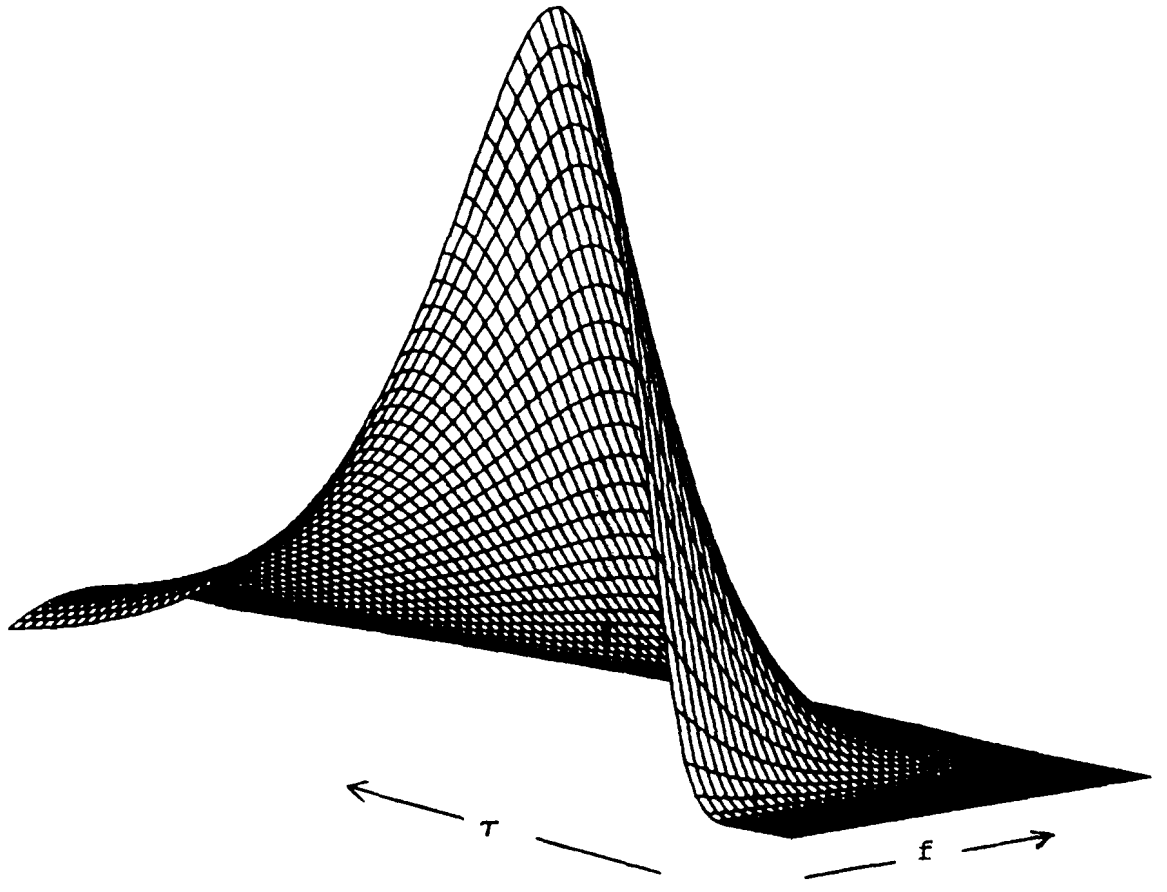

Figure 37. The two-dimensional likelihood function, $\mathcal{L}(\tau, f)$.

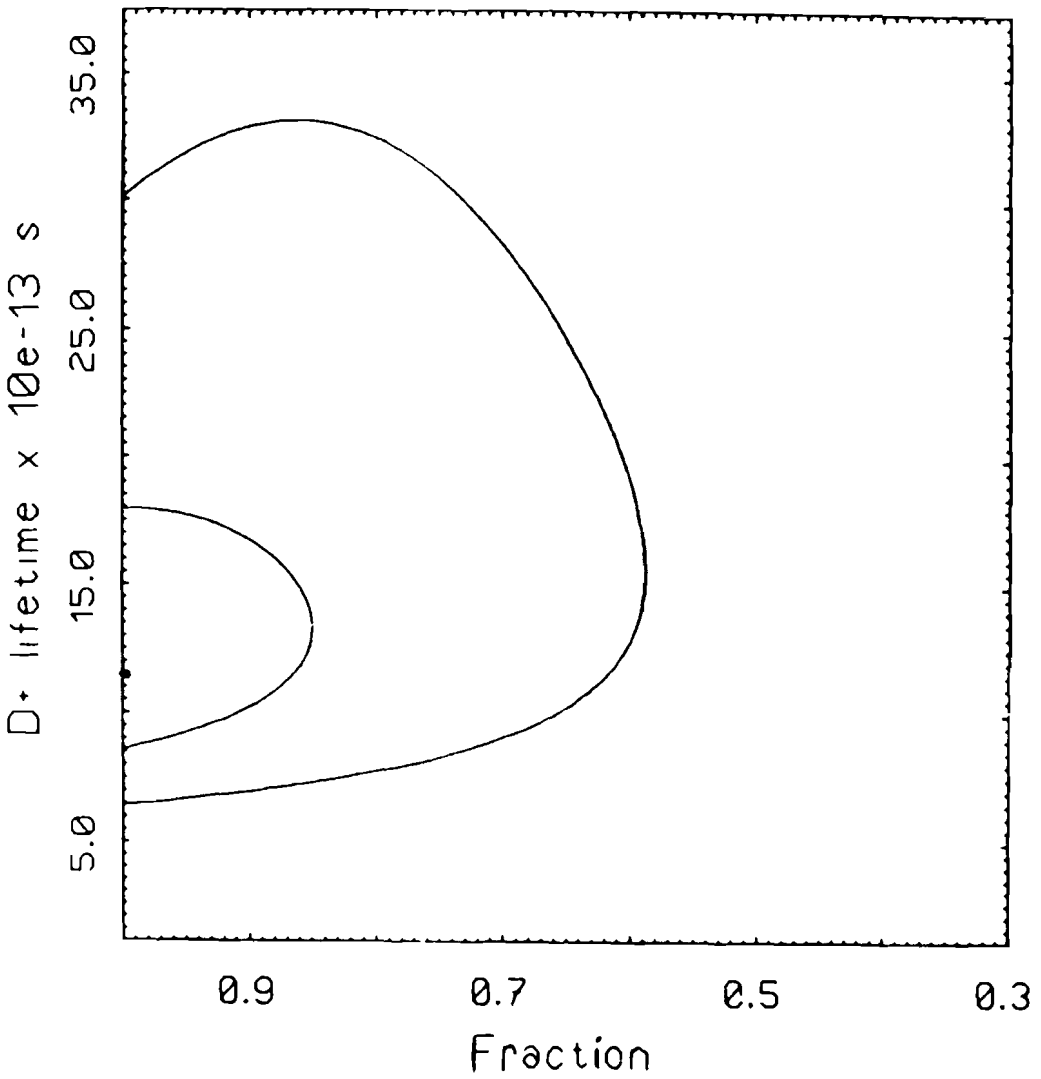

Figure 38. A contour plot of the likelihood function, $\mathcal{L}(\tau, f)$.

$\mathcal{L}_{max}$, of the 2-dimensional likelihood function occurs at τ_D = 11.5 x 10^{-13} s and f_D = 1.0. The first contour, $\mathcal{L} = e^{-0.5}\mathcal{L}_{max}$, represents the traditional 1σ error, provided that only one variable is under consideration while the other remains fixed.[8] By taking the tangents to this contour the errors are obtained: $\tau_D = 11.5^{+6.5}_{-3.0}$ and $f_D = 1.0^{+0.00}_{-0.15}$.

The lifetime of the $D^{\pm}$ is found to be approximately 5 times longer than that of the $F^{\pm}$, the Λ_c^+, and the D^o [Ushida, 1982]. This may be due to the additional annihilation and exchange decay mechanisms which are Cabibbo-favoured for the $F^{\pm}$, Λ_c^+, and the D^o, but which are suppressed for the $D^{\pm}$. The longer lifetime of the $D^{\pm}$ agrees with that measured by a solid-state detector experiment which reports $\tau_{D^{\pm}}$ = 9.5 x 10^{-13} s [Albini, 1982].

Figure 39 is a plot of the invariant masses of the $D^+\pi^o$ combinations. A second smaller peak occurs which is due to the small sample size and which can be made to disappear by eliminating the entries for one event (547-3192). The D^* mass is found to be 2028±19 MeV/c^2.

---

[8] If one considers the joint probabilty for τ and f to be within the contour given by $\mathcal{L} = e^{-0.5}\mathcal{L}_{max}$, then since this probability is the product of the 2 single variable probabilities, the contour does not represent the usual 68% confidence level associated with one standard deviation. Rather the area contained within this contour represents a 46.4% confidence level.

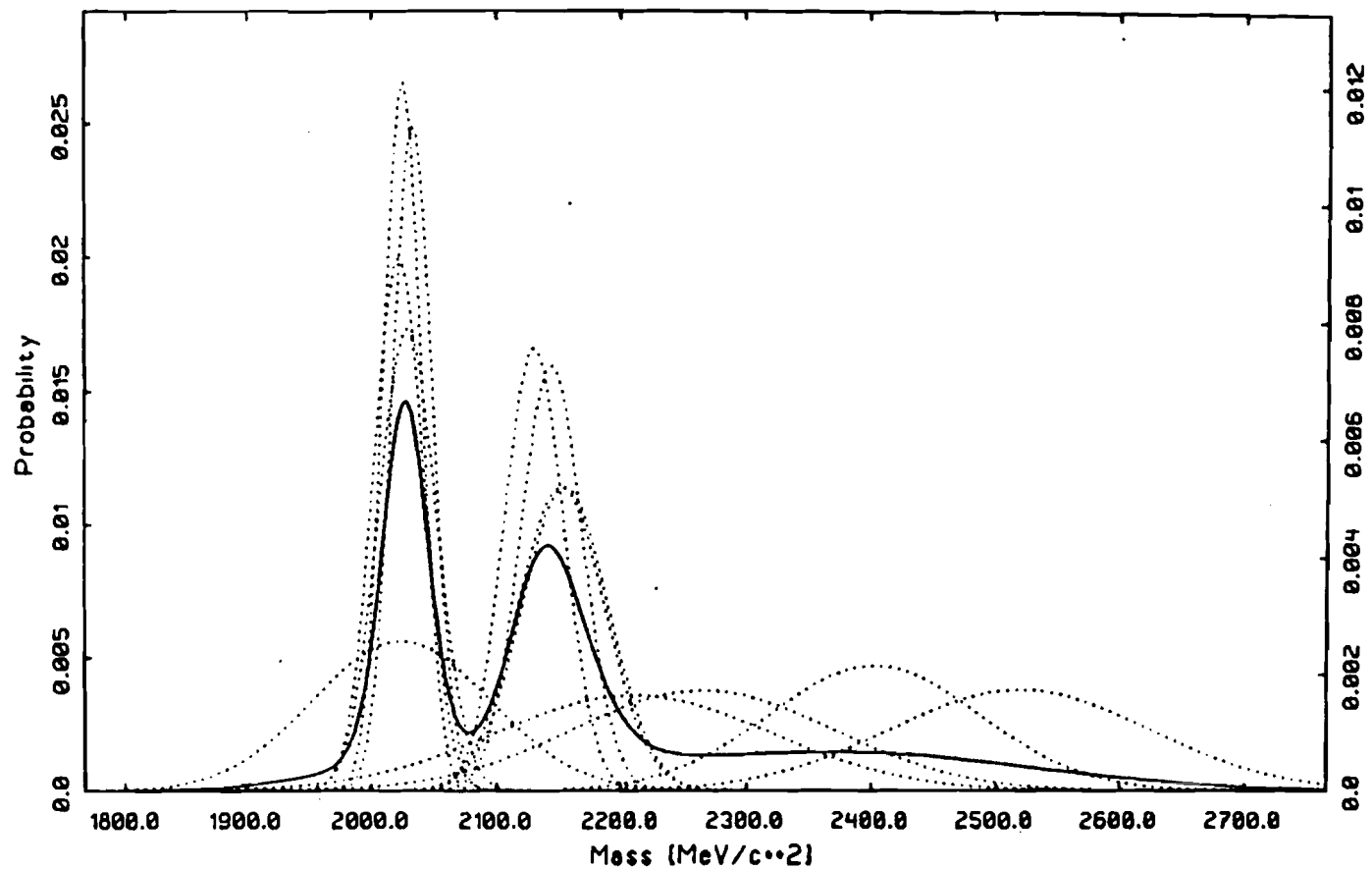

Figure 39. Gaussian ideograms for the invariant masses of all $D^{\pm}\pi^{0}$ combinations. The peak of the solid curve, which is equal to a constant times the sum of the dotted curves, occurs at 2028 MeV/c^2.

TABLE 8. Summary of Exotic Decay Modes

Event	Decay Mode	Fitted Mass (MeV/c^2)
Mesons		
527-3682	$K^-\pi^-\pi^+\pi^0$	2145±57
638-9417	$K^+K^-K^+$	2375±34
656-2631	$K^+K^-K^+$	3200±201
Baryons		
498-4985	$K^+\pi^-\pi^+\Lambda^0$ $\pi^+\pi^-K^+\Lambda^0$	2412±43 2860±24
602-2032	pK^-K^+	2257±12
650-6003	$\pi^+K^+\pi^-\Lambda^0$	2335±41

6.4 The Exotics

Exotic decay hypotheses were possible for some of the charmed decays.[9] The masses for the fitted decay modes are shown in Table 8. Clearly, there is insufficient data to determine a mass for any exotic charm candidate. However, several of the

[9]These are decay modes which are not usually associated with the $D^{\pm}$, $F^{\pm}$, or Λ_c^+, but which might be consistent with 4-quark (meson) or 5-quark (baryon) bound states, for example $c\bar{s}d\bar{s}$ or $cudd\bar{s}$.

hypotheses have masses which are low enough to be those of bound states. Thus, although the data for the charged charm candidates is explained in terms of the decays of the $D^{\pm}$, $F^{\pm}$, and Λ_c^{+}, it does not contradict the possibilty of there being a few charmed exotic hadron decays.

6.5 The Other Multi-prong Events

Four of the multi-prong charm decay candidates were excluded from the lifetime analysis. One of the events occurs in the lucite base and it is therefore impossible to observe the vertex to determine if the event is a nuclear interaction. The other three events, none of which has a constrained fit, are eliminated primarily because the parent momenta are all below 4 GeV/c. Other factors such as low transverse momentum of the decay particles, doubly-Cabibbo-suppressed hypotheses, and extremely long calculated lifetimes, also made these events suspect.

TABLE 9. Summary of Charm Candidates

Parent Particle	Number of Events
Λ_c^+	8
$F^\pm$	4
$D^\pm$	11
Other	4
Total	27

7. A SUMMARY

The lifetimes of the weakly decaying charmed hadrons have been measured using a hybrid emulsion-spectrometer. The lifetime of the $D^{\pm}$ is found to be 11.5×10^{-13} s, a factor of 5 greater than that of the $F^{\pm}$, which is 1.9×10^{-13} s, and that of the Λ_c^+, which is 2.3×10^{-13}s. The mass of the $F^{\pm}$ is measured to be 2057 ± 39 MeV/c^2.

Originally, it was believed that the decay of the weakly decaying charmed particles could be explained in terms of the spectator decay mechanism [Gaillard, 1975], that is, one in which the charm quark decays independently of the other quarks in the decaying parent. This model predicts equal lifetimes for all the low-lying charmed particles. Recently, other models have been proposed which could significantly affect the relative lifetimes. Many of these attribute the shorter lifetime to the additional contributions of annihilation and exchange diagrams, which are Cabibbo-favoured for the D^o, F^+, and Λ_c^+, but which are Cabibbo-suppressed for the D^+. Other models attribute the relative lifetime differences to hard gluon-enhanced amplitudes which interfere destructively for the D^+ [Leveille, 1981].

Although the results of this experiment do not favour either of these two classes, it is interesting to note that one of the

decay candidates for the $F^{\pm}$ has an all-pion decay mode, which does not contain a substantial $s\bar{s}$ component, and which would lend support to the importance of the annihilation mechanism. Since the two classes of models have quite different predictions for the branching ratios of the $F^{\pm}$, the resolution of which model best describes charm decays, awaits the measurement of these branching ratios.

The existence of spin and orbital excitations of the low-lying states was examined by plotting the invariant mass combinations of the $D^{\pm}\pi^{o}$, $F^{\pm}\gamma$, and $\Lambda_c^{+}\pi$. The mass of the D^{+*} -> $D^{+}\pi^{o}$ was found to be 2028 ± 19 MeV/c^2, where the mass of the D^{+} was constrained to be 1868 MeV/c^2.

In taking the invariant masses of the $F^{\pm}\gamma$ combinations, the mass of the $F^{\pm}$ was constrained to be 2030 MeV/c^2. The mass of the F^{+*} -> $F^{\pm}\gamma$ is 2151 ± 14 MeV/c^2, which gives the mass difference, $m_{F^*} - m_F$, 121 ± 14 MeV/c^2.

The invariant masses of all the $\Lambda_c^{+}\pi$ combinations were examined. Both the $\Lambda_c^{+}\pi^{+}$ and the $\Lambda_c^{+}\pi^{-}$ plots show two peaks which appear to be an artifact of limited statistics. When these effects are removed from the data, a distinctive peak at approximately 2495 MeV/c^2 is observed in the $\Lambda_c^{+}\pi^{+}$ and $\Lambda_c^{+}\pi^{-}$ channels. This may be associated with the Σ_c^{*} triplet, which has

$J^P = \frac{3}{2}^+$. Such an interpretation would be consistent with previous experimental evidence for the Σ_c [Baltay, 1979]. The masses of the Σ_c and the Σ_c^* are predicted to be separated by about 60 MeV/c^2 and to be approximately 2500 MeV/c^2. Six of the eight Λ_c^+ events are consistent with the decay of a higher-mass, strongly-decaying charmed baryon state, which is expected theoretically.

APPENDIX A
CHARM EVENTS

A description of the analysis of each of the 23 charged, charm decays is presented below.

Event 476-4449 Λ_c^+

In this event 12 particles are produced at the primary vertex. One of these decays to 3 charged particles after 27.7± 2.8 μ. Of the 3 charged particles one is reconstructed by the spectrometer as a proton with momentum 2.44 GeV/c. The two other particles have up-only tracks. Thus pβ and ionization measurements, which favour pion interpretations for both particles, were made. The transverse momentum imbalance at the decay vertex, before any neutral decay particles are assumed, is 235 MeV/c. An excess of approximately 8 GeV of hadronic energy is observed in the calorimeter and at least three different π^o can be reconstructed using the lead glass data.

TABLE 10. Decay tracks for event 476-4449.

	dx/dz	dy/dz	Momentum (GeV/c)	I/I_o	pβ
P	0.100±0.018	0.094±0.018			
D1	1.513±0.017	-0.092±0.017		1.30±0.04	0.180±0.049
D2	-0.306±0.010	-0.806±0.010		1.05±0.03	0.260±0.068
D3	0.159±0.004	0.224±0.004	2.44±0.02		

None of the reconstructed π^o can be used to balance transverse momentum in the kinematic fit of a charmed baryon

TABLE 11. Summary of unconstrained decay hypothesis for event 476-4449.

Hypothesis	Minimum Mass	Momentum	Decay time	Excited States
	(MeV/c^2)	(GeV/c)	(10^{-13} s)	(MeV/c^2)
$\Lambda_c^+ \to \pi^+\pi^- p(K^o)$	2182±58	4.65	0.45±0.05	

TABLE 12. Summary of constrained decay hypothesis for event 476-4449.

Hypothesis	Mass	Decay Time	2-C Momentum	2-C C.L.	Excited States
	(MeV/c^2)	(10^{-13} s)	(GeV/c)		(MeV/c^2)
$\Lambda_c^+ \to \pi^+\pi^- pK^o$	2365±256	0.36±0.04	5.9±0.2	0.88	2444±28 2488±26 2590±45

decay. A 0-constraint calculation for the hypothesis $\Lambda_c^+ \to \pi^+\pi^- p(K^o)$ was made to predict the position and momentum of the K^o. The low solution is excluded because it gives non-physical values to the various kinematic variables, such as Feynman x. If one uses the angles of lead glass block 39, which contains 1.67 GeV of energy and into which no charged particles are incident, as the angles of the K^o, it is possible to obtain a 2-constraint fit to the decay $\Lambda_c^+ \to \pi^+\pi^- pK^o$, which has a confidence level of 0.88. A 3-constraint fit is not possible since the momentum of

the K^o is unknown. The invariant masses of all the $\Lambda_c^+\pi$ systems were calculated. Several candidates for the Σ_c were found and are given in Table 12.

Event 493-1235 D^+/ambiguous

In this event a charged particle decays to three charged particles after 2203±10 μ. One of the decay particles interacts in the emulsion. Although the other two decay particles are reconstructed as up-to-down tracks in the spectrometer, time-of-flight information is not available for either particle. There is a substantial amount of energy deposited in the hadron calorimeter, 25.7 GeV, which supports the existence of at least one neutral hadron. 21.0 GeV of electromagnetic energy is deposited in the lead glass array, about half of which is due to a reconstructed e^+e^- pair. Two independent π^0 candidates are reconstructed. The transverse momentum imbalance at the decay vertex if a neutral decay particle is not assumed is 653 MeV/c.

TABLE 13. Decay tracks for event 493-1235.

	dx/dz	dy/dz	Momentum (GeV/c)	I/I_0	$p\beta$
P	-0.193±0.011	-0.060±0.005			
D1	0.058±0.011	-0.149±0.005		1.01±0.05	0.555±0.095
D2	-0.304±0.013	0.035±0.006	0.72±0.01	0.96±0.06	
D3	-0.120±0.010	-0.017±0.004	-4.01±0.08	1.01±0.07	

Several 0-constraint decay hypotheses are possible and are

TABLE 14. Summary of decay hypotheses for event 493-1235.

Hypothesis	Minimum Mass	Momentum	Decay time	Excited States
	(MeV/c^2)	(GeV/c)	(10^{-13} s)	(MeV/c^2)
$D^+ \to \pi^+\pi^+\pi^-(K^o)$	1983±171	11.0	12.5±0.5	2053±162
$D^+ \to \pi^+\pi^+K^-(\pi^o)$	1975±180	9.9	13.9±0.7	2040±134
$F^+ \to \pi^+\pi^+K^-(K^o)$	2131±165	10.5	14.1±0.7	2189±108
$F^+ \to \pi^+\pi^+\pi^-(\pi^o)$	1827±186	7.8 16.3	19.0±1.2 9.1±0.3	2160±67
$F^+ \to K^+\pi^+K^-(\pi^o)$	2274±146	9.3	16.0±0.9	2176±88
$\Lambda_c^+ \to \pi^+\pi^+\pi^-(n)$	2306±147	13.1	12.7±0.5	
$\Lambda_c^+ \to \pi^+\pi^+K^-(n)$	2454±142	12.3	13.6±0.6	

given in Table 14. It seems unlikely that the decay is that of a Λ_c^+ since the hypotheses involving a secondary proton are too massive, although zero-constraint calculations exist for hypotheses involving a missing neutron. The data supports both D^+ and F^+ decay hypotheses. The angles and momentum predicted for the missing K^o agree with the location and amount of excess energy in the calorimeter. For the hypotheses involving a missing π^o, the angles predicted for the π^o, are not within the boundaries of the lead glass array. Thus such hypotheses can not be eliminated. None of the reconstructed π^o can be used to balance transverse momentum at the decay vertex.

There are no candidates for the decay $D^{+*} \rightarrow D^{+}\pi^{0}$. Candidates exist for the decays $D^{+*} \rightarrow D^{+}\gamma$ and $F^{+*} \rightarrow F^{+}\gamma$, and the masses of these excited states are given in Table 14.

Event 498-4985 Λ_c^+

In this event a charged particle is observed to decay to three charged particles after 180±5 μ . The three charged particles are reconstructed in the spectrometer, two as up-to-down tracks and one as an up-only track. By TOF measurements and ionization measurements made in the emulsion, all three decay particles are favoured to be charged pions. A vee is observed in the upstream drift chambers. The positively charged decay particle from this vee is reconstructed as an up-to-down track and is identified by TOF as a proton, thus supporting the existence of a π^o. The second decay particle is emitted at a wide angle and therefore has an up-only track.

TABLE 15. Decay tracks for event 498-4985.

	dx/dz	dy/dz	Momentum (GeV/c)	I/I_o	$p\beta$
P	-0.014±0.018	0.132±0.009			
D1	-0.105±0.011	0.158±0.005	3.15±0.03		
D2	0.011±0.010	0.119±0.004	-1.66±0.01	1.02±0.04	
D3	-0.188±0.016	-0.357±0.007	0.59±0.10	0.86±0.04	

TABLE 16. Decay hypotheses for event 498-4985.

Hypothesis	4-C Mass	Decay Time	5-C Momentum	5-C C.L.	Excited States
	(MeV/c^2)	(10^{-13} s)	(GeV/c)		(MeV/c^2)
$\Lambda_c^+ \to \Lambda^o\pi^+\pi^-\pi^+$, $\Lambda^o \to p\pi^-$	2274±44	1.65±0.05	8.30±0.07	0.56	2496±09 2446±05 2911±39 2611±30
$\to \Lambda^o K^+\pi^-\pi^+$, $\Lambda^o \to p\pi^-$	2412±43				
$\to \Lambda^o\pi^+\pi^-K^+$, $\Lambda^o \to p\pi^-$	2860±24				

It is not possible to reconstruct a π^o using the lead glass data -- only one block contains energy which is not due to an incident charged particle, nor does the energy deposited in the calorimeter lend support to the existence of any additional neutral hadrons. The transverse momentum imbalance at the decay vertex is 395 MeV/c, if a neutral decay particle is not added.

Two-vertex constrained fits were performed for the decay $\Lambda_c^+ \to \pi^+\pi^-\pi^+\Lambda^o$ with $\Lambda^o \to p\pi^-$. The momentum of the latter π^- (in addition to those of the Λ_c^+ and Λ^o) was left as an unmeasured parameter to be fitted since it had an up-only track. These fits are shown in Table 16. The existence of higher mass states was

examined by calculating the invariant masses of the $\Lambda_c^+\pi^+$ and $\Lambda_c^+\pi^-$ systems. Also examined were two exotic baryon states.

Event 499-4713 Λ_c^+

A charged particle decays to a single charged particle after $366 \pm 6\,\mu$. The transverse momentum imbalance at the kink vertex is 627 MeV/c. The charged decay particle is reconstructed in the spectrometer and has momentum 2.55 GeV/c. The decay of a Λ^0 is observed in the upstream chambers. The proton from the Λ^0 is reconstructed in an up-to-down track with momentum 1.67 GeV/c. The π^- has an up-only track of momentum 0.274 GeV/c. No excess energy is observed in the lead glass array. The hadron calorimeter contains 16.3 GeV, which supports the existence of a neutral hadron.

TABLE 17. Decay tracks for event 499-4713.

	dx/dz	dy/dz	Momentum (GeV/c)	I/I_0	$p\beta$
P	-0.165 ± 0.016	0.086 ± 0.009			
D	-0.331 ± 0.005	-0.115 ± 0.005	2.55 ± 0.02		

TABLE 18. Summary of decay hypotheses for event 499-4713.

Hypothesis	Mass	Decay Time	3-C Momentum	3-C C.L.	Excited States
	(MeV/c^2)	(10^{-13} s)	(GeV/c^2)		(MeV/c^2)
$\Lambda_c^+ \to \Lambda^o\pi^+$, $\Lambda^o \to p\pi^-$	2157±17	6.53±0.12	4.25±0.03	0.125	
$\Lambda_c^+ \to \Sigma^o\pi^+$, $\Sigma^o \to \Lambda^o\gamma$, $\Lambda^o \to p\pi^-$	2220±25	6.99±0.14	3.97±0.05	0.505	2494±16

Multiple vertex constrained fits were performed for the decay hypotheses:

$$\Lambda_c^+ \to \Lambda^o\pi^+,\ \Lambda^o \to p\pi^- \quad \text{and} \quad \Lambda_c^+ \to \Sigma^o\pi^+,\ \Sigma^o \to \Lambda^o\gamma,\ \Lambda^o \to p\pi^- .$$

The results are shown in Table 18. The decay mode containing a Σ^o is favoured according to the confidence levels. The predicted angles of the γ from the Σ^o do not lie within the boundaries of the lead glass array. The results of the 0-constraint calculations for the decay modes $\pi^+(K^o)$ and $K^+(K^o)$ exclude the possibility of the decay being that of a meson. (The high solutions are incompatible with spectrometer data and the low

solutions are below the nominal momentum cutoff (4 GeV/c) for charmed particles.) The decay is clearly that of a Λ_c^+.

Event 512-5761 D^+/Ambiguous

This decay of a charged particle to three charged secondaries occurs in the vertical emulsion after 457±5 μ. One of the decay particles is identified at the 90% confidence level as a π^+. The two other charged decay particles are excluded as protons but are ambiguous to pion and kaon interpretations. The event cannot be fitted using only the three charged decay particles. The transverse momentum imbalance at the decay vertex, if the existence of a neutral decay particle is not assumed, is 483 MeV/c.

TABLE 19. Decay tracks for event 512-5761.

	dx/dz	dy/dz	Momentum (GeV/c)	I/I_o	$p\beta$
P	0.026±0.004	-0.028±0.004			
D1	0.053±0.003	0.085±0.003	-2.68±0.03		
D2	0.071±0.003	-0.133±0.003	3.31±0.04		
D3	0.071±0.004	-0.206±0.004	1.92±0.01		

There are 11 lead glass blocks in which energy is deposited and at least 10 different (although not independent) π^o can be reconstructed, further complicating the interpretation of the event. Several of the decay hypotheses, selected on the basis of

TABLE 20. Decay hypotheses for event 512-5761.

Hypothesis	Mass	Decay Time	3-C Momentum	3-C C.L.	Excited States
	(MeV/c^2)	(10^{-13} s)	(GeV/c)		(MeV/c^2)
$D^+ \to K^-\pi^+\pi^+\pi_1^0$	1835±38	2.95±0.05	9.65±0.14	0.009	2006±29
$F^+ \to K^-K^+\pi^+\pi_1^0$	2006±36	3.20±0.06	9.63±0.13	0.106	2172±28 2099±22
$D^+ \to K^-\pi^+\pi^+\pi_2^0$	1844±37	2.85±0.05	9.97±0.15	0.097	
$F^+ \to K^-K^+\pi^+\pi_2^0$	2020±35	3.10±0.06	9.94±0.14	0.111	2097±13
$D^+ \to K^-\pi^+\pi^+\pi_3^0$	1841±36	2.76±0.06	10.30±0.16	0.164	
$F^+ \to K^-K^-\pi^+\pi_3^0$	2023±34	3.00±0.06	10.26±0.15	0.212	
$D^+ \to K^-\pi^+\pi^+\pi_4^0$	1827±36	2.82±0.05	10.08±0.15	0.011	
$F^+ \to K^-K^+\pi^+\pi_4^0$	2006±34	3.07±0.06	10.04±0.15	0.016	

π_1^0 uses lead glass blocks 16 and 22

π_2^0 uses lead glass blocks 16 and 23

π_3^0 uses lead glass blocks 16 and 23, 32

π_4^0 uses lead glass blocks 16 and 22, 23

low chi-squared and the fitted masses are given in Table 20. All of the hadronic energy in the calorimeter may be attributed to the charged particles.

All of the decay hypotheses using the decay modes $\pi^-\pi^+\pi^+\pi^0$ and $\pi^-K^+\pi^+\pi^0$ have masses well below that of the D^+ and may therefore be considered unlikely. The chi-squared for those hypotheses involving two independent π^0, that is $\pi^-\pi^+\pi^+\pi^0\pi^0$, $\pi^-K^+\pi^+\pi^0\pi^0$, $K^-\pi^+\pi^+\pi^0\pi^0$, and $K^-K^+\pi^+\pi^0\pi^0$, are too high to be considered acceptable.

Excited charm states D^{+*} and F^{+*} may be postulated. Using energy deposited in the lead glass which has not been used in the π^0 reconstruction, invariant masses for the decay modes $F\gamma$, $D\gamma$, and $D\pi^0$ are calculated. These are shown in Table 20. Since both F^{+*} and D^{+*} hypotheses are possible within the calculated errors, it is unlikely that this event may be rendered unambiguous.

Event 522-2107 D^+/Ambiguous

A positively charged particle decays to three charged particles after 13600±100 μ. All three charged decay particles are reconstructed in the spectrometer, but only one is of low enough momentum, 1.02 GeV/c, to be identified as a π^+. The momenta of the two other particles are 15.8 and 4.4 GeV/c. The transverse momentum imbalance at the decay vertex is 410 MeV/c, if a neutral decay particle is not assumed. The calorimeter contains 27.3 GeV of hadronic energy. A total of 20.9 GeV of energy is deposited in 13 lead glass blocks, from which it is possible to reconstruct more than twenty separate but not independent π^o candidates.

TABLE 21. Decay tracks for event 522-2107.

	dx/dz	dy/dz	Momentum (GeV/c)	I/I_o	$p\beta$
P	0.003±0.006	0.122±0.003			
D1	-0.002±0.010	0.136±0.005	15.77±0.90		
D2	-0.012±0.009	0.072±0.004	1.02±0.01		
D3	-0.065±0.009	0.057±0.004	-4.43±0.07		

TABLE 22. Decay hypotheses for event 522-2107.

Hypothesis	Mass	Decay Time	3-C Momentum	3-C C.L.	Excited States
	(MeV/c^2)	(10^{-13} s)	(GeV/c)		(MeV/c^2)
$D^+ \to \pi^+\pi^+K^-\pi_1^o$	1847±63	35.2±1.2	24.1±0.8	0.253	
$D^+ \to \pi^+\pi^+K^-\pi_2^o$	1846±61	36.3±1.3	23.3±0.8	0.359	
$F^+ \to K^+\pi^+K^-\pi_1^o$	1933±60	36.8±1.4	24.9±0.9	0.173	2122±26 2147±26
$F^+ \to K^+\pi^+K^-\pi_2^o$	1930±57	37.8±1.4	24.2±0.9	0.210	2150±32 2126±20
$\Lambda_c^+ \to p\pi^+K^-\pi_1^o$	2158±51	40.6±1.6	25.4±1.0	0.074	
$\Lambda_c^+ \to p\pi^+K^-\pi_2^o$	2149±49	41.5±1.7	24.8±1.0	0.077	

π_1^o uses lead glass blocks 11, 20 and 1, 9

π_2^o uses lead glass blocks 1, 9 and 30

Zero-constraint calculations were performed for hypotheses which involved either a missing K^o or π^o. Those involving a K^o can be eliminated because there is no evidence for a K^o in the region predicted by the 0-constraint calculation. Although most of the π^o candidates cannot be used to balance the transverse momentum at the decay vertex, there are two which can be used in constrained fits of the decay. The best fits for the decays of the D^+, F^+, and Λ_c^+, all of which have acceptable 3-constraint confidence levels, are given in Table 22.

Event 527-3682 F^-

A charged particle is observed to decay to three charged particles after $670 \pm 4\,\mu$ in a vertical emulsion module. Two of the decay particles, of momenta -1.51 and 1.11 GeV/c, are identified as a π^- and a π^+ respectively. Since the momentum of the third particle is -5.42 GeV/c, it can be a π^- or K^- but not a $\bar{p}$. Energy is deposited in eight lead glass blocks, three of which have incident charged particles. There is 22 GeV of hadronic energy deposited in the calorimeter. The chi-squared for a fit to an exclusive charged particle decay is unacceptable and the transverse momentum imbalance at the decay vertex is 400 MeV/c.

TABLE 23. Decay tracks for event 527-3682.

	dx/dz	dy/dz	Momentum (GeV/c)	I/I_o	$p\beta$
P	0.012±0.008	-0.500±0.005			
D1	-0.041±0.010	-0.114±0.005	-5.42±0.11		
D2	0.345±0.015	-0.076±0.007	-1.51±0.01		
D3	-0.240±0.013	-0.058±0.006	1.11±0.01		

TABLE 24. Decay hypotheses for event 527-3682

Hypothesis	Mass	Decay Time	3-C Momentum	3-C C.L.	Excited States
	(MeV/c^2)	(10^{-13} s)	(GeV/c)		(MeV/c^2)
$F^- \to \pi^-\pi^-\pi^+\pi^0_1$	1983±59	3.83±0.09	11.78±0.26	0.704	2164±22 2089±13
$F^- \to \pi^-\pi^-\pi^+\pi^0_2$	1923±57	3.92±0.09	11.51±0.26	0.120	2153±20 2166±22
$F^- \to \pi^-\pi^-\pi^+\pi^0_3$	2011±61	3.67±0.08	12.31±0.27	0.845	2163±21 2463±54
$F^- \to \pi^-\pi^-\pi^+\pi^0_4$	2021±60	3.65±0.09	12.35±0.28	0.937	2163±21

π^0_1 uses lead glass blocks 20 and 21

π^0_2 uses lead glass blocks 20 and 30

π^0_3 uses lead glass blocks 20, 21, and 30

π^0_4 uses lead glass blocks 30, 20, and 21

Very low chi-squared values are achieved for fits of four-body decays which involve a π^0 reconstructed using lead glass block 20 in combination with 21, 30, or both. These hypotheses are given in Table 24. The chi-squared is unacceptably high if the π^0 is reconstructed using the other lead glass blocks.

The masses of the all-pion decays is in excellent agreement with the expected mass of the F^-, 2030 MeV/c^2. This decay is expected to proceed via a Cabibbo-favoured non-spectator process.

Also calculated were the masses of the $K^-\pi^-\pi^+\pi^0$ system, (not a Cabibbo-favoured decay mode of the D^-), which could be a Cabibbo-favoured decay mode of an exotic meson (for example $\bar{c}s\bar{d}s$). The energy deposited in the remaining lead glass blocks is used to calculate possible F^{+*} states, which are shown in Table 24.

There is some evidence for a K_L^0 in the calorimeter since the hadronic energy is approximately 5 GeV greater than the sum of the energies of the charged tracks. However this can not come from the decay vertex alone, or in combination with any of the π^0 candidates, since it would not balance the transverse momentum at the decay.

Event 529-0271 D^+/Ambiguous

In this event a charged particle decays to a single charged particle after $2547 \pm 30\,\mu$ of vertical emulsion. The transverse momentum imbalance at the kink vertex, before any neutral secondaries have been assumed, is 494 MeV/c. Approximately 25 GeV of excess energy is observed in the hadron calorimeter. The lead glass array contains 11 GeV of energy from which two non-independent π^0 candidates can be reconstructed. One lead glass block (48) contains 8.40 GeV, which is due either to an incident photon or to an interacting hadron.

TABLE 25. Decay tracks for event 529-0271.

	dx/dz	dy/dz	Momentum (GeV/c)	I/I_0	$p\beta$
P	-0.028 ± 0.002	-0.058 ± 0.002			
D1	-0.087 ± 0.002	-0.005 ± 0.002	6.04 ± 0.16		

Several zero-constraint Cabibbo-favoured calculations for D^+, F^+, and Λ_c^+ parent hypotheses are acceptable. The high momentum solution for the $D^+ \rightarrow \pi^+(K^0)$ hypothesis can be excluded since the predicted energy of the K^0, 65 GeV, is clearly inconsistent with that deposited in the calorimeter. The low momentum solutions for all of the D^+, F^+, and Λ_c^+ hypotheses

TABLE 26. Summary of unconstrained decay hypotheses for event 529-0271.

Hypothesis	Minimum Mass	Momentum	Decay Time	Excited States
	(MeV/c^2)	(GeV/c)	(10^{-13} s)	(MeV/c^2)
$D^+ \to \pi^+(K^o)$	1214±33	7.3	26.7±0.3	
$F^+ \to K^+(K^o)$	1399±28	7.1	24.2±0.3	
		46	3.7±0.1	
$\Lambda_c^+ \to p(K^o)$	1762±22	7.0	27.7±0.3	
		25	7.8±0.1	
$D^+ \to \pi^+\pi_1^o(K^o)$	1357±32	8.6	18.4±0.2	
		48	3.3±0.1	
$D^+ \to \pi^+\pi_2^o(K^o)$	1391±36	9.5	16.7±0.2	
		51	3.1±0.1	
$F^+ \to K^+\pi_1^o(K^o)$	1532±28	8.4	20.4±0.2	
		36.5	4.7±0.1	
$F^+ \to K^+\pi_2^o(K^o)$	1578±30	9.4	18.2±0.2	
		37	4.6±0.1	
$\Lambda_c^+ \to p\pi_1^o(K^o)$	1896±23	8.4	23.1±0.3	
		22.5	8.6±0.1	
$p\pi_2^o(K^o)$	1963±26	9.1	21.2±0.3	
		22	8.8±0.1	

contain a K^o emitted at a wide angle ($\frac{dx}{dz} > 0.25$, $\frac{dy}{dz} > 0.25$), and with momentum about 1 GeV/c. Thus none of the low momentum solutions can be excluded. Using the angles of the lead glass block 48, which match almost exactly those predicted by the zero-constraint calculation for the high-momentum solutions, it was possible to perform constrained fits for the decays. The results of these calculations are shown in Table 27.

TABLE 27. Summary of constrained decay hypotheses for event 529-0271.

Hypothesis	Decay Time	2-C Momentum	2-C C.L.	Excited States
	(10^{-13} s)	(GeV/c)		(MeV/c^2)
$D^+ \to \pi^+\pi^0K^0$	3.27±0.24	48.5±3.5	0.92	
$F^+ \to K^+\pi^0K^0$	4.74±0.20	36.2±1.5	0.93	
$\Lambda_c^+ \to p\pi^0K^0$	8.46±0.25	22.9±0.6	0.54	
$\Lambda_c^+ \to pK^0$	7.63±0.21	25.4±0.6	0.70	

Event 533-7152 D^+/Ambiguous

This decay of a charged particle to a single charged particle occurs after 5246±50 μ. The transverse momentum imbalance at the decay vertex is 564 MeV/c. An excess of 23.5 GeV of hadronic energy is observed in the calorimeter and 10 adjacent lead glass blocks in the forward direction contain a total of aproximately 10 GeV of electromagnetic energy. The reconstruction of π^0 candidates was hampered by the fact that all of the lead glass blocks were adjacent.

TABLE 28. Decay tracks for event 533-7152.

	dx/dz	dy/dz	Momentum (GeV/c)	I/I_0	$p\beta$
P	0.019±0.002	0.010±0.002			
D1	-0.023±0.002	-0.084±0.002	5.49±0.1		

Many 0-constraint, Cabibbo-favoured, hypotheses were examined and found to be acceptable. None of the low momentum solutions was excluded by experimental evidence. Some of the high momentum solutions could be eliminated, since the calculated energy of the missing neutral clearly exceeded that deposited in the lead glass of the calorimeter. The energy deposited in the lead glass could not balance the transverse momentum at the decay vertex.

TABLE 29. Summary of decay hypotheses for event 533-7152.

Hypothesis	Minimum Mass	Momentum	Decay Time	Excited States
	(MeV/c^2)	(GeV/c)	(10^{-13} s)	(MeV/c^2)
$D^+ \to \pi^+(K^o)$	1332±31	6.6 46	49.5±0.5 7.1±0.1	
$\Lambda_c^+ \to p(K^o)$	1846±22	6.3 20.2	63.1±0.6 19.7±0.2	
$F^+ \to \pi^+(\pi^o)$	1159±35	5.9	59.9±0.6	
$D^+ \to \pi^+\pi^o(K^o)$	1621±59	13 38	25.1±0.2 8.6±0.1	
$F^+ \to K^+\pi^o(K^o)$	1842±59	13 30	27.1±0.3 10.9±0.1	
$\Lambda_c^+ \to p\pi^o(K^o)$	2274±48	16	24.8±0.2	
$\Lambda_c^+ \to \pi^+(\Lambda^o)$	1830±26	8	49.7±0.5	
$\Lambda_c^+ \to K^+(n)$	1844±23	7	56.8±0.5	
$\to K^+(\Lambda^o)$	1999±22	7.7		

Event 546-1339 D^+/ambiguous

A charged particle decays in a horizontal emulsion module to three charge particles after 2150±50 μ. One of the decay particles is identified as a μ^+ since it passes through both planes of the muon scintillation counters. The two other charged particles (-3.92 and +3.22 GeV/c) may be either pions or kaons. There is one lead glass block, 40, which contains 2.44±0.23 GeV of energy, and 11.5 GeV of energy is deposited in the calorimeter. The transverse momentum imbalance at the decay vertex, without the addition of a neutral decay particle, is 530 MeV/c.

TABLE 30. Decay tracks for event 546-1339.

	dx/dz	dy/dz	Momentum (GeV/c)	I/I_0	$p\beta$
P	-0.029±0.008	-0.052±0.005			
D1	-0.043±0.011	-0.160±0.005	-3.92±0.08	0.10±0.04	
D2	0.004±0.008	-0.042±0.004	4.67±0.11	1.08±0.04	
D3	0.079±0.009	-0.032±0.004	3.22±0.05	1.03±0.04	

The emulsion and computer calculated angles for the reconstructed tracks differ significantly in dx/dz. The difference is systematic and may be attributed to a rotation of

TABLE 31. Summary of decay hypotheses for event 546-1339.

Hypothesis	Minimum Mass	Momentum	Decay Time	Excited States
	(MeV/c^2)	(GeV/c)	(10^{-13} s)	(MeV/c^2)
$D^+ \to \pi^-\mu^+\pi^+(\nu_\mu)$	1622±93	29.9 13.5	4.5±0.1 9.9±0.2	
$F^+ \to \pi^-\mu^+\pi^+(\nu_\mu)$	1622±93	36.6 13.0	4.0±0.1 11.1±0.3	2100±46
$F^+ \to \pi^-\mu^+K^+(\nu_\mu)$	1949±87	20.2 14.1	7.2±0.2 10.3±0.2	
$D^+ \to K^-\mu^+\pi^+(\nu_\mu)$	1897±85	16.5	8.1±0.2	2003±16
$F^+ \to K^-\mu^+K^+(\nu_\mu)$	2171±83	15.5	9.3±0.2	

16 mr in dx/dz and 0 mr in dy/dz. Therefore, in fitting the event, such a rotation was assumed and the computer-calculated dx/dz measurements were used as the input to the fitting programs. Because of the existence of the unobserved ν_μ, constrained fits were not possible. The results of the 0-constraint calculations are shown in Table 31. All of the energy in the calorimeter may be attributed to incident charged hadrons.

If one assumes the presence of a γ in lead glass block 41, the invariant masses of the F^+ and D^+ can be calculated and are also shown in Table 31. These masses are consistent respectively with that of the F^{+*} and the D^{+*}. The branching ratio of $F^{+*} \to$

$F\gamma$ is not known although several theoretical predictions place it at 100%. For the $D^{+*} \rightarrow D\gamma$, the branching ratio is 7±8%.

Event 547-3192 D^+/ambiguous

This decay of a charged particle to three charged particles occurs after 185±10 μ . In addition there were ten other tracks from the primary vertex which were found in the emulsion. One of the charged secondaries interacts in the emulsion producing 6 black tracks and one minimum-ionizing track. Another of the charged secondaries hits a support post and scatters significantly. Only one of the three secondaries can be reconstructed using the spectrometer data, and this is an upstream-only track. Ionization and $p\beta$ measurements were therefore performed on the three secondaries, in an attempt to gain some information about the decay.

TABLE 32. Decay tracks for event 547-3192.

	dx/dz	dy/dz	Momentum (GeV/c)	I/I_0	$p\beta$
P	-0.023±0.011	-0.110±0.005			
D1	0.084±0.018	0.478±0.008	0.68±0.30	0.97±0.04	0.38±0.10
D2	-0.007±0.010	0.066±0.005		1.01±0.04	2.60±0.97
D3	-0.021±0.012	-0.218±0.005		0.95±0.04	3.80±1.36

These measurements allow for two of the secondaries to be either pions or kaons, while the third is identified as a pion. The

TABLE 33. Summary of constrained decay hypotheses for event 547-3192.

Hypothesis	2-C Mass	Decay Time	3-C Momentum	3-C C.L.	Excited States
	(MeV/c^2)	(10^{-13} s)	(GeV/c)		(MeV/c^2)
$D^+ \to \pi^+\pi^+K^-$	1717±260	1.23±0.08	9.4±0.3	0.602	
$\to K^+\pi^+\pi^-$	2558±333				
$\to K^+\pi^+K^-$	2619±323				
$F^+ \to \pi^+\pi^+\pi^-\pi_1^0$	2239±313	1.14±0.07	10.8±0.3	0.762	2110±21
$D^+ \to \pi^+\pi^+K^-\pi_1^0$	2323±292	1.28±0.08	9.0±0.3	0.303	2027±15 2035±16
$F^+ \to \pi^+\pi^+\pi^-\pi_2^0$	2209±323	1.15±0.07	10.8±0.3	0.786	2110±21
$D^+ \to \pi^+\pi^+K^-\pi_2^0$	2286±215	1.28±0.08	9.0±0.2	0.359	
$F^+ \to \pi^+\pi^+\pi^-\pi_3^0$	1929±311	1.07±0.07	11.7±0.4	0.601	
$D^+ \to \pi^+\pi^+K^-\pi_3^0$	2036±291	1.19±0.07	9.7±0.3	0.570	

π_1^0 uses lead glass blocks 12 and 55

π_2^0 uses lead glass blocks 12 and 64

π_3^0 uses lead glass blocks 37 and 56

TABLE 34. Summary of unconstrained decay hypotheses for event 547-3192.

Hypothesis	Minimum Mass (MeV/c^2)	Momentum (GeV/c)	Decay Time (10^{-13} s)
$D^+ \to \pi^+\pi^+\pi^-(K^o)$	2107±458	9.5	1.2±0.1
$F^+ \to \pi^+\pi^+K^-(K^o)$	2238±400	9.4	1.3±0.1
$\Lambda_c^+ \to \pi^+\pi^+K^-(n)$	2556±244	11.0	1.3±0.1
$\Lambda_c^+ \to \pi^+\pi^+\pi^-(\Lambda^o)$	2590±257	12.1	1.2±0.1

charges of the three cannot be determined from the emulsion measurements, but the parent is assumed to be positively charged because there is a 17.2 GeV μ^-, which penetrates both planes of muon counters. There is 16.0 GeV of energy deposited in the calorimeter, which supports the existence of a neutral hadron. Ten lead glass blocks contain energy, only three of which have incident charged particles, and can be used to reconstruct five separate but not independent π^o candidates. The transverse momentum imbalance at the decay vertex is approximately 300 MeV/c.

The analysis of the decay was performed using the momenta measured in the emulsion. It was possible to fit a charged-only decay mode, $\pi^+\pi^+K^-$ for the D^+, which has a confidence level of

0.602. There are also several acceptable hypotheses of $D^+ \rightarrow \pi^+\pi^+K^-\pi^0$ and $F^+ \rightarrow \pi^+\pi^+K^-\pi^0$ using the various π^0 candidates. Zero-constraint hypotheses involving missing neutrals are also possible and are shown in Table 34. These are $D^+ \rightarrow \pi^+\pi^+\pi^-(K^0)$, $F^+ \rightarrow \pi^+\pi^+K^-(K^0)$, $\Lambda_c^+ \rightarrow \pi^+\pi^+\pi^-(\pi^0)$, and $\Lambda_c^+ \rightarrow \pi^+\pi^+K^-(n)$. Several downstream track segments and excess hadronic energy support the existence of such neutrals, whose angles and momenta were calculated.

Using the energy deposited in the lead glass, candidates for both the D^{+*} and F^{+*} were found assuming the decay modes $D^{+*} \rightarrow D^+\pi^0$ and $F^{+*} \rightarrow F^+\gamma$. The masses of the D^{+*} and F^{+*} candidates do not change significantly when the momentum of the D^+ and F^+ are varied slightly, as happens when different π^0 are used in the D^+ or F^+ decay hypothesis.

Since the charges of none of the decay particles can be determined, the interpretation of this event is uncertain.

Event 549-4068 Λ_c^+ or Non-charm

A charged particle is observed to decay to three charged particles after $20.6 \pm 2.0\ \mu$. One of the three particles is reconstructed as a positively charged, 1 GeV/c, up-only track by the spectrometer. It is identified using $p\beta$ and ionization measurements as a proton. A second decay particle, which was emitted backward in the laboratory frame, is identified as a 47 MeV/c π^+, by observation in the emulsion of the decay chain

$$\pi^+ \rightarrow \mu^+\nu$$
$$\quad\quad \hookrightarrow e^+\nu\bar{\nu}.$$

The $p\beta$ and ionization measurements for the third decay particle, which was not reconstructed from spectrometer data, cannot resolve the ambiguity between kaon and proton interpretations although the latter is favoured. Two lead glass blocks contain energy due to incident charged particles from the primary vertex. The calorimeter contains 15 GeV of hadronic energy, which supports the existence of a neutral hadron. Transverse momentum imbalance at the decay vertex is 287 MeV/c.

The interpretation of this event as the decay of a charmed particle (as opposed to a nuclear interaction) can be made only if the third decay particle is assumed to be a K^-. Using this

TABLE 35. Decay tracks for event 549-4068.

	dx/dz	dy/dz	Momentum (GeV/c)	I/I_o	$p\beta$
P	-0.236±0.025	0.025±0.025			
D1	0.097±0.003	-0.129±0.003		1.10±0.06	0.85±0.24
D2	-0.339±0.007	0.451±0.007	0.80±0.12	1.31±0.07	0.63±0.22
D3	3.756±0.100	-10.321±0.300			0.047±0.001

TABLE 36. Summary of decay hypotheses for event 549-4068.

Hypothesis	Minimum Mass	Momentum	Decay Time	Excited States
	(MeV/c^2)	(GeV/c)	(10^{-13} s)	(MeV/c^2)
$\Lambda_c^+ \to p\pi^+K^-(\pi^o)$	2155±123	1.7	0.92±0.09	2560±31
		2.6	0.60±0.06	2543±31

assumption and the existence of an unobserved π^o, 0-constraint calculations were performed. The two solutions for the decay $\Lambda_c^+ \to K^-p\pi^+(\pi^o)$ are given in Table 36. (The minimum mass of a $K^-p\pi^+(K^o)$ system is 2417±100 MeV/c^2.)

For both 0-constraint solutions the momentum of the decaying Λ_c^+ is considerably less than any momentum cutoff (~4 GeV/c) below which background nuclear interactions are quite likely. This fact, in additon to the fact that a kaon is not the favoured

identification for the third decay particle, render the interpretation of the event as a charmed particle decay somewhat doubtful.

Event 567-2596 Λ_c^+

In this event, a charged particle is observed to kink after 175±5 μ. The daughter track, reconstructed in the spectrometer, has momentum 1.62 GeV/c and is identified as a proton. The transverse momentum imbalance at the kink point is 543 GeV/c, if a neutral secondary is not assumed. Five other particles, all of whose tracks are reconstructed in the spectrometer, are produced at the primary vertex. No evidence of electromagnetic energy, in excess of that attributed to the incident charged particles, is observed in the lead glass array. There is approximately 4 GeV of energy in one column of the calorimeter in excess of that deposited by the incident charged hadrons.

TABLE 37. Decay tracks for event 567-2596.

	dx/dz	dy/dz	Momentum (GeV/c)	I/I_o	$p\beta$
P	0.096±0.010	-0.010±0.005			
D1	0.466±0.018	0.023±0.008	1.62±0.01		

TABLE 38. Summary of decay hypotheses for event 567-2596.

Hypothesis	Minimum Mass	Momentum	Decay Time	Excited States
	(MeV/c^2)	(GeV/c)	(10^{-13} s)	(MeV/c^2)
Λ_c^+ -> p(K^o)	1821±22	1.33	10.0±0.3	
		6.20	2.1±0.1	2473±13
				2499±15
				2550±13
				2558±22

A 0-constraint calculation for the decay hypothesis Λ_c^+ -> p(K^o) was performed to predict the position and energy of the K^o. These were in good agreement with the observations of the calorimeter. The existence of strongly-decaying resonant states was examined by calculating the invariant masses of the Λ_c^+ with the pions produced at the primary vertex. These invariant masses are summarized in Table 38.

Event 580-4508 D^-

In this event a negatively charged particle decays to three charged secondaries after $2307 \pm 50\ \mu$. A 6.4 GeV/c μ^+ from the primary vertex is identified by both planes of muon counters. There is 14.6 GeV of energy deposited in the hadron calorimeter. Of the three charged decay particles two have been reconstructed as up-to-down tracks with momenta 1.52 and -4.28 GeV/c and the third is an up-only track of momentum -0.85 GeV/c and is therefore not identified. The 1.52 GeV/c track is identified as a K^+ by TOF. The -4.28 GeV/c track enters a lead glass block, in which is deposited 5.70 GeV of energy, and it is therefore identified as an electron. No other particles either from the primary or secondary vertex enter this block. Since the electron is expected to radiate photons by the bremsstrahlung process as it traverses the emulsion, the energy of the lead glass system should be a more reliable measurement of the energy of the electron. Including the energy of an adjacent block, into which no charged particles are incident, the energy of the electron is 5.79 ± 0.36 GeV. Evidence for the existence of a neutral hadron is observed in one column of the calorimeter, which measured 8.6 GeV of hadronic energy, and into which a K^+ of energy 1.52 GeV was incident.

Because of the missing $\bar{\nu}_e$, the analysis of this event was

TABLE 39. Decay tracks for event 580-4508.

	dx/dz	dy/dz	Momentum (GeV/c)	I/I_o	$p\beta$
P	-0.003±0.003	-0.049±0.003			
D1	0.062±0.002	-0.038±0.002	-4.28±0.28		
D2	0.075±0.004	-0.213±0.004	-0.85±0.28		
D3	-0.267±0.004	-0.027±0.004	1.52±0.01		

TABLE 40. Summary of decay hypotheses for event 580-4508.

Hypothesis	Minimum Mass (MeV/c^2)	Momentum (GeV/c)	Decay Time (10^{-13} s)
$D^- \to e^-\pi^-K^+(\bar{\nu}_e)$	1716±173	8.12 10.36	17.7±0.4 13.9±0.3
$F^- \to e^-K^-K^+(\bar{\nu}_e)$	2252±152		

limited to zero-constraint calculations, which favour the interpretation $D^- \to e^-\pi^-K^+(\bar{\nu}_e)$. The minimum mass of the decay mode $e^-K^-K^+(\bar{\nu}_e)$ is 1.5 standard deviations above the mass of the F^-, 2030 MeV/c^2. If one includes a K^o or $\bar{K}^o$ as one of the decay products, using a dx/dz consistent with the the measurements of the calorimeter and a dy/dz which would minimize the parent mass, then for minimal values for the momentum, 1 GeV/c, the parent mass precludes an F^- interpretation. The minimum parent mass is

2590 MeV/c^2 for the $e^-\pi^-K^+(\bar{\nu}_e)K^o$ system. In any case it would be unlikely for the neutral hadron to have momentum of only 1 GeV/c when 7.6 GeV of energy is unaccounted for. One would have to conclude that the neutral hadron originated at the primary vertex. Although there is one isolated lead glass block which contains 350 MeV of energy, there is not a D^{-*} candidate.

Event 597-1851 F^+

In this event, a charged particle decays to three charged particles after 130±11 μ. The momentum of all three decay particles is less than 3 GeV/c, enabling hadron particle identification by TOF. The transverse momentum imbalance at the decay vertex is 629 MeV/c if a neutral decay particle is not assumed. Two lead glass blocks (38 and 51) contain small amounts of energy (0.14 and 0.09 GeV) which cannot be attributed to incident charged particles. However, the invariant mass calculated using the energy of these blocks, is far below that of a π^o. The amount of energy in the hadron calorimeter is 10.3 GeV. There is no muon identified in this event as none of the charged particles penetrate the muon steel. The existence of a muon cannot be excluded though, since there are several wide-angle tracks which do not pass through the magnet gap.

TABLE 41. Decay tracks for event 597-1851.

	dx/dz	dy/dz	Momentum (GeV/c)	I/I_o	$p\beta$
P	-0.105±0.018	-0.002±0.013			
D1	-0.091±0.003	-0.078±0.003	2.19±0.01		
D2	-0.070±0.002	0.027±0.002	-1.60±0.01		
D3	0.089±0.003	0.114±0.003	2.69±0.03		

TABLE 42. Summary of decay hypotheses for event 597-1851.

Hypothesis	Mass	Decay Time	3-C Momentum	3-C C.L.	Excited States
	(MeV/c^2)	(10^{-13} s)	(GeV/c)		(MeV/c^2)
$F^+ \rightarrow K^+\pi^-\pi^+K^o$	2082±71	1.00±0.09	8.79±0.23	0.47	

Two decay hypotheses were examined using zero-constraint calculations: $K^+\pi^-\pi^+\pi^o$ and $K^+\pi^-\pi^+K^o$. The hypothesis, $K^+\pi^-\pi^+\pi^o$ is a Cabibbo-suppressed decay mode of the F^+ and is not a decay mode of the D^+. One of the kinematic solutions of $F^+ \rightarrow K^+\pi^-\pi^+\pi^o$ can be excluded because there is no evidence for the π^o in the lead glass array in the direction calculated by the zero-constraint program. For the second solution, the direction of the π^o, as calculated by the program falls just barely beyond the boundaries of the lead glass array.

The minimum mass for the decay hypothesis $K^+\pi^-\pi^+\pi^o$ is 1991± 161 MeV/c^2; for the hypothesis $K^+\pi^-\pi^+K^o$ the minimum mass is 2150± 140 MeV/c^2, which excludes the Cabibbo-suppressed D^+ hypothesis. There is only one kinematic solution for the $F^+ \rightarrow K^+\pi^-\pi^+K^o$ hypothesis, at the minimum of the -1-constraint curve. At this point, the calculated energy of the missing K^o is in good agreement with the information of the calorimeter. The predicted angles agree with those of lead glass block 51. Since the

interaction length of the lead glass is 40 cm, it is quite plausible for a hadron to interact in the lead glass, leaving traces of its energy. Using the angles of the lead glass, a constrained fit for the F^+ decay was obtained and is shown in Table 42. No F^{+*} candidates were found.

In summary, the decay cannot be that of a Λ_c^+ or a D^+, and is explained by the hypothesis $F^+ \rightarrow K^+\pi^-\pi^+K^o$.

Event 598-1759 D/ambiguous

In this event a charged particles decays to three charged particles after 1802±15 μ. One of the charged particles is identified by TOF as a π^+. The other two, however, are too energetic (6.4 and 8.1 GeV/c) to be identified. The transverse momentum imbalance at the decay vertex is 174 MeV/c. There are nine lead glass blocks in which energy is deposited. Although the upstream drift chambers contain no hits in addition to those used for the fitted tracks, there appear to be downstream-only track segments. That these segments are due to charged particles is supported by information of the TOF II counters. It appears that a neutral particle (K^o) may have decayed within the magnet gap. The energy deposited in the calorimeter is 21 GeV of which 18 GeV may be attributed to the three charged decay particles and the muon from the primary vertex. (No other charged particles are observed in this event.)

The addition of a neutral secondary at the decay vertex is not warranted by the transverse momentum imbalance. However, none of the three-body decay modes has a parent mass within 4 standard deviations of the appropriate charmed particle. Therefore several hypotheses were examined: those which involved a missing π^o and those involving a K^o. All of the π^o which could be reconstructed using the lead glass data were cycled through using two-vertex

TABLE 43. Decay tracks for event 598-1759.

	dx/dz	dy/dz	Momentum (GeV/c)	I/I_o	$p\beta$
P	-0.096±0.003	-0.045±0.003			
D1	-0.130±0.003	0.011±0.003	-6.40±0.14		
D2	-0.118±0.003	-0.063±0.003	8.05±0.20		
D3	0.100±0.003	-0.084±0.003	1.57±0.07		

TABLE 44. Summary of constrained decay hypotheses for event 598-1759.

Hypothesis	Mass	Decay Time	3-C Momentum	C.L.	Excited States
	(MeV/c^2)	(10^{-13} s)	(GeV/c)		
$D^+ \to K^-K^+\pi^+\pi^o$	1847±46	6.34±0.09	17.7±0.2	0.747	
$\Lambda_c^+ \to K^-p\pi^+\pi^o$	2191±42	7.54±0.14	18.1±0.3	0.303	

constrained fits. The two hypotheses which produced masses in the appropriate range (and therefore acceptable 3-C confidence levels) were $D^+ \to K^-K^+\pi^+\pi^o$ and $\Lambda_c^+ \to K^-p\pi^+\pi^o$. No D^{+*} candidates can be reconstructed in association with the D^+, for which this decay mode is Cabibbo-suppressed.

There are solutions for both D^+ and F^+ hypotheses for zero-constraint calculations which involve a missing K^o. The range in

TABLE 45. Summary of unconstrained decay hypotheses for event 598-1759.

Hypothesis	Minimum Mass	Momentum	Decay Time	Excited States
	(MeV/c^2)	(GeV/c)	(10^{-13} s)	(MeV/c^2)
$D^+ \to \pi^-\pi^+\pi^+(K^o)$	1871±45	22.25	5.1±0.1	1958±74 (γ) 2024±71 (π^o)
$F^+ \to K^-\pi^+\pi^+(K^o)$	2066±43	21.5	5.6±0.1	2071±67 (γ) 2114±65 (γ) 2181±62 (π^o)
$F^+ \to \pi^-K^+\pi^+(K^o)$	2029±43	21.75	5.6±0.1	2072±68 (γ) 2115±66 (γ) 2181±64 (π^o)

the angles and momenta for the K^o predicted by the calculations are compatible with what is observed in the spectrometer. For both the D^+ and F^+ hypotheses, there are candidates for associated D^{+*} and F^{+*}. The values for the masses of the D^{+*} and the F^{+*} should be examined qualitatively since there are other points on the -1-constraint curves within one standard deviation of the D^+ and F^+, and for which the momenta are different (which would affect the values of the masses of the D^{+*} and the F^{+*}).

Event 602-2032 Λ_c^+

In this event a charged particle decays to three charged particles after 282.5±5.0 μ.[10] One of the decay particles scatters in the emulsion and is then observed in the spectrometer as an up-to-down track of momentum 1.88±0.02 GeV/c. It is identified as a proton. The two other decay particles are reconstructed as up-only tracks with extremely poorly measured momenta. Two downstream track segments are reconstructed which do not appear to be part of any of the tracks observed in the emulsion. There is also a multitude of hits in the upstream chambers. The lead glass array contains no evidence for a π^0. The energy in the hadron calorimeter exceeds that of the incident charged hadrons by a few GeV.

The analysis of this event was limited because the momenta of two of the decay tracks were so poorly measured and since ionization and pβ measurements were not available (except to confirm that the two particles were minimum ionizing). It was assumed, however, that the decay was that of a charmed baryon because of the identification of one of the decay particles as a proton.

---

[10] In addition a nuclear interaction is observed in the emulsion.

TABLE 46. Decay tracks for event 602-2032.

	dx/dz	dy/dz	Momentum (GeV/c)	I/I_o	$p\beta$
P	0.016±0.002	-0.099±0.002			
D1	-0.048±0.005	0.106±0.005	1.88±0.02		
D1k	-0.107±0.003	0.166±0.003	1.88±0.02		
D2	0.271±0.005	-0.188±0.005	-2.16±3.58		
D3	-0.125±0.008	-0.594±0.008	1.90±1.26		

TABLE 47. Summary of unconstrained decay hypothesis for event 602-2032.

Hypothesis	Minimum Mass	Momentum	Decay time	Excited States
	(MeV/c^2)	(GeV/c)	(10^{-13} s)	(MeV/c^2)
$\Lambda_c^+ \to p\pi^-\pi^+(K^o)$	2041±78	3.3 6.4	6.51±0.12 3.36±0.06	

The only constrained hypothesis which had an acceptable confidence level was the Cabibbo unfavoured $\Lambda_c^+ \to pK^-K^+$, shown in Table 48. 0-constraint hypotheses for $\Lambda_c^+ \to p\pi^-\pi^+(K^o)$ were examined using different momenta for the pions. The upper and lower bounds for the momentum of the Λ_c^+, 6.4 Gev/c and 3.3 GeV/c, are obtained by assuming both pions have momentum equal to 0.5 GeV/c. (Any increase in the momentum of the two pions will move

TABLE 48. Summary of constrained decay hypothesis for event 602-2032.

Hypothesis	Mass	Decay Time	2-C Momentum	2-C C.L.	Excited States
	(MeV/c^2)	(10^{-13} s)	(GeV/c)		(MeV/c^2)
$\Lambda_c^+ \to p\pi^-\pi^+$	1764±24				
$\Lambda_c^+ \to pK^-\pi^+$	2007±18				
$\Lambda_c^+ \to pK^-K^+$	2257±12	5.40±0.11	3.98±0.04	0.06	

the minimum and maximum closer together.) For the purposes of the Λ_c^+ lifetime calculation, the decay time for this event was taken to be 4.48±1.4 x 10^{-13} s.

Event 610-4088 Λ_c^+

In this event, there are only two charged particles produced at the primary vertex: a muon, which is reconstructed by the spectrometer and a charged particle which decays to three charged particles after 221±4 μ. Of the three decay particles one is reconstructed by the spectrometer and is identified as a 1.48 GeV/c pion. The two other particles are emitted at very wide angles and although the tracks of the particles are observed in a few of the most upstream chambers, reliable fits for these tracks and the momenta cannot be obtained. Measurements of pβ were made on the emulsion tracks of these two decay particles. Both are favoured to be pions with momenta less than 500 MeV/c.

TABLE 49. Decay tracks for event 610-4088.

	dx/dz	dy/dz	Momentum (GeV/c)	I/I_0	pβ
P	0.236±0.007	0.123±0.007			
D1	0.196±0.004	-0.140±0.004	1.48±0.01		
D2	-0.079±0.015	1.331±0.015	-0.82±0.25		0.17±0.03
D3	0.387±0.011	0.901±0.011	-1.61±1.14		0.32±0.13

In addition, a vee is observed in the drift chambers: a cluster of hits lies in the most downstream of the upstream

TABLE 50. Summary of decay hypothesis for event 610-4088.

Hypothesis	Minimum Mass	Momentum	Decay time	Excited States
	(MeV/c^2)	(GeV/c)	(10^{-13} s)	(MeV/c^2)
$\Lambda_c^+ \to \pi^+\pi^+\pi^-(\Lambda^o)$	2127±49	6.39	2.62	

chambers, and there are two track segments in the downstream chambers, one of which passes through the TOF II array, while the other is at too wide an angle. Quite fortunately, it is the positively charged particle from the vee which enters a TOF II counter. Since the decay point of the vee particle is known, it is determined to be a $\Lambda^o \to p\pi^-$, based on the TOF information which supports the hypothesis that the positive decay particle is a proton. The vee cannot be that of a $K^o \to \pi^-\pi^+$.

All of the energy deposited in the lead glass is due to the three incident charged particles. No excess energy is observed in the hadron calorimeter.

The charm decay cannot be fitted using a charged-only decay mode. The predictions of the zero-constraint calculation for the angles and momenta of the Λ^o of the decay $\Lambda_c^+ \to \pi^+\pi^+\pi^-(\Lambda^o)$ are in excellent agreement with the observations of the spectrometer.

Event 638-9417 F^+

In this event a positively charged particle decays to three particles after $153 \pm 8\ \mu$. Two of the three decay particles have TOF identification: one is identified as a K^+ and the second is ambiguous as to K^- and $\bar{p}$ interpretations, but can be excluded as a π^-. The probability of there being a $\bar{p}$ is extremely small, since the emulsion is not composed of valence antiquarks. The third decay particle has an upstream-only track and therefore cannot be identified by TOF. In addition, a gamma conversion to an electron-positron pair occurs in the emulsion and the electromagnetic shower continues into the upstream chambers. The energy deposited in the calorimeter is 6.1 GeV. Energy is deposited in nine lead glass blocks, (including that due to incident charged particles), from which several π^0 candidates may be reconstructed. Transverse momentum imbalance at the decay vertex if a neutral decay particle is not assumed, is 635 MeV/c^2.

None of the reconstructed π^0 candidates are in the direction which would balance transverse momentum at the decay vertex. Nor can a K^0 be inferred from the calorimeter since the measured hadronic energy may be attributed in total to the charged hadrons. It is possible however to reconstruct a π^0 using the emulsion information regarding the gamma conversion, and an additional upstream-only track, which one could assume to be an

TABLE 51. Decay tracks for event 638-9417.

	dx/dz	dy/dz	Momentum (GeV/c)	I/I_o	$p\beta$
P	-0.002±0.005	-0.213±0.015			
D1	0.041±0.002	-0.045±0.002	1.92±0.02		
D2	-0.009±0.002	-0.046±0.002	2.20±0.02		
D3	-0.174±0.005	-0.275±0.005	2.61±3.13		

TABLE 52. Summary of decay hypotheses for event 638-9417.

Hypothesis	Mass	Decay Time	3-C Momentum	3-C C.L.	Excited States
	(MeV/c^2)	(10^{-13} s)	(GeV/c)		(MeV/c^2)
$F^+ \to K^+K^-\pi^+\pi^o$	2077±51	1.69±0.09	6.09±0.09	0.116	2136±33 2107±21 2124±23

electron/positron from the conversion of a second gamma. The transverse momentum of this π^o balances quite well the observed momentum imbalance at the decay vertex.

Two-vertex constrained fits were performed on this event, in which the momenta of both the decaying parent and the π^o were fitted. The angles of the π^o were also allowed to be fitted during one of the sessions, as a check of the assumptions made. The results of these fits are shown in Table 52.

Clearly the only acceptable interpretation for this event is that it is a decay of a F^+ meson. The fitted baryon mass is above that of the Λ_c^+, and there are no hypotheses consistent with the decay of the D^+.

Even if the π^o seems dubious, it is interesting to note that the results of the zero-constraint calculations support the conclusions made concerning the parent particle species. The minimum masses for the zero-constraint calculations are rather high for the D^+ and Λ_c^+ for their appropriate decay modes, yet are quite consistent with the mass of the F^+ for the decay $F^+ \rightarrow K^+K^- \pi^+\pi^o$. There are two independent candidates for the F^{+*}, assuming the decay mode $F^{+*} \rightarrow F^+\gamma$.

Event 650-6003 Λ_c^+

In this event, a charged particle decays in a vertical emulsion module to three charged particles after 40.6±2.0 μ. Two of the decay particles are reconstructed in the spectrometer. One particle is seen in both the upstream and the downstream chambers and is identified as a 1.21 GeV/c π^+; the second is seen in only the upstream chambers and has a momentum of -0.44 GeV/c. Ionization and pβ measurements performed in the emulsion identified the second particle as a π^-. The third particle, which is not reconstructed in the spectrometer, and which is assumed to be positively charged, is most probably a pion on the basis of emulsion measurements. The transverse momentum imbalance at the decay vertex is 381 MeV/c. There is no evidence for a neutral hadron in the calorimeter nor can a π^0 be reconstructed using the lead glass.

TABLE 53. Decay tracks for event 650-6003.

	dx/dz	dy/dz	Momentum (GeV/c)	I/I_0	pβ
P	-0.167±0.038	-0.038±0.015			
D1	-0.397±0.006	-0.121±0.006	1.21±0.01		
D2	-0.220±0.005	-0.256±0.005		0.80±0.05	0.800±0.365
D3	-0.387±0.007	-0.308±0.007	-0.44±0.13	0.89±0.05	0.380±0.137

TABLE 54. Decay hypotheses for event 650-6003.

Hypothesis	Mass	Decay Time	3-C Momentum	3-C C.L.	Excited States
	(MeV/c^2)	(10^{-13} s)	(GeV/c)		(MeV/c^2)
$\Lambda_c^+ \to \pi^+\pi^+\pi^-\Lambda^o$	2135±75	0.53±0.3	5.77±0.07	0.90	
$\to \pi^+K^+\pi^-\Lambda^o$	2335±41				

The decay of a neutral particle to two charged particles is observed in the upstream chambers. One of the decay particles is identified by TOF as a proton, while the other decay particle has an upstream-only track and is assumed to be a π^-. The invariant mass of the $p\pi^-$ pair agrees with the mass of the Λ^o.

The only hypothesis for which a constrained fit can be made is $\Lambda_c^+ \to \pi^+\pi^+\pi^-\Lambda^o$. Decay hypotheses for D^+ or F^+ parent particles are not possible since the only neutral particle reconstructed in the spectrometer is the Λ^o. The results of the two-vertex constrained fits are given in Table 54.

Event 656-2631 D^+/Ambiguous

In this event, a charged particle decays to three charged particles after 570±11 μ. Two of the three charged decay particles are reconstructed as up-to-down tracks in the spectrometer but are too energetic (the momenta are 11.4 and 19.3 GeV/c) to be identified by TOF. The third particle is an upstream-only track and therefore is also not identified. The transverse momentum imbalance at the decay vertex is 49.5 MeV/c. There is no evidence for a neutral hadron in the calorimeter, since all of the energy deposited, 26.0 GeV, may be attributed to incident charged particles. The lead glass contains 10.6 GeV of electromagnetic energy, from which seven separate but not independent π^0 candidates may be reconstructed.

TABLE 55. Decay Tracks for event 656-2631

	dx/dz	dy/dz	Momentum (GeV/c)	I/I_0	$p\beta$
P	0.015±0.002	0.043±0.002			
D1	0.018±0.002	0.030±0.002	11.4±0.7		
D2	0.027±0.002	0.053±0.002	-19.3±1.8		
D3	-0.225±0.004	0.001±0.004	0.9±0.3		

TABLE 56. Summary of decay hypotheses for event 656-2631.

Hypothesis	Mass	Decay Time	3-C Momentum	3-C C.L.	Excited States
	(MeV/c^2)	(10^{-13} s)	(GeV/c)		(MeV/c^2)
$D^+ \to \pi^+K^-\pi^+$	1759±256	1.09±0.06	32.5±1.5	0.847	2022±20
$F^+ \to K^+K^-\pi^+$	1928±248	1.19±0.06	32.4±1.5	0.876	
$\Lambda_c^+ \to pK^-\pi^+$	2340±24	1.42±0.06	30.5±1.2	0.883	
$D^+ \to \pi^+K^-\pi^+\pi^o$	1888±89	0.99±0.04	35.9±1.4	0.997	2029±23
$F^+ \to K^+K^-\pi^+\pi^o$	2069±87	1.34±0.05	35.2±1.2	0.987	
$\Lambda_c^+ \to pK^-\pi^+\pi^o$	2498±99	1.51±0.05	28.7±0.8	0.210	
$F^+ \to \pi^+\pi^-\pi^+\pi^o\pi^o$	2098±112	1.06±0.04	36.2±1.2	0.746	

Several decay hypotheses for the D^+, F^+ and Λ_c^+ may be fitted with acceptable confidence levels. There are the charged-only decay modes $D^+ \to \pi^+K^-\pi^+$, $F^+ \to K^+K^-\pi^+$ and $\Lambda_c^+ \to pK^-\pi^+$, as well as decay modes which involve a π^o. Different π^o candidates can be used in these fits, although only the best fits for the parent D^+, F^+ and Λ_c^+ are shown in Table 56. It was also possible to fit the decay $F^+ \to \pi^+\pi^-\pi^+\pi^o\pi^o$, using two independent π^o candidates.

No evidence for the decay $F^{+*} \to F^+\gamma$ was found. Several candidates for the decay $D^{*+} \to D^+\pi^o$ were found and are shown in Table 56.

Event 663-7758 D^+/Ambiguous

A charged particle decays to 3 charged particles in the vertical emulsion after 13000±50 μ. The three decay particles have momenta +14.59, +22.06, and -39.5 GeV/c, and are thus too energetic for TOF identification. The particles all enter the same lead glass block, 41, in which 19.92 GeV of energy is deposited. Adjacent to this block are two blocks each containing approximately 2 GeV of energy. Three other blocks, not in the immediate vicinity of the charged tracks, have energy deposited in them. The transverse momentum imbalance at the decay vertex, if a neutral secondary is not assumed, is 681 MeV/c. There is 55 GeV of hadronic energy in the calorimeter.

TABLE 57. Decay tracks for event 663-7758.

	dx/dz	dy/dz	Momentum (GeV/c)	I/I_o	$p\beta$
P	-0.004±0.002	-0.003±0.002			
D1	0.000±0.002	-0.008±0.002	22.06±2.38		
D2	-0.018±0.002	-0.009±0.002	39.50±8.22		
D3	-0.016±0.002	0.001±0.002	14.59±1.06		

The large amount of energy in block 41 indicates the existence of an electron or positron. The most likely interpretation is that the 14.59 GeV/c particle is a positron.

TABLE 58. Summary of decay hypotheses for event 663-7758.

Hypothesis	Minimum Mass	Momentum	Decay Time	Excited States
	(MeV/c^2)	(GeV/c)	(10^{-13} s)	(MeV/c^2)
$D^+ \to \pi^+\pi^-e^+(\nu_e)$	1713±367	97.49 195.13	8.3 4.1	2403±85
$F^+ \to \pi^+\pi^-e^+(\nu_e)$	1712±367	91.03 246.9	9.7 3.6	2445±97 2052±32 2062±34
$D^+ \to \pi^+K^-e^+(\nu_e)$	1907±322	123.5	6.6	2520±105
$F^+ \to K^+\pi^-e^+(\nu_e)$	2037±354	115.0	7.6	2875±100 2158±26 2140±26
$F^+ \to K^+K^-e^+(\nu_e)$	2190±316	113.5	7.8	2532±118 2057±50 2066±52
$\Lambda_c^+ \to p\pi^-e^+(\nu_e)$	2690±341	103.5	9.6	
$\Lambda_c^+ \to pK^-e^+(\nu_e)$	2795±327	102.0	9.7	
$F^+ \to e^+\pi^-\pi^+(\nu_e)$	1729±369	91.3 238.6	9.6 3.7	
$F^+ \to e^+\pi^-K^+(\nu_e)$	2189±339	113.0	7.8	
$D^+ \to e^+K^-\pi^+(\nu_e)$	1919±327	121.0	6.7	
$F^+ \to e^+K^-K^+(\nu_e)$	2370±257	124.5	7.1	
$\Lambda_c^+ \to e^+\pi^-p(\nu_e)$	3109±250	112.0	8.8	
$\Lambda_c^+ \to e^+K^-p(\nu_e)$	3135±330	98.5	10.0	

The remainder of the electromagnetic energy in this block and its two neighbours would be attributed to that deposited by the other incident charged, minimum-ionizing particles and the energy due to photons radiated by the e^+ through the bremsstrahlung process. (In addition two tracks from the primary vertex enter this block.) The possible decay hypotheses using this assumption are shown in Table 58. It is also possible that the 22.06 GeV/c particle is a positron. However, one would have to assume that some of the electromagnetic energy has not been contained by the lead glass. Decay hypotheses for this assumption are shown in Table 58. In both cases, the energy in the calorimeter, may be attributed to incident charged hadrons, and thus there is no evidence for the existence of a K^o or neutron. An electron neutrino has been included for lepton conservation which also serves to balance the transverse momentum.

All of the decay hypotheses containing a proton have masses well beyond that of the Λ_c^+ baryon (2285 MeV/c^2), thus eliminating that particle from consideration as the parent. The three lead glass blocks which do not have incident charged particles were used in the calculation of D^{+*} and F^{+*} candidates. It was assumed that the F^{+*} decays exclusively to $F\gamma$ while the D^{+*} may decay to $D\gamma$ or $D\pi^o$. The findings for the excited charm states unfortunately do not resolve the ambiguity between a D^+ and a F^+ interpretation for the event.

Event 671-7015 F^+

In this event a charged particle decays to a single charged particle after 65.0±5 μ. The decay particle is reconstructed in the spectrometer as an up-only track with momentum 0.49±0.25 GeV/c. By ionization and pβ measurements made in the emulsion, the particle is favoured to be a K^+. The transverse momentum imbalance at the kink vertex is 350 MeV/c. Three lead glass blocks contain energy. The energy in one is accounted for by an incident charged particles while the two other blocks, 15 (0.51 GeV) and 22 (0.34 GeV), have no incident charged particles. There are two vee candidates in the drift chambers. The first vee has one reconstructed up-to-down track with momentum 0.25 GeV/c, which cannot originate at the production or decay vertex. Because of its wide angle it misses the TOF array. The second track in this vee candidate is not reconstructed although several hits (<6) exist in the first few upstream chambers at wide angles. The second vee candidate has one up-to-down track with momentum 1.30±0.05 GeV/c and a second up-only track with momentum -0.45±0.05 GeV/c. The invariant mass of this pair is 451±33 MeV/c^2.

0-constraint calculations were performed for the decay hypotheses $K^+(\pi^o)$ and $K^+(K^o)$. The low-momentum solution for the $K^+(\pi^o)$ hypothesis cannot be excluded since the predicted angles

TABLE 59. Decay tracks for event 671-7015.

	dx/dz	dy/dz	Momentum (GeV/c)	I/I_o	$p\beta$
P	0.181±0.002	0.060±0.002			
D1	0.847±0.010	-0.285±0.005	0.49±0.25	1.19±0.06	0.49±0.19

TABLE 60. Summary of decay hypotheses for event 671-7015.

Hypothesis	Mass	Decay Time	3-C Momentum	3-C C.L.	Excited States
	(MeV/c^2)	(10^{-13} s)	(GeV/c)		(MeV/c^2)
$F^+ \to K^+K^o$	2055±94	1.5±0.1	2.89±0.06	0.16	2253±48 2155±35

of the π^o do not lie within the boundaries of the lead glass array. The high-momentum solution is excluded by the lead glass data. Constrained fits can be made for the hypothesis $F^+ \to K^+K^o$ using the second of the K^o candidates. The results of this fit are shown in Table 60. Using the energy in lead glass block 22, a candidate $F^{+*} \to F^+\gamma$ can be found. The interpretation of this event as the decay of a charmed particle is subject to some doubt since the momentum of the F^+, 2.89 GeV/c, lies in the region (less than 4 GeV/c) for which there is a large background to charm decays.

REFERENCES

H. Abramowicz et al., Phys. Lett. 109B (1982) 115.

E. Albini et al., Phys. Lett. 110B (1982) 339.

D. Allasia et al., Nuclear Physics B 176 (1980) 13.

R. D. Ammar et al., Phys. Lett. 94B (1980) 118.

C. Angelini et al., Phys. Lett. 80B (1979) 428.

C. Angelini et al., Phys. Lett. 84B (1979b) 150.

J. J. Aubert et al., Phys. Rev. Lett. 33 (1974) 1404.

J.-E. Augustin et al., Phys. Rev. Lett. 33 (1974) 1406.

David C. Bailey, Neutrino Charm Production and a Limit to Neutrino Oscillations, Ph.D. Thesis, McGill University, 1983.

C. Baltay et al., Phys. Rev. Lett. 42 (1979) 1721.

I. Bars et al., Phys. Rev. Lett. 29 (1972) 969.

I. Bars et al., Phys. Rev. D 7 (1973) 1233.

G. Bellini et al., Phys. Rep. 83 (1982) 1.

A. Benvenuti et al., Phys. Rev. Lett. 35 (1975) 1199.

B. J. Bjorken and S. L. Glashow, Phys. Lett. 11 (1964) 255.

A. Bodek, Proceedings of the Calorimeter Workshop (M. Atac, Fermilab) (1975) 229.

E. H. S. Burhop et al., Phys. Lett. 65B (1976) 299.

Bruce A. Campbell, Current Induced Interactions in Quantum Chromodynamics, Ph.D. Thesis, McGill University, 1980.

L. A. Copley, Nathan Isgur and Gabriel Karl, Phys. Rev. D 20 (1979) 768.

A. de Rujula, Howard Georgi and S.L. Glashow, Phys. Rev. D 12 (1975) 147.

B. de Wit et al., Nucl. Phys. B57 (1973) 237.

Roland M. Egloff, Measurements of Elastic Rho, Omega and Phi Meson Photoproduction Cross Sections on Protons from 30 to 180 GeV, Ph.D. Thesis, University of Toronto, 1979.

Steven M. Errede, Measurement of the Lifetimes of the Charmed D^+, F^+ Mesons and the Λ_c^+ Charmed Baryon, Ph.D. Thesis, The Ohio State University, 1981.

A. G. Frodesen, O. Skjeggestad, and H. Tofte, Probability and Statistics in Particle Physics, Bergen, Universitetsforlaget, 1979.

M. K. Gaillard, B.W. Lee and J. Rosner, Rev. Mod. Phys. 47 (1975) 277.

M. K. Gaillard, S.A. Jackson and D.V. Nanopoulos, Nucl. Phys. B 102 (1976) 326; Nucl. Phys. B 112 (1976) 545.

Sheldon L. Glashow, Nucl. Phys. 22 (1961) 579.

S. L. Glashow, J. Iliopoulos and L. Maiani, Phys. Rev. D 2 (1970) 1285.

G. Goldhaber et al., Phys. Rev. Lett. 37 (1976), 255.

Michael Gutzwiller, The Lifetime of the D^o Charmed Meson, Ph.D. Thesis, The Ohio State University, 1981.

J. Hanlon et al., Phys. Rev. Lett. 45 (1980) 1817.

J. Hanlon, private communication, 1981.

Toshio Hara, Ph.D. Thesis, Osaka City University, 1982.

S. W. Herb et al., Phys. Rev. Lett. 39 (1977) 252.

Peter W. Higgs, Phys. Rev. Lett. 13 (1964), 508.

M. Kaplon, B. Peters and D. Ritson, Phys. Rev. 85 (1952) 900.

T. Kafka et al., Phys. Rev. Lett. 48 (1982) 910.

M. Kobayashi and T. Maskawa, Prog. Theor. Phys. 49 (1973) 652.

Benjamin W. Lee, C. Quigg and Jonathan L. Rosner, Phys. Rev. D 15 (1977) 157.

Jacques P. Leveille, University of Michigan preprint UMHE 81-18.

V. A. Lubimov et al., Phys. Lett. 94B (1980) 266.

K. Maltman and N. Isgur, Phys. Rev. D 22 (1980) 1701.

S. Mori, Fermilab technical publication TM 888 1979, unpublished.

K. Nishikawa et al., Phys. Soc. Japan Journal 14 (1959) 880.

K. Niu, E. Mikumo and Y. Maeda, Prog. Theor. Phys. 46 (1971) 1644.

I. Peruzzi et al. Phys. Rev. Lett. 37 (1976) 569.

M. Piccolo et al., Phys. Rev. Lett. 39 (1977) 1503.

Dale Pitman, Construction, Testing and Use of Large Scale Drift Chambers in Fermilab Experiment 531, M. Sc. Thesis, University of Toronto, 1979.

A. L. Read et al., Phys. Rev. D 19 (1979) 1287.

F. Reines, H. W. Sobel, and E. Pasierb, Phys. Rev. Lett. 45 (1980) 1307.

A. Salam, Proceedings of the Eighth Nobel Symposium (Almqvist and Wiksells, Stockholm), 1968.

Hiroshi Shibuya, Ph.D. Thesis, Nagoya Universtiy, 1982.

D. Son et al., Phys. Rev. Lett. 49 (1982) 1128.

George H. Trilling, Phys. Rep. 75 (1981) 57.

G. t'Hooft, Nucl. Phys. B33 (1971) 173.

N. Ushida et al., Phys. Rev. Lett. 45 (1980) 1049.

N. Ushida et al., Phys. Rev. Lett. 45 (1980) 1053.

N. Ushida et al., Phys. Rev. Lett. 47 (1981) 1694.

N. Ushida et al., Phys. Rev. Lett. 48 (1982) 844.

N. Ushida et al., to be submitted to Nuclear Instruments and Methods (1983).

Steven Weinberg, Phys. Rev. Lett. 19 (1967) 1264.